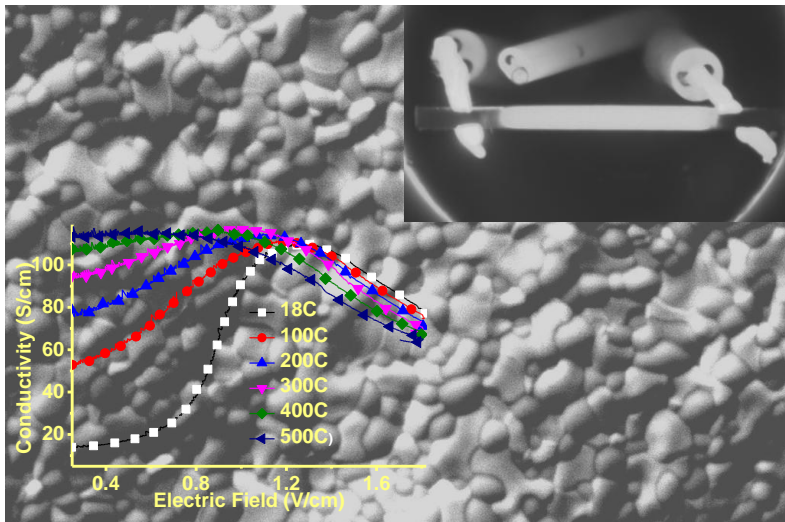




Doctoral School in Materials Science and Engineering

Flash-Sintering of MnCo_2O_4 and $(\text{La}, \text{Sr})(\text{Co}, \text{Fe})\text{O}_3$ Ceramics for Potential Application in SOFC

Anshu



June 2014

**FLASH-SINTERING OF MnCO_2O_4 AND $(\text{La, Sr})(\text{Co, Fe})\text{O}_3$
CERAMICS FOR POTENTIAL APPLICATION IN SOFC**

Anshu

E-mail: gauranshu20@gmail.com

Approved by:

Prof. Vincenzo M. Sglavo, Advisor
Department of Industrial Engineering
University of Trento, Italy.

Ph.D. Commission:

Prof. Vincenzo M. Sglavo,
Department of Industrial Engineering
University of Trento, Italy.

Prof. Rajesh Prasad,
Department of Applied Mechanics
*Indian Institute of Technology Delhi,
India.*

Prof. Lorella Ceschini,
Department of Industrial Engineering
Alma Mater Studiorum
University of Bologna, Italy.

University of Trento,
Department of Industrial Engineering

June 2014

University of Trento- Department of Materials Science and Engineering

Doctoral Thesis

Anshu - 2014

Published in Trento (Italy) – by University of Trento

To My Parents & My 'Sir'



Candidate's Declaration

I hereby declare that the work which is presented in the present PhD thesis entitled, "**Flash-sintering of MnCo_2O_4 and $(\text{La, Sr})(\text{Co Fe})\text{O}_4$ ceramics for potential application in SOFC**" in partial fulfillment of the award of the degree of Doctor of Philosophy in 'Materials Science and Engineering', submitted in the Department of Industrial Engineering, University of Trento, Italy is an authentic record of my own work carried out during the period from January, 2011 to December, 2013 under the esteemed guidance of Dr. Vincenzo M Sglavo, Professor, Department of Industrial Engineering, University of Trento, Italy.

The matter presented in the thesis has not been submitted by me for the award of any other degree of this or any other Institute.

(ANSHU)

Supervisor

This is to certify that the above statement made by the candidate is correct to the best of my knowledge.

The Ph.D. Viva-Voice Examination of **Miss Anshu**, PhD Student, has been held on 16/06/2014.

Date: 16/06/2014
Place: Trento, Italy

(Dr. Vincenzo M. Sglavo)
Professor, Department of Industrial Engineering,
University of Trento, Italy

Abstract

The innovative flash-sintering technique has been considered to investigate the effect of DC electric field on sintering and electrical conductivity of two oxide ceramics MnCo_2O_4 and $\text{La}_{0.6}\text{Sr}_{0.4}\text{Co}_{0.2}\text{Fe}_{0.8}\text{O}_3$ (LSCF). These oxides are renowned for their high electrical conductivity and oxygen reduction properties, and therefore find application in solid oxide fuel cell as interconnect coating and cathode respectively. Flash-sintering of LSCF composite with 10 mol% Gd doped ceria (GDC), which is considered more promising than pure LSCF for cathodic application, is also reported. In flash-sintering-effect, when an adequately high DC electric field is applied on a green specimen, which is subjected to heating at a constant rate, the field drives rapid increase in the conductivity at a suitable furnace temperature. This event drives sintering, and the rate of shrinkage is so rapid that the material, generally, sinters in a couple of seconds without requiring elevated temperature. The aim of the present work is to better understand such electric field effect on sintering as it may affect the material properties (microstructure, conductivity etc.). Till now, the technique has been mostly reported for weakly conducting or insulating materials. The present work deals with the conducting-edge materials to point out the versatility of flash-sintering technique.

The present work demonstrates the flash-sintering of conductive oxides, MnCo_2O_4 and LSCF. These oxides are sintered under electric field ranging from 7.5 to 12.5 V/cm at furnace temperatures 100-200°C, which are 1000°C lower than traditional heat treatments. LSCF, being highly conductive, surprisingly sinters at 25°C under 12.5 V/cm. On the other hand, the composite phases (LSCF/GDC: 60/40, 50/50 and 40/60 weight ratios) flash sinters at higher temperatures and electric fields which is systematic with GDC additions. The role of electric field and temperature in sintering is realized from specimen temperature which helps to understand the observed outstanding event. The flash-sintering occurs at conventional sintering temperatures and therefore, enhanced sintering at a particular temperature at this stage is expected to result from increased defect concentrations. Rapid increase in the conductivity possibly provides diffusion-able sites at rapid rate and the high sintering

rate can be explained to occur using these sites. At drastic conductivity increase, the thermal effect is so dominant that ions diffuse for sintering more with the support of local temperature and less by the electric field. The extent of sintering is confirmed through scanning electron microscopy. The microstructural analysis carried on flash-sintered samples suggests that the surface morphology and grain growth homogeneity resemble that of traditionally-sintered samples. With the proper choice of processing parameters (electric field and current density), dense and pore-free microstructure for MnCo_2O_4 coating and porous microstructure of LSCF for cathodic application are obtained in very short sintering time. From the case of composites, current is clearly pointed to be a determining parameter in controlling the density. An enhanced electric field effect is recorded on the microstructure of MnCo_2O_4 starting at 1100°C . No such temperature discrimination is observed for LSCF, the sintering effects being regular with the temperature. From XRD analysis, MnCo_2O_4 undergoes to a significant phase reduction for the specimen temperature in excess of 1100°C . The LSCF and its composite phase are stable and compatible with GDC10 against flash-sintering. These observations are in agreement with conventional sintering. The flash-effect is investigated by analyzing electrical conductivity property of dense specimen. Consistent changes in current-voltage characteristics with temperature suggest that the electric field controls the conductivity in the same way as temperature does. At sufficient temperature, the electric field enhances the conductivity by increasing thermal excitation of charge carrier. At low temperature, the field enhances the conductivity by direct energy transfer; these temperature and field has a fundamental role in flash-sintering. On the basis of conductivity analysis, flash-sintering is proposed to be accelerated by utilizing defect complexes formed during the "polaron-hopping" which is the usual conduction mechanism of these materials, MnCo_2O_4 and LSCF. On the basis of correlation between the microstructure and phase stability, a constraint about the utilization of defect complex is realized. Sintering is enhanced when there is stabilization of reduction reaction in hopping process. This condition assures the availability of defect complexes for sintering; under equal probability of hopping transitions, the reduction is more under the tendency of oxidation. It was realized in the sintering of MnCo_2O_4 is enhanced over conventional for temperatures higher than 1080°C which corresponds to the reduction temperature.

Such implication was verified on LSCF where sintering is found to be enhanced for all the considered temperatures as it undergoes reduction as sintering starts. Therefore, sintering is proposed to occur by the movement of reduced transition metal cations during usual hopping mechanism. Sintering at unusually low temperatures, in very short times and involving quite usual ionic transitions shows its potentials for ceramics manufacturing especially in multilayer production and temperature sensitive application.

Table of Contents

Chapter I

Introduction.....	1
-------------------	---

Chapter II

Background and Literature Review	8
2.1. Sintering of Ceramic Materials	8
2.1.1 Sintering Mechanism.....	9
2.1.2 Grain growth and Coarsening.....	11
2.1.3 Sintering Analysis.....	12
2.1.3.1 Sintering Activation Energy.....	12
2.1.3.2 Sintering Mechanism.....	14
2.1.4 Sintering Activation.....	15
2.1.4.1 By increasing driving force.....	16
2.1.4.2 By increasing sintering kinetics.....	16
2.2. Assisted Sintering Techniques	16
2.2.1 Un-assisted sintering.....	16
2.2.2 Pressure Assisted.....	17
2.2.3 Electromagnetic Field Assisted.....	18
2.2.4 Electric field Assisted Sintering.....	19
2.2.4.1 High Electric Field-assisted (Electric Discharge Compaction) & High Electric Current-assisted (Spark Plasma Sintering).19	
2.2.4.2 Flash and FAST.....	21
2.3 Flash-sintering: State of the Art.....	23
2.3.1 The method.....	23
2.3.2 Electrical and Sintering Behaviour	24
2.3.3 Flash-sintering Effect Analysis.....	29
2.3.3.1 Estimate of Local Temperature.....	30
2.3.3.1.1 Specimen Temperature.....	30
2.3.3.1.2 Grain Boundary Temperature.....	34
2.3.3.2 Microstructure and Grain-growth	35
2.3.3.3 Electrical Conductivity.....	37

2.3.4	Widely Suggested Mechanism.....	40
2.3.5	Development in Flash-sintering/Experiments	41
2.3.5.1	Flash-sintering of Multilayer.....	41
2.3.5.2	Flash-sintering of Composite.....	42
2.3.5.3	Sintering of circular SOFC cell.....	43
2.4	Solid Oxide Fuel Cell	43
2.5	Manganese Cobaltite.....	45
2.5.1	Application as Interconnect Coating	45
2.5.2	Crystal Structure and Electrical Conductivity.....	47
2.6	(La, Sr)(Co, Fe)O₃.....	48
2.6.1	Application as SOFC cathode.....	48
2.6.2	Crystal Structure and Electrical Conductivity.....	50

Chapter III

Experimental Methods: Materials, Equipments and Characteriza-

tions.....		52
3.1	Materials.....	52
3.1.1	Manganese Cobaltite and (La, Sr)(Co, Fe)O ₃ Powders.....	52
3.1.2	Binder.....	54
3.2	Sample Preparation.....	54
3.3	Flash-sintering Experiment.....	55
3.3.1	Experimental-arrangement.....	55
3.3.2	Power Supply: Sorensen XG6025.....	57
3.3.3	Multimeters: Keithley 2000 and 2100 Digital Multimeter.....	57
3.3.4	Pyrometer.....	57
3.3.5	Data Collection.....	58
3.3.5.1	Interface environment and language.....	58
3.3.5.2	Data Acquisition Hardware used.....	58
3.4	Sample Characterization Techniques.....	59
3.4.1	Dilatometry	59
3.4.2	X-ray Diffractometry.....	59
3.4.2.1	Calculation of amount of phase.....	60
3.4.3	Scanning Electron Microscopy.....	61
3.4.4	Electrical Conductivity.....	62
3.4.5	Thermo-gravimetry (TG)/Differential Thermal Analyzer (DTA)..	63

Chapter IV

Results and Discussions	65
4.1 Flash-sintering of $MnCo_2O_4$	65
4.1.1 Flash-sintering	65
4.1.1.1 Power Dissipation and Shrinkage.....	65
4.1.1.2 Relation of flash-parameter with Density.....	67
4.1.1.3 Specimen Temperature.....	68
4.1.2 Microstructure Evolution	70
4.1.3 Spinel Phase-stability Analysis	74
4.1.4 Electrical conductivity	77
4.1.4.1 On green specimen: Maximum current under flash-effect of different electric field.....	78
4.1.4.2 Effect of sintering temperature on conductivity.....	78
4.1.4.3 On dense specimen.....	80
4.1.4.3.1 Conductivity versus Electric field.....	80
4.1.4.3.2 Conductivity versus Temperature.....	82
4.1.4.3.3 Role of thermal effect/Joule heating.....	84
4.1.4.3.4 Hysteretic behavior.....	86
4.1.5 Discussion	88
4.1.5.1 Electric field dependent Conductivity: Literature review.....	88
4.1.5.2 Flash-sintering Mechanism.....	91
4.1.6 Summary	94
4.2 Flash-sintering of LSCF	96
4.2.1 Flash-sintering	96
4.2.1.1 Power Dissipation and Shrinkage.....	96
4.2.1.2 Specimen Temperature.....	98
4.2.1.3 Comparison with $MnCo_2O_4$	99
4.2.1.4 Importance of Specimen Temperature and Electric field.....	100
4.2.2 Microstructure Evolution	101
4.2.3 Phase stability	103
4.2.4 Electrical Conductivity	104
4.2.4.1 On Green Specimen.....	104
4.2.4.2 On Dense Specimen.....	106
4.2.4.2.1 Conductivity versus Electric field.....	106

4.2.4.2.2	Conductivity versus Temperature.....	108
4.2.4.2.3	Comparison with MnCo ₂ O ₄	111
4.2.5	Discussion.....	113
4.2.5.1	Flash-sintering Mechanism.....	113
4.2.5.2	Role of Reduction reaction: Correlation with MnCo ₂ O ₄	115
4.2.5.3	Comparison with Reported System.....	117
4.2.6	Summary.....	118
4.3	Flash-sintering of LSCF/GDC Composite.....	120
4.3.1	Flash-sintering.....	120
4.3.1.1	Power dissipation.....	120
4.3.2	Microstructure evolution.....	123
4.3.3	Phase-Compatibility.....	125
4.3.4	Electrical conductivity.....	126
4.3.4.1	Conductivity versus temperature.....	126
4.3.4.2	Conductivity versus electric field.....	127
4.3.5	Summary.....	128

Chapter V

Conclusion and Future Perspectives.....	129
------------------------------------------------	------------

References	135
-------------------------	------------

Curriculum Vitae.....	148
------------------------------	------------

Acknowledgements.....	151
------------------------------	------------

Chapter I

Introduction

Ceramic materials have become immensely popular in the modern time for their 'wide range' of 'tailorable' properties [1–4]. These are backbone of many industrial/manufacturing/household/transportation /energy areas for their technological applications [5]. This class of ceramic, separated from traditional ones, is distinguishably honored as advanced ceramics and became prominent in the 20th century when the materials systems turned more purified, and different compounds and processes were developed for structural and electronic applications [6]. This new class of ceramics is renowned for their high chemical purity, careful processing and functional properties [6]. According to their properties and applications advanced ceramics are broadly categorized into structural, electro- and bio-ceramics. About 90% of present ceramic use relies on their insulating, dielectric, piezoelectric, magnetic, optical, and lately, superconducting properties which led their use in electronic and electrical applications, these are referred as electroceramics [6]. Their applications include the piezoelectric lead zirconate titanate (PZT) elements in telephones and autofocus cameras, capacitors made of barium titanate in televisions, radios and almost all the electronic equipment, the microwave dielectric ceramics used in highly selective filters for cellular phones and satellite communication systems [6]. Fuel cells utilize zirconia as solid electrolyte [7], rare earth and transition metal based oxide ceramics for electrical or electrochemical applications [8,9]. The other 10% of ceramics use constitutes the structural ceramics in which the mechanical properties such as strength, modulus, toughness, wear resistance, hardness etc. are of primary interest. For example, amongst oxides, alumina are extensively in demand for its hardness, inertness and in high temperature application as refractories [10], zirconia for thermal barrier coating [11,12]. Non-oxides, silicon carbide and tungsten carbide are first choice for cutting and abrasive tools for its hardness and wear resistance properties [13]. Also, these are well used as heating elements for its high melting temperature. Ceramics has also gained attention for bio-applications where these are used inside the human body as hip and bone transplants, as supports for directed delivery

and as components in implant devices such as pace makers. Their biocompatibility and adequate mechanical strength makes some ceramics such as zirconia [14], hydroxylapatite [15], β -tricalcium phosphate [16,17] the ideal materials for these applications.

For any application, ceramic powders are first consolidated in the desired shape to produce a "green body". It is usually done by applying a pressure (150-200 MPa) to reach adequate density, of about 50-60%, for handling. To convert into useful structure, the green body is fired between 700-1700°C depending upon the ceramic, which causes a drastic reduction in porosity and makes the structure strong. The material/sintering is controlled and manipulated in order to reach desired properties.

Ceramics find one essential application in solid oxide fuel cells (SOFC) [18], where different layers of oxide-ceramics with different structural, electrical properties are arranged together to generate power by an electrochemical reaction [19]. Engineered-sintering of layers for selective/specific growth of microstructures is the key to create an efficient cell. In a general sense, high temperature processing of ceramics, renders issues on its processing in terms of time and cost (of equipments and environment); zirconia (8YSZ) which is widely accepted as SOFC electrolyte demands 1400°C for full densification. High temperature, sometimes, is an issue if material or its environment (in multilayer or composite) is sensitive to temperature. For example, electrolyte in SOFC should be fully-dense whereas the adjacent cathode and anode layers need to be porous. Therefore, materials demand selective treatment; sintering of layers with different requirements is a challenge. In other case, SOFC interconnect ceramic coating should be without open porosity but the materials sintering is restricted to 800°C for metal usage, this temperature is very low for adequate densification. Moreover, some high temperature reactions are undesirable, for example reduction of MnCo_2O_4 phase decreases its conductivity thereby degrading its electrical properties for coating application in SOFC [9].

The discovery of flash-sintering techniques provides a solution to many of such sintering issues. Flash-sintering is an electric field assisted sintering technique which

can produce dense/porous (as per requirement) samples in a couple of seconds and limited temperatures; 8YSZ is flash-sintered to full density in less than 5 s [20], without requiring 'any' higher temperature [21]. Shorter time-temperature processing may help to control or completely eliminate the undesirable reactions of high temperature [22] and can also lead to reduced sintering stresses and improved interfaces in SOFC multilayer development. Also, there can be selective flash-sintering effect depending upon the conductivity of materials [23]. Moreover, the technique allows lesser use of processing equipments and thereby lesser production of harmful or unwanted waste. The electrolyte, interconnect coating, composite anode (NiO/YSZ) materials of SOFC technology has been reported to be flash-sintered with requisite properties in a flash of time [23]. The reason of such fastness is not totally understood, though understanding the mechanism is crucial in controlling the properties. The conductivity based flash-sintering is mostly reported and discussed on weakly conducting materials like YSZ, MgO-doped alumina etc [20,24–26]. The present work moves to the other end and deals with the flash-sintering of electrically conductive ceramics, MnCo_2O_4 and $(\text{La}, \text{Sr})(\text{Co}, \text{Fe})\text{O}_3$ which are candidate materials for interconnect coating and cathode in SOFC, respectively. These are also prominent in other applications for their high electrical conductivity and oxygen reduction property. These materials are at a large gap in conductivity among the already reported materials in flash-sintering applications. The possibility of flash-sintering LSCF/GDC- $\text{Gd}_{0.1}\text{Ce}_{0.9}\text{O}_2$ composites containing different amounts of GDC is also investigated. This composite is considered as more promising for cathode than pure LSCF phase. The aim of the work is to analyze the flash-sintering behavior and mechanism in order to better control the microstructure and, therefore, the properties under fairly new sintering method.

The flash-sintering effect in a sample occurs when applied electric field is greater than a certain threshold and is suitably paired with a temperature. The effect starts with unusual rapid increase in the conductivity and heating by Joule effect. Thereafter, sample shrinks in an instantaneous manner. All these events occur within less than a minute. Initially, this fast sintering was thought to be due to rapid thermally-driven-diffusion effect. Nevertheless, under rapid heating as in flash-sintering, the

kinetic factor restricts the rate of ionic diffusion and, therefore, to achieve a particular degree of sintering significantly higher temperature is required [21]. The analysis of temperatures in flash-sintering revealed that rapid diffusion could not be the only effect [21]. The retarded grain growth, occurring as a result of fast heating, is almost ruled out by the observation of similar/increased grain size in zirconia and MnCo_2O_4 compared to that of conventionally produced samples [22,27]. Paired-defect formation under electric field is the most discussed theory of flash-sintering as this allows to explain both the increase in conductivity and the geometrical shrinkage [24,28]. However, there is no final confirmation or visualization of such argument. How do materials with different conductivities-mechanisms and different compositions, oxide or non-oxides undergo similar kind of flash-effect is still an open question. And although it is related to defects formation, more detailed analyses are required about conductivity and defect structure of materials in order to construct a robust background for flash-sintering of materials. Therefore, a part of the research work regarding flash-sintering is dedicated to understand its causes and it is one of the prime concerns of the present work.

Manganese cobalt oxide (MnCo_2O_4) is the most conductive material from the family of ceramic materials that have been densified using flash-sintering [10]. The high conductivity of the spinel made it suitable for application as interconnect-coating in solid oxide fuel cells (SOFC) [29,30]. The purpose of using MnCo_2O_4 as a coating is to maintain the conductivity of the interconnect steel along with protecting it from oxidation [15] and the cell from Cr-poisoning [31,32] at high temperature. The SOFC demands dense coating for interconnects which should not possess open porosity. On the other hand MnCo_2O_4 sintering demands temperatures as high as 850-1300°C [9] which are not sustainable for Crofer steel. Several hours of sintering at low temperature are responsible for the growth of chromia layer, which increases the resistance of the stack [30,33,34]. Flash-sintering is a promising approach in such temperature sensitive application for its 'very low time and lower temperature' demand. The ability of flash-sintering of Mn-Co oxide is reported [27]. The treatment without current control produced very high power dissipation. It is not clear if such high values are the necessary requirement for sintering. The unusual fastness in

temperature-increase during flash-sintering can cause the mechanical fracture of the ceramic specimen. Therefore, the minimum of parameters (power dissipation in terms of electric field and current density) are required to estimate in order to better control the processing of spinel oxide. The other issue with the sintering of MnCo_2O_4 is related to its phase stability at high temperature [9]. Conventional sintering leads to the formation of secondary phases which subsequently results in a decreased conductivity [9]. Thereby, it diminishes the role of MnCo_2O_4 which is preferably used for its higher conductivity in SOFC and as a conducting phase for mixed ionic-electronically conductive (MIEC) application [9]. Because of this reason, in practical applications, an optimal value for sintering temperature and time are chosen in order to achieve the optimal mechanical and electrical properties [19]. The drastically reduced time and lower temperature typical for flash-sintering are expected to be helpful to obtain the desired spinel phase structure of MnCo_2O_4 . Moreover, it will also be useful to analyze the correlation between sintering and stability of spinel phase during flash-sintering.

$\text{La}_{1-x}\text{Sr}_x\text{Co}_{1-y}\text{Fe}_y\text{O}_3$ (LSCF), which makes the other part of the thesis, is an electrically conductive material whose conductivity, in a part, is based on the same polaron-hopping mechanism as found in MnCo_2O_4 . LSCF a mixed oxide is developed for cathodic application in SOFC from parent LaFeO_3 and LaCoO_3 oxides which are well known compounds for their electrochemical properties and applications [35,36]. A particular composition, $\text{La}_{0.6}\text{Sr}_{0.4}\text{Co}_{0.2}\text{Fe}_{0.8}\text{O}_4$ (LSCF), is specially chosen for its good high electronic and ionic conductivity [36]. As a cathode, it facilitates oxygen reduction and transportation to the adjacent electrolyte through the porous structure. In the present SOFC scenario (in anode or electrolyte supported configuration with 8YSZ electrolyte), the cathode is generally sintered on the electrolyte at the later/final stage of the cell production in order to preserve the porosity and to develop the requisite properties [37]. During sintering, even at temperature lower than 900°C , LSCF forms a weakly conducting phase at the YSZ/LSCF interface which is highly undesirable [38]. In order to overcome such sintering issue, Gd doped ceria (GDC) barrier layer is usually inserted between the two since LSCF was found to be compatible with doped ceria although also YSZ-GDC sintering is not exempt from problems [39].

Without adding structural complication, flash-sintering of LSCF is promising for developing YSZ/LSCF layer since sintering for few seconds can result in improved interface properties. An additional interest regards the possibility of flash-sintering very high electrical conductivity (250-330 S/cm at 600-800°C [36]) material like LSCF, which possesses conductivity 3-4 times larger than MnCo_2O_4 [9] and more than two orders from others [25,40]. This can increase the knowledge of the still rather obscure electrically-driven flash-sintering phenomenon. In addition, LSCF as like MnCo_2O_4 contains transition metal cations and its conductivity, in part, is controlled by similar hopping activity [36,41] thus allowing a comparison between the two material systems flash-effect and sintering behavior. Therefore, flash-sintering results of LSCF are, here, compared with those of MnCo_2O_4 in order to provide a more general understanding of flash sintering phenomenon which would be helpful in understanding and controlling the material properties.

In the light of the discussed conventional sintering issues for MnCo_2O_4 and LSCF, the novel flash-sintering method is considered and investigated in order to resolve them. The main objectives of the present work are:

- to estimate the sintering parameters, e.g. electric field, current density, temperature to deal with in order to control the microstructure (grain growth, density/porosity etc) and phase stability properties;
- to analyze sintering behavior in terms of specimen temperature for understanding the role of electric field and temperature in flash-sintering;
- to analyze the electrical conductivity under electric field/temperature in order to understand the flash-sintering-effect;
- to compare the results of electric field assisted flash-sintering and electrical conductivity of the two materials in order to present a rather general understanding of the effect and the mechanism.

The flash-sintering on green specimen and electrical conductivity behavior on dense specimen is experimentally studied under different electric fields. The results are compared with those collected under conventional conditions. On the basis of the

results an attempt is made to understand the mechanisms involved in the flash-sintering of the materials. Finally, the proposed mechanism is compared to propose a more general physical model for describing the flash-sintering phenomenon.

Chapter II

Background and Literature Review

2.1 Sintering of Ceramic Materials

Sintering is processing of powders in order to produce objects, of desired (geometrical, mechanical, electrical etc) properties. Sintering occurs through atomistic diffusion, and is achieved by the heat treatment of powder compacts to elevated temperatures, usually at $T, T_m > T > 0.5 T_m$, where diffusional mass transport is appreciable. Figure 2.1 shows the four steps involved in the formation process via sintering, these are 1) physical touching of particles via building powder compact, at this stage structure is termed as green body, 2) formation of sharply concave necks between individual particles which is the onset of increase of the mechanical strength of the structure and the process is often termed as pre-sintering, 3) evolution of necks and formation of grain boundaries and interconnected pores and 4) the last, pore removal and grain growth. Successful sintering usually results in a dense polycrystalline solid. Sintering can proceed only locally (i.e. at contact point of grains), without any appreciable change in the average overall density of a powder compact. The last three steps of Fig. 2.1 define stages of sintering in terms of shrinkage level namely initial (<10%), intermediate (~95%) and final stage which results to isolation of pores, elimination of porosity via grain growth.

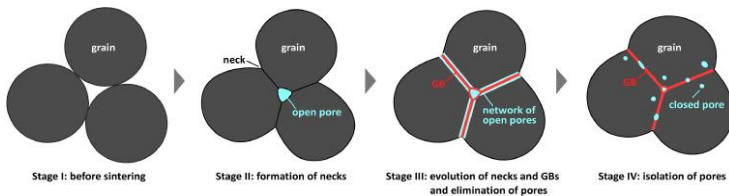


Figure 2.1: Three particle model for showing different stages of sintering [42]

From the energy point of view, sintering is a natural process where material-system tries to reduce its free energy due to elimination of internal surface area associated with the pores. Therefore, surface curvature of particles and an externally

applied pressure become driving force for sintering, and on the variation of these, sintering can occur at faster or slower rate [43,44]. Additionally, occurrence of a chemical reaction also drives the sintering process [4,5]. E.g. sintering occurs during the reaction between silicon and carbon in the formation of SiC; it is attributed by exothermic heat released during the reaction. Such kind of reaction sintering can lower the processing temperature of SiC to 1400-1500°C [46] compared to 1700-1800°C of hot pressing method. An schematic of sintering processes related to three driving forces along with their energy equations, which move towards minimization during sintering, are shown in Fig. 2.2,

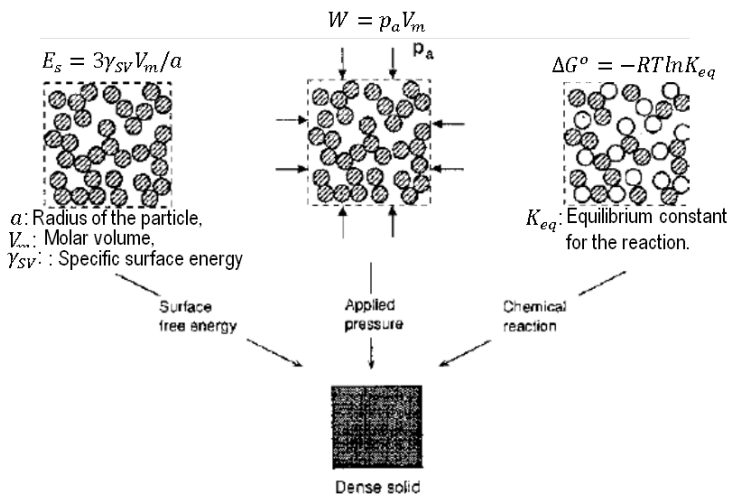


Figure 2.2: Schematic diagram showing three main driving forces of sintering [47]

2.1.1 Sintering Mechanism

Mechanism in the context of sintering simply describes the way or path matter can move through for providing or controlling densification. Under the mentioned forces, in the process of minimization of energy, ions/particles move through structural/crystal defects which are always available in a real system in the form of surface, grain boundary, point defects etc. Depending on existence of various defects there are six possible diffusion paths in a polycrystalline material, as depicted in Fig.

2.3, through which matter can move to the particle necks for providing inter-particle connection at the first, and densification at later stage. These are,

- 1) Surface diffusion, from surface, via surface,
- 2) Lattice diffusion, from surface, via the lattice,
- 3) Vapor transport, from surface, via the evaporation,
- 4) Grain boundary diffusion, from and via grain boundary,
- 5) Lattice diffusion, from grain boundary via the lattice, and
- 6) Plastic flow, dislocation motion

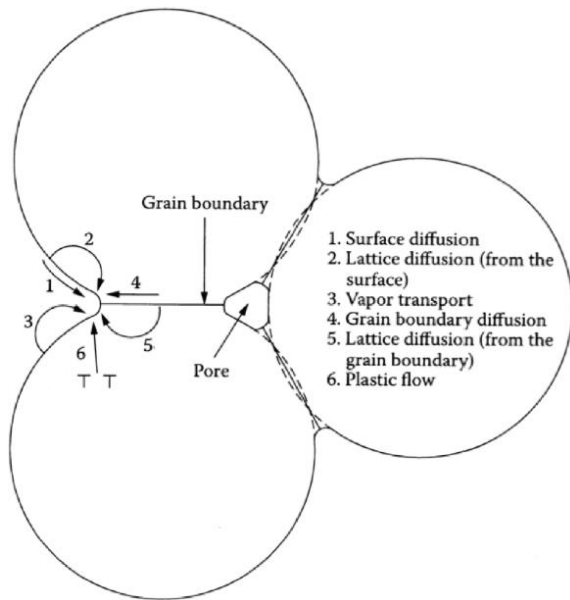


Figure 2.3: Various diffusion paths [47]

Among these possibilities, diffusions numbered by 4 and 5, when occur, decrease distance between particles resulting compaction; such diffusion processes thereby are termed as densifying-mechanisms. Others numbered by 1, 2 and 3 which do not involve with decreasing distance between particles are termed as non-densifying mechanisms; they are important for that even they do not cause densification, they play a major role in controlling the densifying-diffusion processes.

2.1.2 Grain growth and Coarsening

Grain growth, refers to the increase in the grain size, like sintering is a natural process which occurs for the reduction in free energy related to the total grain boundary area. Conversely, coarsening is a word to describe the process of grain growth coupled with pore size. Many engineering properties of materials are dependent on the grain size, e.g the dielectric constant of BaTiO₃ capacitors is found to increase with decreasing grain size down to 1 μm while the fracture strength of many ceramics is found to increase by decreasing size as $1/G^{1/2}$, where G represents grain size. Therefore, the materials should be processed in controlled way in order to achieve desired grain microstructure. The grain growth process also affects the densification rate and final density of materials. At a given temperature and density, the dependence of densification rate on the grain size is given as [47],

$$\frac{1}{\rho} \frac{d\rho}{dt} = \frac{K}{G^m} \quad (2.1)$$

Where K is a temperature dependent constant, the exponent $m = 3$ for lattice diffusion, and $m = 4$ for grain boundary diffusion. The rapid diffusion for sintering requires the diffusion distance to be small, thus requiring smaller grains. Rapid grain growth cause reduction in densification rate. And abnormal grain growth results to the trapped pores which are very difficult to remove. Coarsening refers to the abnormal grain growth where one grain grow at the expense of other one, resulting into a large grain size distribution. In order to achieve finer grain size microstructure with high density mostly, following things can be done:

- If a material has high activation energy for densification, the high heating rate can skip the step of intensive grain growth of lower temperatures.
- Addition of dopants also seen to control the grain, as in one possibility it segregates at grain boundary and reduce the grain boundary mobility. Dopant may also affect the densification rate.

- Sintering with external pressure usually increases rate of densification, resulting to smaller grains.

2.1.3 Sintering Analysis

In the age of novel processing and characterization techniques, materials for any applications are often produced in an engineered way where the desired properties are nicely put or grown by controlling them at smaller scales, at its microstructure. In order to develop a material with high performance, it is important to understand the relationship between particle structure and the mechanism of material transport, and the sintering control-factors. Below is discussed briefly an example of determining the sintering activation energy and the sintering-mechanism with the help of 3YSZ (3YS) and Al₂O₃ doped-3YSZ (3YSE) sintering data [48].

2.1.3.1 Sintering Activation Energy

Constant Rate of Heating (CRH) Analysis

Under constant rates of heating (CRH), the relation related to sintering valid for initial stage (~initial 3.5% of fractional shrinkage) is given for grain boundary (GBD) and volume diffusions (VD) separately as [48],

$$\frac{d\left(\frac{\Delta L}{L_0}\right)}{dT} \cong \left(\frac{2.14\gamma\Omega b D_{0B}RT}{ka^4cQ}\right)^{\frac{1}{3}} \left(\frac{Q}{3RT^2}\right) \times \exp\left(-\frac{Q}{3RT}\right) \quad (2.2)$$

$$\frac{d\left(\frac{\Delta L}{L_0}\right)}{dT} \cong \left(\frac{5.34\gamma\Omega D_{0V}RT}{ka^3cQ}\right)^{\frac{1}{2}} \left(\frac{Q}{2RT^2}\right) \times \exp\left(-\frac{Q}{2RT}\right) \quad (2.3)$$

where ΔL is the change in the length of the specimen, L_0 the initial length of the specimen, γ the surface energy, Ω the atomic volume, T the absolute temperature, k the Boltzmann's constant, and a the particle radius, c is the heating rate (dT/dt), D_{0B} and D_{0V} represent constant terms that are given as, $bD_B = D_{0B} \exp\left(-\frac{Q}{RT}\right)$ and $D_{BV} = D_{0V} \exp\left(-\frac{Q}{RT}\right)$, bD_B the grain boundary diffusion coefficient, b is the

effective grain-boundary width, D_V the volume diffusion coefficient, Q is the activation energy for respective mechanisms.

Another equation is developed where temperature, grain size and density dependent quantities are separated into different terms as [48],

$$\ln \left[T \left(\frac{dT}{dt} \right) \left(\frac{d\rho}{dT} \right) \right] = -\frac{Q}{RT} + \alpha_{B,V} \quad (2.4)$$

where $\alpha_{B,V} = \ln[f(\rho)] + \ln \frac{C\gamma V^{2/3}}{R} - N \ln d$

Here, ρ is the density, $f(\rho)$ a function of density, C a constant, V the molar volume, d the grain size, and N the grain size power law ($N = 3$ for lattice diffusion, $N = 4$: grain boundary diffusion). In order to determine the sintering activation energy, shrinkage profile of green samples pressed under same conditions is recorded at different heating rates. Assuming isotropic shrinkage, density $\rho(T)$ at a given temperature T is calculated by the following equation,

$$\rho(T) = \left(\frac{L_f}{L(T)} \right)^3 \rho_f \quad (2.5)$$

where L_f and $L(T)$ are the final length and the length at temperature T of the specimen, respectively. ρ_f indicates the final density that can be measured by the Archimedes method. For different heating rates, the T and $d\rho/dT$ values at the same relative density (at the fractional shrinkages of <4%, which satisfy the condition of sintering without grain growth) is determined, and their values are plotted in Arrhenius-type plot of $T(dT/dt)(d\rho/dT)$ against $1/T$. The activation energy is determined from the slope of the straight line at each relative density (Eq. 2.4). For example at a relative density of 50%, the activation energies of 3YS and 3YSE is reported to have similar values, and on exceeding 50%, activation energies of 3YSE were lower than those of 3YS. Averaging the activation energies of 3YS and 3YSE determined at the relative density range of 50–54% consecutively, it was seen that the Q value of 3YSE was smaller than that of 3YS. The value of $\alpha_{B,V}$ term, which is related to surface energy for constant density and grain size, is determined from the intercept of the straight line in the Fig. 2.4(a). The low $\alpha_{B,V}$ value reported for 3YSE sugg-

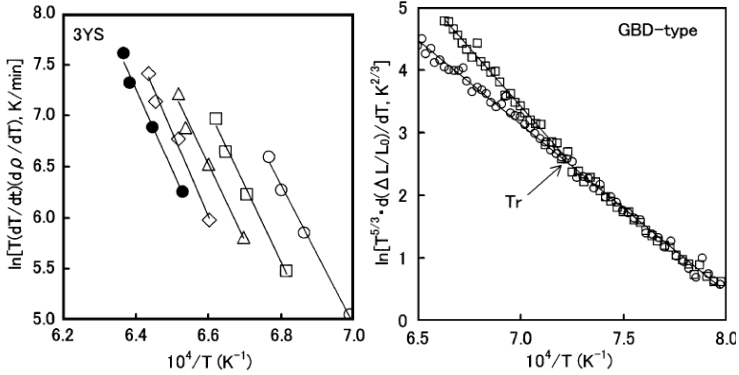


Figure 2.4: a) Arrhenius type plot for the estimate of activation energy of sintering, (○),(□), (Δ), (◇) and (●) represent 50%, 51%, 52%, 53 and 54% relative densities respectively b) Grain boundary diffusion type plots of 3YSZ (○) and Al₂O₃ doped 3YSZ (□) [48].

est that the surface energy and average activation energy of 3YSZ powder is reduced by including a small amount of Al₂O₃.

2.1.3.2 Sintering Mechanism: Diffusion Parameters

Sintering mechanism is determined using Eqs. 2.2 and 2.3, from the slope S_2 of the plot of $\ln[T^{5/3}d(\Delta L/L_0)/dT]$ or $\ln[T^{3/2}d(\Delta L/L_0)/dT]$ versus $1/T$ by assuming GBD or VD; the m value is calculated using Q and S_2 by the simplified relation of $Q/m = -RS_2$ where $m = 3$ for GBD and $m = 2$ for VD. In the example, for 3YS both the relations for GBD and VD were linear and m -value was close to 3 suggesting dominance of GBD. For 3YSE, the relation deviated in response to Al₂O₃ addition from linear starting from 1110°C (corresponding to a relative density of 49%); its m -value was close to 2 indicating VD.

Isothermal Shrinkage Analysis

The above analysis is validated using isothermal shrinkage measurements. The sintering rate equation of isothermal shrinkage at the initial sintering is as follows,

$$\left(\frac{\Delta L}{L_0}\right) = \left(\frac{K\gamma\Omega D}{kT\alpha^p}\right)^n t^n \quad (2.6)$$

$$\log \left(\frac{\Delta L}{L_0} \right) = n \log t + n \log \left(\frac{K \gamma \Omega D}{k T a^p} \right) \quad (2.7)$$

Where K is a numerical constant, D is the diffusion coefficient, p a constant, n the order depending on the diffusion mechanism. Equation is applicable to the fractional shrinkages of <4%, which satisfy the initial sintering condition. Using the isothermal shrinkage data, $\log \left(\frac{\Delta L}{L_0} \right)$ is plotted against $\log t$ and from the slope n value is determined. According to two sphere shrinkage model, n value for GBD and VD range between $n = 0.31-0.33$ and $0.40-0.50$, respectively. The n values of 3YS and 3YSE were 0.32 and 0.41, respectively. Compared with above n values, it was confirmed that the diffusion mechanism of 3YS and 3YSE were GBD and VD respectively.

2.1.4 Sintering Activation

Because of strong bonding forces, solid state diffusion is a slow process and requires elevated temperatures for its effective occurrence for sintering. For example processing of alumina requires at 1100-1700°C [24,49], zirconia 1100-1450°C [20], and this way, demands high temperature sustainable instruments and inert/vacuum environment leading to a large production costs. In order to overcome processing issues, often efforts are made to decrease the sintering temperature and/or time by increasing the sinter-ability of materials; such process is termed as sintering-activation. In addition to above mentioned factors, activated sintering is sometimes required based on material's specific application and environment. For example sintering of MnCo_2O_4 coating on metallic interconnects for solid oxide fuel cell application is restricted to lower temperatures [29,33,50]. In order to make a better compromise with time and temperature, the sintering is reaction-activated where spinel phase is first reduced to constituent oxides in reducing atmosphere and then is oxidized in air to form MnCo_2O_4 with improved connectivity and sintering of coating. Other example includes addition of gadolinium to ceria which not only increases its ionic conductivity but also causes sintering to happen at lower temperature [51]. Following from force and mechanism of sintering, the mass diffusions are accelerated in below mentioned two ways [52].

2.1.4.1 By increasing driving force

Changes in interfacial properties such as higher surface energy or lower grain boundary energies may induce higher driving forces. Milling [43], dopant addition [48,49,53], choosing controlled temperature-time profile [54], assistance of pressure [55] etc is usually employed to stimulate the sintering process.

2.1.4.2 By increasing sintering kinetics

In other scheme, apart from directly increasing the heating rate for increased kinetics [56], increase in defect concentration may also activate the diffusion process, thereby, sintering. Such scenario of enhanced sintering can be achieved by some physical treatment such as applying electric field accelerates the diffusion by Joule-heating [56] and can also cause increased defect concentration [28]. Similarly, some chemical treatment can do the same [57–59]. Addition of dopant also can serve for increasing the defect centers [48].

2.2 Assisted Sintering Techniques

Assisted sintering is used to enhance the conventional sintering process in order to reduce the sintering time and temperature. These techniques are enthusiastically accepted for ceramics which generally require very high processing temperatures. The method employs the assistance of external parameters such as pressure, electric field etc during conventional sintering. Brief descriptions of different assisted-sintering techniques are given in the following sections first briefing the traditional.

2.2.1 Un-assisted Conventional Sintering

Conventional-sintering is a free sintering of powder compact kept in a furnace which is heated with a constant rate, isothermal hold is given as per requirement. Sintering happens by the ionic-diffusion generally through defects when thermal energy is sufficiently available. Therefore, particle size, purity of powder, time, temperature, heating rate etc. control the sintering process.

2.2.2 Pressure Assisted Sintering

Sintering can be activated by applying a pressure, high enough to interact with or affect the contact pressure between particles. Such pressure enhances the densifying mechanism by increasing the driving force for the sintering, so the effect of the non-densifying mechanism is reduced. As a result, densification rate is enhanced greatly relative to the coarsening rate resulting in to the attainment of high density and fine grain size. Under high pressure, these factors lead to the reduction of sintering temperature as low as half of the melting point. Depending on the amount of applied pressure, assisted sintering is termed as hot pressing and sinter-forging (20-40 MPa) [60,61], hot iso-static pressing (200-300 MPa) [44] and high pressure assisted sintering (2-8 GPa) [62–65]. In hot pressing, the pressure is applied by uniaxial load on the powder compact placed in a die; sinterforging uses the same loading concept with the difference that it has lateral edges free which helps eliminate porosity and packing defects. In hot iso-static technique, pressure is applied isotropically by means of a gas which makes it a costly technique. High pressure system uses die-press concept, employing load over smaller area sample to produce high pressure. Sample is usually placed in a pressure transmitting medium such as Ar gas, In, Pb and NaCl [65] etc in order to homogenize the pressure. Heating, if required, is mostly provided by laser or electric current through graphite die depending upon the type of HP cell. The sample diameter in this case could be as small as 0.2 mm (in the range of 0.2-5 mm). Hot pressing, sinter-forging and high pressure is commonly used for simple shape samples. For complex shapes iso-static pressing is the option.

One nice usage of pressure assisted technique is in production of γ - phase of Al_2O_3 . The $\gamma\text{-Al}_2\text{O}_3$ is one of the transition aluminas widely used in technology, in the form of powder or thin film, as adsorbents, catalysts or catalysts carriers, coatings, and soft abrasives because of their fine particle size, high surface area, and catalytic activity [66]. It is difficult to produce due to phase transformation sequences that occur during the conventional sintering process at ambient pressure: $\gamma(750^\circ\text{C}) \rightarrow$

$\delta(900^\circ\text{C}) \rightarrow \theta(> 1000^\circ\text{C}) \rightarrow \alpha$. The use of the HP technique provides the means to overcome this difficulty.

The effect of HP assistance (5-7 GPa for 1-15 min) on microstructure of alumina sample is reported [63]. An intensive grain coarsening is observed in 15 min of time, for change of pressure from 5 to 7 GPa. Conversely, under 7 GPa decreasing time from 15 to 1 min showed homogeneously grown microstructure with smaller grains. Alumina samples produced at 1000°C confirmed the strong effect of high pressure in controlling the microstructure and, significant difference in processing parameters [63].

2.2.3 Electromagnetic-field (Microwave/UV) Assisted Sintering

In electromagnetic field such as microwave-assisted sintering, energy is directly transferred to the material through the interaction of microwaves with molecules. Such interaction in dielectric materials gives rise to the formation of electric dipoles which in response to variations of electric field change their orientation rapidly and result to the heating. It is unlike to the energy in conventional thermal processing where it is transferred to the materials through convection, conduction, and radiation of heat from the surface. Microwave processing can achieve the rapid and uniform heating of materials, and can also be utilized for the selective heating. The molecular structure affects the ability of microwaves to interact with materials, so, if a sample is combined with several materials having different dielectric properties, the microwaves will selectively couple with a high loss material. Therefore, it may be possible to process multiple phase materials with new or unique micro structures by microwave processing. A dense material with improved microstructure of smaller grain size can be obtained by microwave processing in a much shorter time due to higher heating rate and shorter sintering cycles compared to the conventional processes.

Sintering set-up mostly employs commonly used microwave oven operating at frequency of 2.45 GHz with typical power of 500 W to 1.5 kW. Sample is usually placed on a microwave absorber to improve the heating of the materials such as alumina, zircon which are poor microwave absorber at room temperature. In order to

record specimen temperature, a platinum/rhodium thermocouple is inserted in the chamber, encased in metal sheathes and designed such that they do not interact with the microwave field; in other scheme, a pyrometer is focused directly over the sample for temperature.

The effectiveness of microwave for sintering is shown via the microstructure of aluminum borate samples sintered by microwave assistance [67]. Aluminum borate samples are shown to have straight morphologies with the average lengths ranging from 300–400 nm in conventional sintering and 2.5- 5 μm in microwave sintering, both with average diameters below 100 nm. The microwave samples retained the original morphology of the $\text{Al}_4\text{B}_2\text{O}_9$ nano-rods and is more homogeneously grown compared to conventional sample produced at the same sintering temperature; in the conventional sample, some of the rods have outgrowth morphology. The results showed potential of microwave heating in substantially accelerating the sintering process and allowing for highly densified solidification by eliminating the pores and increasing the shrinkage rate.

2.2.4 Electric field Assisted Sintering

2.2.4.1 High Electric-field Assisted (Electric discharge compaction-EDC) and High Current Assisted (spark plasma sintering-SPS)

In electric field assisted sintering, generally there are two parameters to work with, current and voltage or field. In some application, a very high voltage is used to draw heating by a single electrical discharge, and at other place, large current is used to generate sufficient energy.

High electric field assisted, EDC technique is mostly used for producing nano-crystalline bulk solid sample with densities close to theoretical [68]. Schematic of EDC setup is shown in Fig. 2.5(a). The principle of EDC is to discharge a high-voltage (up to 30 kV), high-density current (10 kA/cm^2) pulse (for less than 500 μs) from a capacitor bank through the powders under external pressure, resulting in a

temperature rise of more than 2500 K, instantaneously to weld nano-crystalline powders together. This discharge time is long enough for densification, yet too short for extensive grain growth. Advantages of the technique are short sintering time (less than one second), no need for controlled atmosphere even during sintering of highly reactive materials such as titanium, the ability to obtain nano-crystalline materials.

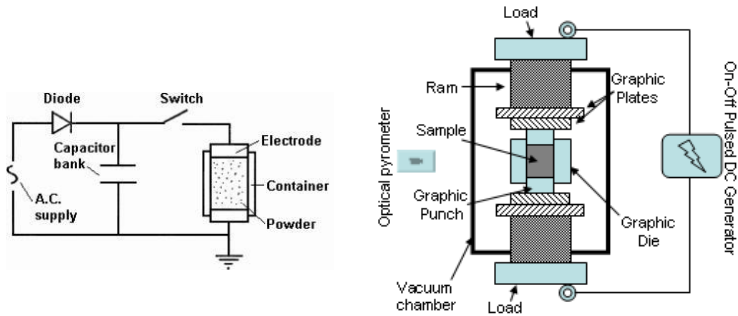


Figure 2.5: Schematic of a) electric discharge compaction and b) spark plasma sintering set-up

In other case, current is majorly used for providing heat for sintering/formation. The consolidation process mainly consists of two stages: an initial activation through the application of a voltage, and the subsequent heating and densification by using DC current. A typical heating for sintering is achieved by the application of a low voltage (approximately 10 V) and 600–1000 A current. The sintering in such case is suggested to occur by local Joule heating, melting or plasma formation at the particle-particle contacts. With the initial presumption of local plasma formation, the technique is better or also known as spark plasma sintering. However, till date, there is no conclusive evidence for the effect of a plasma generation/melting in SPS. The technique is more versatile as a range of materials, metal, ceramics and composites with conductive, non-conductive and insulating behaviors are shown treated using SPS. The clear benefit of SPS is the significant savings of time and energy and the ability to retain nanostructures as a result of fast heating. The equipment consists of a mechanical device capable of applying uniaxial pressure and electrical components to apply current and voltages. The powder materials are directly stacked without any additives between the die and punch on the sintering stage in the chamber between

the graphite electrodes. The pressure is usually limited to <100 MPa. The system is equipped with controlled environment. A rapid heating is achieved by applying and electrical discharge of typical values between 10-15 V and 1000A. The powders are mainly heated by Joule effect. This effect heats the conductive sample directly, but non conductive sample are heated up by heat transfer from die and plungers.

The effect of heating rate on Alumina samples produced by this technique is reported [69]. A high heating rate resulted into significantly smaller grains, as it did not allow surface diffusion to coarsen the grains at low temperature, it quickly takes the powder to higher temperature where sintering is predominant [69].

2.2.4.2 Flash and FAST Sintering

Flash-sintering is a branch of electric field assisted sintering observed with ceramic materials (so far) having semiconducting trend of conductivity. Specialty of in flash-sintering lies in that, the material undergoes a large conductivity change in a couple of seconds, subsequent Joule heating, and sintering in further few more seconds [22,70]. Such fast heating-sintering effect comes by the inherent property of

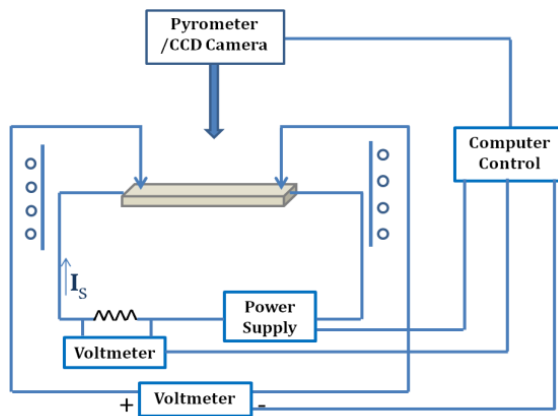


Figure 2.6: Schematic of flash-sintering set-up

materials when the applied field is greater than a threshold value and not forcefully because of high voltage electrical discharge as in EDC [71] or by a huge amount of

current as in SPS [52]. Therefore, the sintering effect, Joule heating or any other, if there, is developed all of a sudden by the property of material, at a right combination of electric field and temperature. For example, electrically conductive MnCo_2O_4 requires a minimum of (5 V/cm, 450°C) [22,27], weakly conductive 8YSZ needs (24-30 V/cm, 1000°C) [20,70] and insulating MgO-doped Al_2O_3 demands 500-750 V/cm [24]. If the field, lower than this threshold value is applied across the green sample,

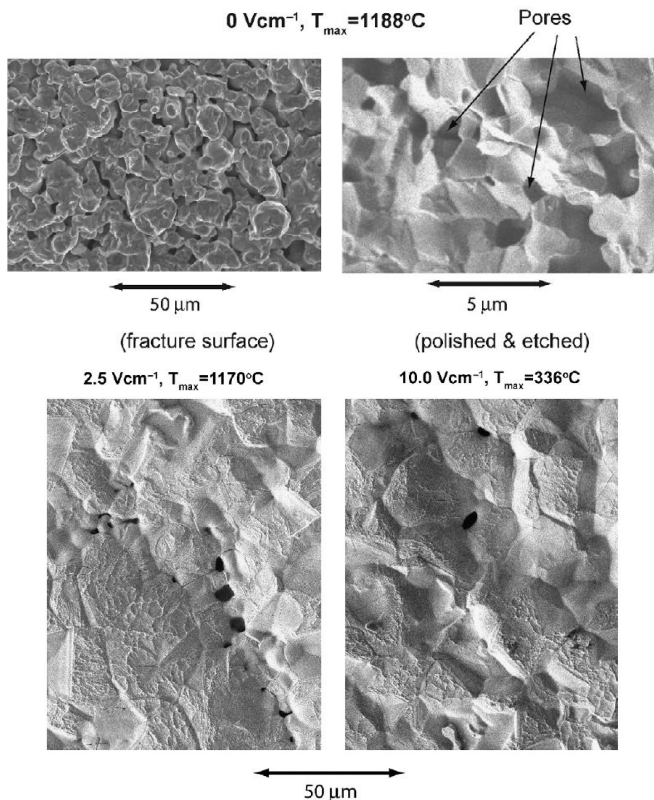


Figure 2.7: Microstructure of a) and b) conventionally, c) FA under 2.5 V/cm and d) flash-sintered under 10 V/cm MnCo_2O_4 samples [27]

gradually accelerated sintering but similar to conventional behavior is observed and such techniques is usually referred by FAST- field assisted sintering. In FAST, processing temperature is reduced by 100-200°C [20,24] and sintering time is of same

order whereas in flash-sintering, the processing temperature is reduced by more than 700-800°C and sintering time is of the order of seconds [20,22]. Figure 2.6 shows the schematic of experimental arrangement used for flash-sintering. Sintering is performed on free-standing sample which is held through two conducting electrodes in an electrical circuit which contains power supply and other measuring devices. A CCD camera or pyrometer is focused over sample to record shrinkage and specimen temperature respectively. The technique employs no pressure, but may need a small load for making proper electrical connection.

Figure 2.7 shows the microstructure of MnCo_2O_4 samples, sintered under 0, 2.5 and 10 V/cm [27]. Three values of electric field define three sintering techniques conventional, FAST and flash, which clearly reflect the significant differences in the processing temperatures required. In case of flash-sintering processing temperature is reduced by more than 800°C. In order to reach the same microstructure under 2.5 V/cm, temperature needs to reach up to 1180°C whereas for the same temperature of 1170-1180°C conventionally sintered sample is significantly porous. Such kind of observation for processing temperature is important for selective treatment/sintering in multilayer structures.

2.3 Flash-sintering: State of the Art

2.3.1 The method

The fascinating method of flash-sintering is first discovered during 2010 in yttria stabilized zirconia, 3YSZ, where shrinkage is shown to achieve almost instantly when the applied field was 60 V/cm and higher [72]. This sintering to full density is achieved in less than 5 s under constant field of 120 V/cm, at 850°C of furnace which was heated with a constant rate of 10°C/min. It is shown that for fields lower than 60 V/cm, the sintering is found accelerated but the order of time and temperature requires is not as significant as in flash-sintering. For example under 20 V/cm, in the same CRH experiment sintering completes at 1300°C, 100°C earlier than of conventional 1400°C; the same order of time is 10-15 min lesser [72]. Also, there are previous reports on accelerated sintering [72–76] under DC/AC electric field where the

effects are explained on the basis of retarded grain growth [73–75]. The unusual finding of flash-sintering in 3YSZ is explained by the local Joule heating at grain boundaries, which, on the one hand, promotes grain boundary diffusion (a kinetic effect), while at the same time restricts grain growth (a thermodynamic effect). The smaller grain size and the higher temperature at grain boundaries act synergistically to enhance the rate of sintering. The results pointed to have a bearing on spark plasma and microwave sintering. After this, another composition of zirconia, i.e. 8YSZ is examined under flash-sintering and observed to show the similar effect but under lower electric field and temperature for being more (ionically) conductive than 3YSZ [77].

Later on the method is tested over a number of ceramic materials, listed in Table. 2.1. It displays the threshold values (electric field, temperature) and the conductivity related information of materials. It shows conductivity dependent need of parameters for flash-sintering. The effect which starts with a rapid increase in the conductivity is observed on various types of conduction properties materials such as electronic/ionic, largely/weakly-conducting; all with a common feature that these have a tendency of increasing conductivity with temperature [20,25,27]. Most of them are non-stoichiometric oxides, with recent observation of the flash-sintering on non-oxide SiC [26].

Table 2.1: Flash-sintering parameters of materials along with their conductivity

Material	Threshold Field V/cm	Threshold Temperature °C
3YSZ [72]	30	1150
8YSZ [20]	60	1025
MnCo ₂ O ₄ [27]	5	450
MgO doped Al ₂ O ₃ [24]	500	1320
SrTiO ₃ [40]	500	900
GDC10 [78]	20	1100
SiC [26]	50	1670
TiO ₂ [25]	250	820
Hydroxyapatite	-	-
Gd- doped BaCeO ₃ [79]	-	-

2.3.2 Electrical and Sintering Behavior

2.3.2.1 Threshold Electric field, Temperature and Power dissipation

First data for flash-sintering is in the form of power dissipation and shrinkage against furnace temperature in constant rate of heating (CRH) experiment [20,22] and against time in isothermal experiment [80]. In the CRH experiment, a constant voltage is applied across the sample kept in a furnace which is heated with a constant rate. Electric field across and current density through the specimen is recorded.

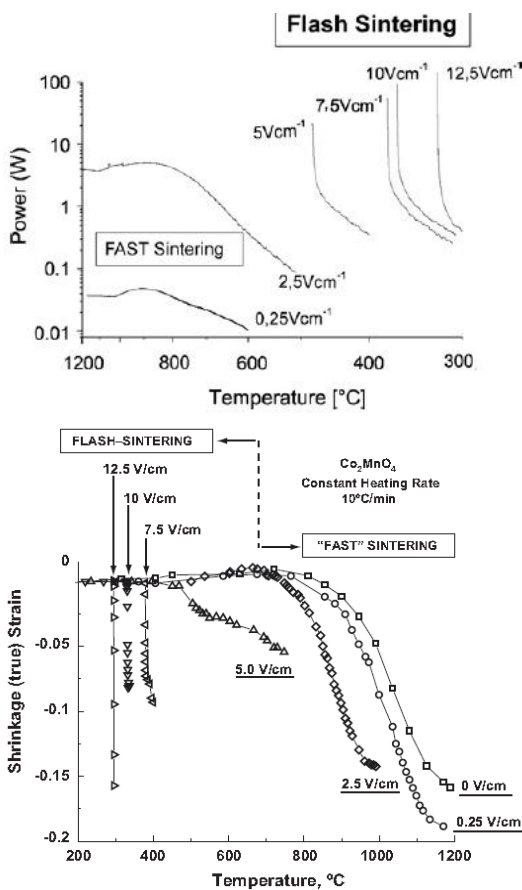


Figure 2.8: Power Dissipation and shrinkage as a function of furnace temperature during flash-sintering of MnCo_2O_4 [27]

Power dissipation is calculated from the multiplication of the two and is plotted against temperature which is manually noted from the furnace display bar or recorded automatically using thermocouple measurement device. Sintering, in free standing sample, is evaluated by linear shrinkage using a CCD camera. Such graphs for MnCo_2O_4 are shown in Fig. 2.8. The left figure shows initial smooth growth in power dissipation with temperature for gradual increase in the conductivity; at certain temperature, this increase becomes rapid giving sign of flash-sintering as shown in Fig. 2.8(b) by vertical lines. The graphs of power dissipation and shrinkage clearly differentiates two regimes of electric field effect, FAST where the changes are smooth, and other flash where changes are instant, observable by vertical line. The field and the temperature at the transition of these two behaviors are termed as threshold field and temperature for that material (mentioned in Table. 2.1). For each material depending on the conductivity, a particular combination of temperature and electric field is required to see flash-sintering. For example, YSZ is shown to be sintered under 60-150 V/cm, at 750-1100°C [20] whereas for MnCo_2O_4 the parameters are 7-12 V/cm with 250-450°C [27].

A nice work for the evaluation of critical parameters came by giving a mathematical relation between electric field and temperature [70]. In the work, Zirconia was

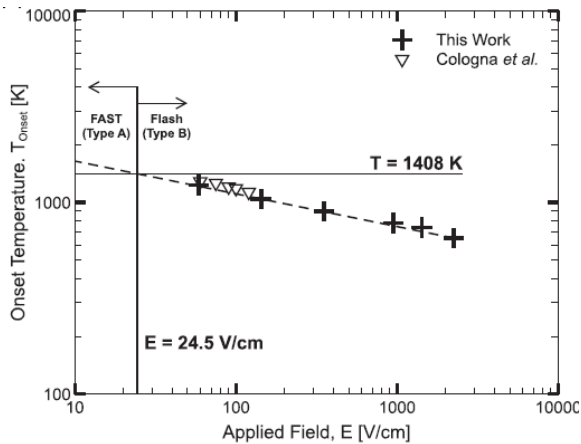


Figure 2.9: Log-log plot of onset temperature for flash-sintering as function of electric field [70]

sintered by applying electric fields ranging from 30 V/cm to 2.5 kV/cm and was plotted against onset temperature as shown in Fig. 2.9. The data was found in agreement from the previously reported results of smaller field values [20]. A relation of $T_{Onset} = 2440E^{-1/5.85}$ was developed using the fitting methods. Using the fitted curve, the FAST to flash transition field is determined graphically to be 24.5 V/cm which is close to the reported 30 V/cm [20]. This way acceptability and applicability of the proposed relation is confirmed.

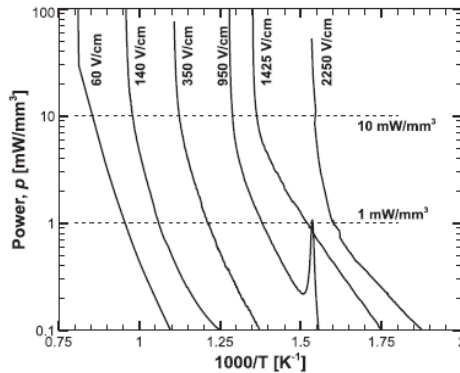


Figure 2.10: Arrhenius type plot of power dissipation with temperature showing threshold power level [70]

Apart from electric field and temperature, a threshold in the power dissipation is also observed. Sample enters into flash-effect at the development of certain power level. The value of this minimum power dissipation remains invariable with respect to the field. In Fig. 2.8(a) $MnCo_2O_4$ shows the flash effect at ~ 10 mW/mm³ for all the field values higher than threshold. In case of 8YSZ, almost similar value is observed for the threshold [77]. The invariability of such observation is strengthened when the electric field for YSZ was increased to 2.25 kV/cm from nominal 100-150 V/cm (Fig. 2.10) and for all the threshold power dissipation was found to be in the range of 1-10 mW/mm³ [70]. Such invariability is seen with different materials and was found not very different from that of each other, e.g. the threshold power dissipation of comparatively conducting $MnCo_2O_4$ [22,27] and insulating MgO doped alumina [24] lies close to 10 mW/mm³ only.

2.3.2.2 Importance of Current and Power dissipation

It is mentioned at several places that for the onset of fast-effect, electric field is important but for density, current is a more determining parameter. The importance of current density for shrinkage is shown in Fig. 2.11(a) for 3YSZ at a particular electric field of 100 V/cm, where a series of density level is produced upon systematically increasing the current density from 20-100 mA/mm² [80]. In the Fig. 2.11(b), the level of shrinkage is shown to increase or saturate with time under the same current densities. The two plots clearly suggest the importance of current in controlling the density which might be related with the specimen temperature.

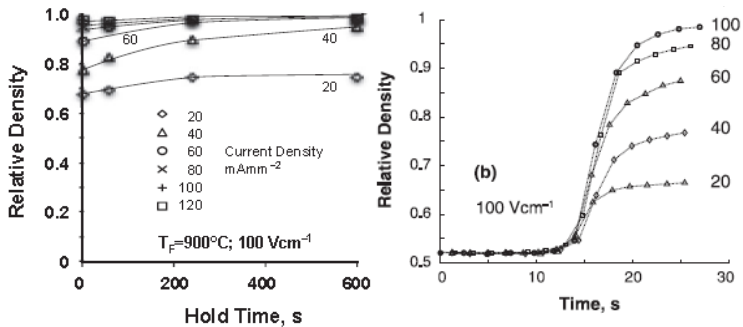


Figure 2.11: Plot of relative density as function of time for different current densities [80].

Table 2.2: The highest current and the corresponding voltage measured in the flash-sintering experiment of MnCo₂O₄ [27]

Applied Field V/cm	Maximum Current A/mm ²	Maximum Power Dissipation W
12.5	9.7	243
10	7.54	151
7.5	6.67	100
5.0	4.48	45
2.5	2.48	12
0.25	0.25	0.125

In another scenario, power dissipation is emphasized not to be as valuable as current density. In case of conducting samples, as for MnCo₂O₄ shown in Table 2.2 the power dissipation is reported to be very high which cannot account for the actual sintering temperatures (measured by pyrometer) if calculated from black body rela-

tion [22,27]. These experiments were performed without any control on current, but there is no report for excessive heating or melting of samples [27]. In case of 8YSZ, it is reported that after passing the critical power dissipation, current density becomes a more important factor in controlling the densification rather than power density [70]. Table 2.3 lists the power data for sample sintered under different electric field and utilizing two set of current densities, mA for 60-140 V/cm 650 and 120 mA for 350-2250 V/cm, over same sample dimension. Even with power densities as high as 5.2 W/mm³, shrinkage did not exceed 10%. However, samples sintered with smaller electric fields, but with higher current densities had shrinkages up to 28.1% despite the maximum power dissipation being only 257.7 mW/mm³. In other reports also, the importance of current is expressed by level of density calculation. As like electric field temperature and power dissipation which are important for onset of flash-sintering effect, a critical value of current density is required to ensure full sintering and plays an important role in matter transport.

Table 2.3: Applied electric field, onset temperature, linear shrinkage and maximum power dissipation of 8YSZ [70]

Applied Field V/cm	Onset Temperature °C	Linear Shrinkage %	Maximum Power Dissipation mW/mm ³
60	960	-28.1	257.7
140	768	-24.7	113.6
350	629	-11.8	827.1
950	508	-10.0	105.9
1425	467	-9.7	374.8
2250	390	-8.5	5285

These discussions were mostly based on sintering under constant electric field and varying temperature. Sintering experiment can be performed by working with parameters in other ways such as by keeping the temperature and voltage constant, or by keeping the temperature constant and increasing the voltage. In all such cases only the form of electric data will be different.

2.3.3 Flash-sintering Effect Analysis

The effect includes rapid increase in the conductivity represented by power dissipation data, Joule heating and thereby sintering close to full density in a very short

period of time. The possible reason for such fast sintering effect is suggested to be Joule heating at grain boundaries, Frenkel defect formation, space charge formation at the grain boundaries which can interact with external electric field etc. The following section will put forward different observations regarding such fast-effect.

2.3.3.1 Estimate of Local Temperature

2.3.3.1.1 Specimen Temperature

The flash-effect starts with sharp increase in the conductivity at remarkably low furnace temperature which causes to heat the sample up by Joule effect. Therefore, there are two kinds of temperature that needs to be reported, furnace and the local temperature while discussing flash-sintering-effect. The local specimen temperature is measured experimentally using a pyrometer or estimated using black body relation (eq. 1) from steady state power dissipation. A result of pyrometric measurement in flash-sintering experiment of zirconia has been shown in Fig. 2.12. It shows that the furnace temperature and the specimen temperature agree perfectly until the

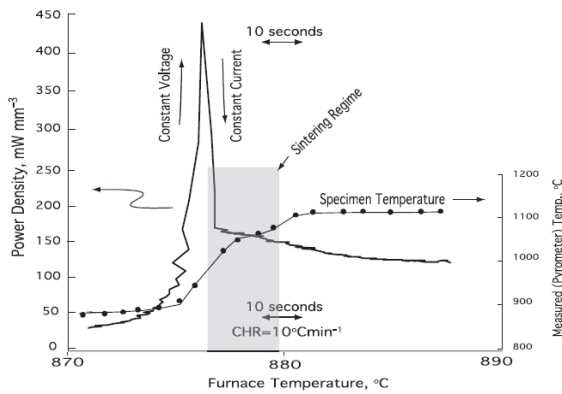


Figure 2.12: Power dissipation and specimen temperature as function of temperature [21].

onset of power surge. The peak like appearance of power dissipation is because power supply turned from voltage control to current control, such setting has been done to avoid thermal runaway. After the peak, the voltage starts dropping for any increase in the conductivity, so the power dissipation. Following power dissipation,

specimen temperature begins to overtake the furnace temperature, attains a steady state. The difference of the two temperatures is almost 200°C. Sintering for 8YSZ is reported to occur in the stabilization region of power dissipation and specimen temperature. The full sintering experiment does not take more than 10-20 s.

The specimen temperature is also estimated from the black body relation $E = \sigma T^4$, where E is the heat radiated from the body per unit area, $\sigma = 5.67 \times 10^{-8} \text{ W/m}^2 \cdot \text{K}^4$ is a universal constant and $T(K)$ is the temperature. The specimen temperature T is calculated by equating the steady state power dissipation under electric field to the heat radiated through the body by the relation,

$$W = \sigma AT^4 \quad (2.8)$$

$$T = \left[T_0^4 + \frac{W}{A\sigma} \right]^{1/4} \quad (2.9)$$

$$\frac{T}{T_0} = \alpha \left[1 + \frac{1000W_V (\text{mW mm}^{-3}) \left(\frac{V}{A} (\text{mm}) \right) \right]^{1/4}, \quad W_V = \frac{W}{V} \quad (2.10)$$

where W is power dissipation in watts, T_0 ambient furnace temperature, W_V is the power dissipation calculated in mW/mm^3 . The results of such a calculation are presented in Fig. 2.13 for volume to area ratios of 0.5 and 0.75 mm assuming the emissivity of 1. The calculation considers different values of power dissipation (200-1000 mW/mm^3) and furnace temperature (700-1800°C) for each V/A . Using these maps, the required power dissipation in order to reach a certain temperature can be calculated. E.g. if the furnace is at 1100°C, then in order to reach a specimen temperature of 1450°C for a sample with $V/A=0.5$ mm power density of 600 mW/mm^3 and for $V/A=0.75$, 410 mW/mm^3 is required. From the calculation is also clear that, for decreasing the furnace temperature, from 1100→900→700°C (the case of conducting sample), to reach the same specimen temperature of 1450°C higher power dissipation of 600→800→900 mW/mm^3 for $V/A=0.5$ is required. It also suggest that in case of conducting samples such as MnCo_2O_4 , for which flash-sintering effect occurs at very low furnace temperature require comparatively higher value of power dissipation in order to reach the same specimen temperature because of high heat capacity (the

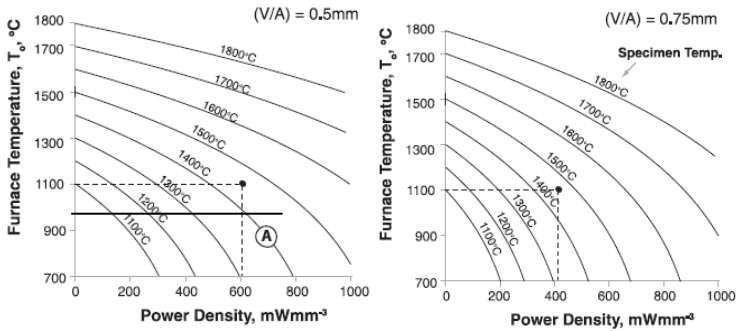


Figure 2.13: Maps for estimating specimen temperature from furnace temperature and the power dissipation in the specimen for volume to area ratio of 0.5 and 0.75 mm [21]

property related to thermal and/or electrical conductivity), it supports the observation of higher power dissipation values in MnCo_2O_4 [22,27]. Results of specimen temperature calculation, from black body relation, of a 95% dense sample of 8YSZ with $V/A=1.0$ mm at 1200°C furnace temperature, is compared with experimentally observed temperature which is estimated from volumetric thermal expansion. There is a fair agreement between the two data with a deviation of 100°C at 400 mW/mm^3 .

In the Fig. 2.12 the maximum power dissipation value is reasonably high compared to the steady state, almost half or less than the peak. At the initiation of instability, large increase in the energy through power dissipation is associated with the heat capacity of the material. Initial part of the energy represented through power spike is suggested to be absorbed by the heat capacity property of the material. The calculation is done considering a triangular shape of the spike having width at half maximum to be 1s. Energy dissipated as heat during this 1 s period is estimated to be $1\text{J}/\text{mm}^3$ for 1000 mW/mm^3 power maximum. Using density of zirconia as 5.67 g/cm^3 , heat capacity 80 $\text{J}/\text{K}\cdot\text{mol}$ (average of 75 - 85 $\text{J}/\text{K}\cdot\text{mol}$) heat capacity of unit volume came out to be 0.004 $\text{J}/\text{K}\cdot\text{mm}^3$ which corresponds to 250°C rise in temperature for $1\text{J}/\text{mm}^3$. The temperature calculated from spike-energy is far less than the temperature observed experimentally or predicted by black body relation. This way, whatever heat is dissipated during initial stage, all goes absorbed by the materials by the heat capacity. The rapid increase in the conductivity heats the materials up by

the Joule effect as shown in Fig. 2.12. Under this fast, effect sintering to full density is sometimes achieved in <5 s [72]. The idea of local temperature for producing fully dense specimen in such short can be made from an equation which governs the temperature dependence of sintering rate and is given as [21],

$$\log_{10} \frac{\text{Rate}_2}{\text{Rate}_1} = \frac{Q}{2.3R} \left(\frac{1}{T_1} - \frac{1}{T_2} \right) \quad (2.13)$$

where T_1 and T_2 are the maximum temperatures that need to reach to attain a specific density while sintering with rates R_1 and R_2 in constant heating rate experiments. From this equation an estimate of sintering temperature can be made for an approximated sintering rate during flash-sintering as shown in Fig. 2.14.

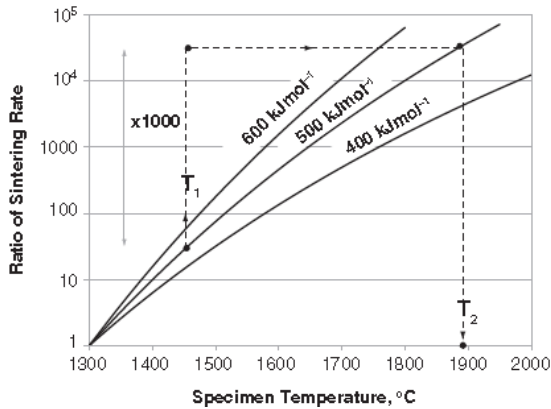


Figure 2.14: Sintering rate as function of specimen temperature [21]

It shows that if a sample conventionally sinters at 1450°C in 1h (3600 s), In order to sinter it in 3.6 s, means by a rate 1000 time higher the temperature need to reach is 1900°C. It suggest that under such fast heating as observed in flash-sintering, the kinetic factors does not allow diffusion of ions/atoms to occur at such a fast rate that sintering can be achieved in less than a minute of time. And in order to achieve equivalent degree of sintering, temperature required is very high which is on contrary to the temperature observed in flash-sintering. So from here, it is not just the Joule heating and thermal effect that causes sudden densification but some additional factors are involved.

2.3.3.1.2 Grain-boundary Temperature

Another possible reason for quick sintering is suggested to be resistive heating at grain boundaries. High temperature at these grain boundaries can affect the grain boundary diffusion and the sintering. It can be calculated from the sintering rate equation given below [72],

$$\dot{\rho} = \frac{Af(\rho)}{Td^4} e^{\frac{Q_B}{RT}} \quad (2.14)$$

where A is a material constant, Q_B is the activation energy for self-diffusion at grain boundaries, $f(\rho)$ is a function of the density, T is the temperature in K , and d is the grain size. The grain size exponent of 4 applies to boundary diffusion-dominated mass transport. The equation can be applied to zirconia where sintering is assumed to occur by the dominance of grain boundary mechanism (lattice/volume diffusion is dominant in large grain size materials). If ρ_0 is the densification under zero applied field at temperature T_0 , and ρ_E is the densification measured under an applied field. The grain boundary temperature is calculated by using the above relation as,

$$\ln \left(\frac{\dot{\rho}_E T_E}{\dot{\rho}_0 T_0} \right) = \frac{Q}{T} \left(\frac{1}{T_E} - \frac{1}{T_0} \right) \quad (2.15)$$

where both the densification rates are to be measured at the same relative density, and the densities should be under the constant grain size, which is possible when the pores remain interconnected. Result of grain boundary temperature calculation of 8YSZ for densities in the range of 60-75% considering activation energy for grain boundary diffusion to be $Q_B = 720$ kJ/mol [48] is shown in Fig. 2.15. The status of furnace temperature for FAST and flash event are shown in left figure where the FAST samples are produced at different furnace temperatures for different densities whereas under flash-sintering, the same is taken to be achieved at same temperatures. From Fig. 2.26(a), the estimated grain-boundary temperatures for zero field or 20 V/cm which belongs to the FAST is close to the furnace temperature. Conversely for flash-sintered samples, the difference of grain boundary temperature from furnace

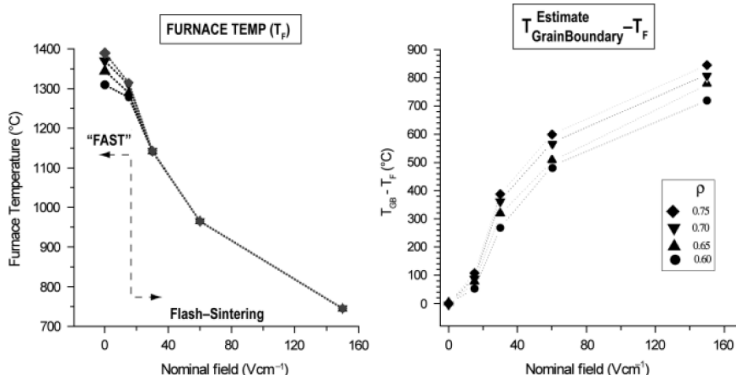


Figure 2.15: Furnace temperature and difference between the furnace temperature and estimated grain boundary temperature under different applied electric fields [77]

temperature is as high as 800°C under 160 V/cm [77]. The grain boundary temperature is significantly higher than the specimen temperature, estimated from black body relation shown in Fig. 2.12 and 2.13. Such local concentration of energy at the grain boundaries can be the reason for enhanced sintering.

2.3.3.2 Microstructure and Grain-growth

The interest towards finding the cause of enhanced sintering rate investigates the micro-structural evolution of materials under electric field assisted FAST and flash-sintering. The two techniques are distinct from each other on sintering rates. In the FAST process, there a gradual increase in the sintering rate with applied electric field, and in flash sintering, sintering occurs almost instantaneously with the field, above a threshold value and at remarkably low temperatures. The increased sintering rate in case of FAST is due to retarded grain growth [76] and follows from the well established fact that the sintering rates are highly sensitive to grain size. The equation for grain size dependent sintering rate is given in eq. 2.16. Under comparable sintering rates as observed in FAST, at a constant density, grain size can be related with the temperature by the equation, where temperature dependence of temperature is determined by the exponential factor,

$$n \ln \frac{d_E}{d_0} = -\frac{Q}{R} \left(\frac{1}{T_E} - \frac{1}{T_0} \right) \quad (2.16)$$

where d_E and d_0 are the grain sizes with and without the electric fields at the same densification rate, and same density; these correspond to T_E and T_0 temperatures, respectively. The above equation is applied to sintering data, with and without electric field, of 3YSZ assuming $Q = 500$ kJ/mol. Figure 2.16 shows the sintering curve for 0 and 20 V/cm, the horizontal at a density level of 0.73 (sintering rates are nearly equal) helps giving the value of $T_E = 1473$ K and $T_0 = 1548$ K. Using eq. 2.16, the grain size ratio is calculated and shown in the Fig. 2.17. It shows that with the increase of the electric field grain size continuously goes down, providing support to the concept that the enhanced sintering is a result of the finer grain size. Following from FAST concept of grain size dependent sintering, the instant flash-sintering, at the first, is expected to drive in the similar way from the retarded grain growth. However, the grain size of the 3YSZ sample that was flash sintered at 850°C was measured to be 150 nm, confirmed by TEM, not remarkably different from the grain size of the FAST sintered sample [72]. Larger grain size in flash-sintering is reported for MnCo_2O_4 [27]. In case of alumina, conventionally sintered specimen (1550°C for 1 h) had an average grain size of 1.9 μm , while the flash-sintered specimen (1260°C

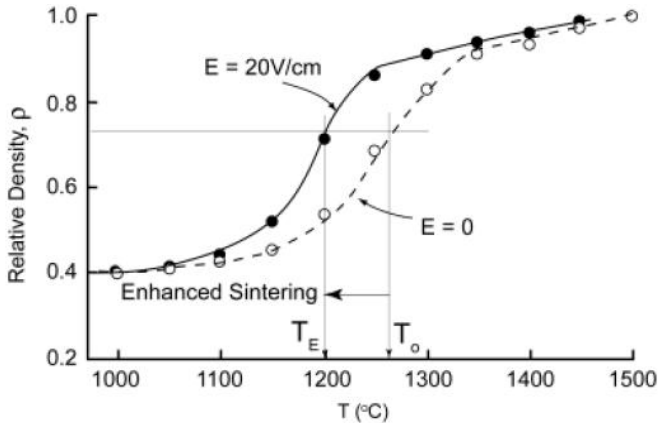


Figure 2.16: Densification rate as function of temperature [76]

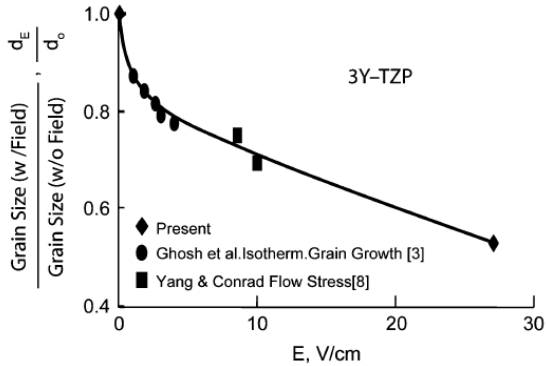


Figure 2.17: Normalized value of grain size as function of electric field [76]

under 1000 V/cm) had a smaller grain size of 0.8 μm [24]. A consistent decrease in the grain size with electric field is observed for GDC samples [78]; the result is expected as to be the result of Joule heating which raises the specimen temperature and the heating rate. Comparing the different results on grain growth of materials under electric field, it does not lead to the ultimate conclusion that the enhanced sintering is because of higher rate of heating and retarded grain growth.

2.3.3.3 Electrical conductivity

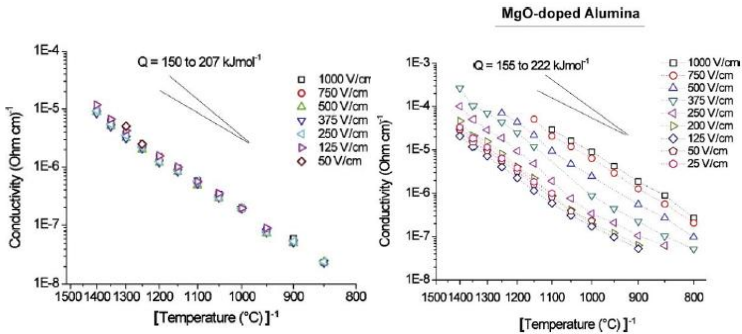


Figure 2.18: Arrhenius type conductivity curves for pure and MgO doped alumina [24]

The flash-sintering-effect initiated with rapid increase in the conductivity is investigated in alumina by observing the I-V behavior on dense specimens by applying electric fields of the range that is needed for flash-sintering (up to 1000°C). I-V char-

acteristics of pure and MgO doped alumina is reported at different temperatures, 900-1400°C. These graphs are linear up to 500 V/cm in case of pure alumina; small non-linearity at higher fields is associated with Joule heating. Using the same data, the conductivity is calculated and presented in Fig. 2.18(a) as functions of temperature under different electric fields. The conductivity curves are observed to be overlapped for all the fields, with small deviation at higher values. Activation energy is calculated from Arrhenius plot and is found to be in the range of 150-207 kJ/mol [24]. This low value of activation energy precluded the possibility of any ionic diffusion.

Conversely, similar I-V graphs of MgO doped alumina shows strong non-linearity at fields higher than 250 V/cm. This non-linearity appeared almost at the same electric field, regardless of the temperature. The conductivities measured under different fields are found shifted to upwards (Fig. 2.18(b)), higher conductivity for higher field and suggesting larger increase in the conductivity under electric field. The slopes are independent of temperature. The activation energy calculated from the slope matches closely with that of pure alumina. Since Q in the equation $\sigma = Ae^{-\frac{Q}{RT}}$ reflects the activation barrier for the mobility of the charged defects, while the pre-exponential A is related to the concentration of the defects, it is inferred that the field has the effect of increasing the concentration of defects in MgO doped alumina which is more pronounced at higher electric fields. This increase in conducti-

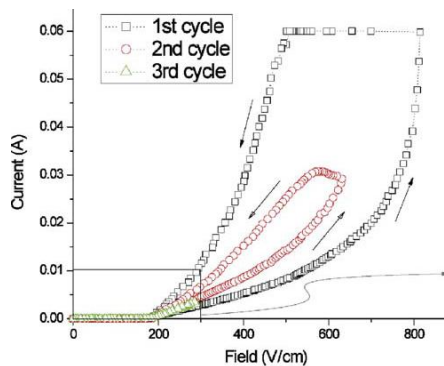


Figure 2.19: Cyclic current voltage response upon the application of field controlled cycles of increasing amplitude [24]

-ivity is associated with the generation of defects under high electric field. In order to have some insight, the electric field is applied in steps up to a maximum and then traversed back following the same. Figure 2.19 shows the current field behavior of the MgO doped alumina while the field is raised to 300, 650 and 750 V/cm with a changing rate of 30 V/s and rest period of 30 s. The behavior is linear and reversible when the amplitude was held up to 300 V/cm. A hysteretic behavior is observed for the field of 600 V/cm. Under 750 V/cm a similar behavior, though more pronounced, is seen. Such remanence of the conductivity is suggested to come from defects nucleation at higher electric fields and which got survived when the field is brought down. The idea of Joule heating is discarded because of quite abrupt reversible (300 V/cm) to hysteretic transition (600 and 750 V/cm).

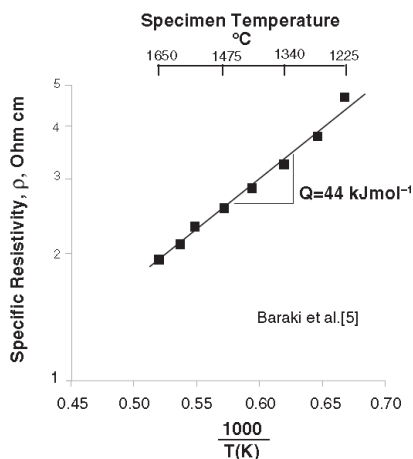


Figure 2.20: Arrhenius plot for the specific resistivity of 8YSZ as a function of temperature [21]

One more discussion about conductivity is with 8YSZ [21]. The resistivity of 8YSZ under different electric fields is plotted against specimen temperature calculated from thermal expansion and is shown in Fig. 2.20. An increase factor of 2.5 is reported for the temperature increase from 1275°C to 1700°C. From the plot activation energy is calculated to be 0.46 eV. It is suggested that in flash-regime the material behaves like a semiconductor with a small band gap. The conductivity of YSZ under flash-conditions, as discussed above, is suggested to be electronic, rather

than ionic. Implication is made as: the diffusion energy of oxygen ion is higher than 0.46 eV. Though it decreases with the increase of yttria content and the temperature, the lowest it can not achieve lower than the value for hopping energy for oxygen ions, which has been calculated to be 0.63 eV. Other support is from the observation of no-reduction of Zirconia into zirconium metal.

2.3.4 Widely Suggested Mechanisms

The effect of quick sintering is extensively suggested to occur by increased kinetics, and not by the change in barrier height of ionic diffusion (activation energy of sintering). Therefore, increased conductivity and rapid sintering is believed to occur by the formation of defects (e.g. Frenkel pair). In support of this, the hysteretic behavior in the conductivity of MgO doped alumina is associated with the increased concentration of defects [24]. The high concentration of defects in electric field treated MgO is correlated with flash-sintering phenomenon [28]. MgO samples treated with higher fields (>1000 V/cm) at high temperatures (>1000°C) showed the presence of vacancy concentrations over two orders of magnitude, some interstitials, and high density of impurity precipitates. It is suggested that these defects interact with elastic and electronic fields of dislocations and grain boundaries, and this defect segregation enhances the mobility of dislocations and increases diffusion along dislocations and grain boundaries. At higher fields, ionic and electronic conduction can lead to an avalanche, where grain boundaries are selectively heated to melting which leads to flash-sintering.

Defect structure analysis on flash-sintered SrTiO₃ sample is reported using ultrafast optical microscopy, XRD and HRTEM [40]. These are shown to have some grains having irregularly placed line features in HRTEM; these defects are associated with the local deviations and with the formation of secondary phase. The results are correlated with the structural distortions in stoichiometric SrTiO₃ under an applied electric field and explained by the ordering of oxygen vacancies and electromigration of SrO ion complexes. Flash-sintering is suggested to be enhanced through these ionic migrations. In zirconia, a kind of reduction reaction under similar

range of electric field as in flash-sintering leads to blackening effect [81–83]; fast sintering effect is suggested to be mediated by the same reduction reaction [81].

Overall, the formation of defects is widely raised/discussed possible cause for enhanced sintering in ceramics. However, the mechanism of defect formation might be different in different materials. Looking at the flash-sintering of different oxides, it might have been associated with oxygen stoichiometry, as discussed with strontium titanate and zirconia, but the recent observation of flash-sintering on non-oxide SiC [26] open a new opportunity and also a challenge for understanding the sintering mechanism in ceramics.

2.3.5 Development in Flash-sintering Experiments

2.3.5.1 Flash-sintering of Multilayer

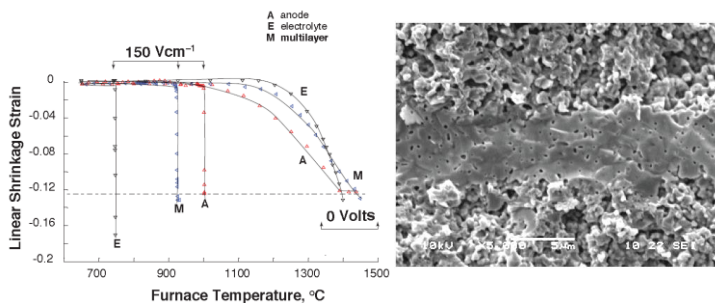


Figure 2.21: a) Shrinkage as a function of furnace temperature and b) SEM micrographs of anode-electrolyte multilayer sample, with electrolyte sandwiched between two anode layers [23]

In the direction of development, flash-sintering anode electrolyte multilayer is a nice effort [23]. The most discussed papers dealt with the dog-bone shape samples. In this case, the sample was prepared from thermo-compressing of tape casted layers at 75°C under pressure of 12 MPa. After this, these were cut into bar-shape samples 20 mm long with rectangular cross section of 2.75 x 3.25 mm². The thickness of the prepared stack consisted of 2.97 mm (8 layers) of anode and 0.28mm (7 layers) of electrolyte. It was hung between two platinum wire-electrodes similar to dog bone samples. The parameters required (temperature and electric field) for

flash-sintering was higher than that required for sintering of electrolyte and lower than that of anode (Fig. 2.21(a)), based on their conductivities. The cross-sectional view of the multilayer in Fig. 2.21(b) showed well adhered layers. The electrolyte is fully sintered with some closed porosity. Anode layers observed to be porous according to the requirement of SOFC anode. The comparatively denser microstructure of electrolyte layer is probably the result of its comparatively lower conductivity. Therefore, the results showed that NiO–zirconia anode and cubic zirconia electrolyte can be sintered below 1000°C in a few seconds.

2.3.5.2 Sintering of Composite

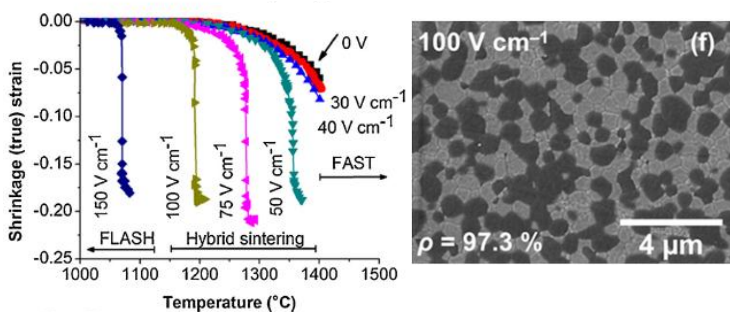


Figure 2.22: a) Shrinkage of alumina-zirconia composite subjected to different electric fields as function of temperature and b) microstructure of composite, flash-sintered under 100 V/cm [84].

Like multilayer of different compositions, composite mixture of alumina and zirconia in 50-50 volume% is sintered to almost full-density under the effect of electric field. Composite requires electric fields in the range of what required for zirconia but flash occurs at comparatively higher temperature. Pure alumina which resists flash-sintering at fields up to 1000 V/cm exhibits this behavior in case of composite at low fields. Between FAST and flash, a hybrid behavior of sintering is shown where a FAST-like sintering is followed with flash-like behavior. Microstructure of the composite produced under 100 V/cm is shown to reach a density of ~ 97% of theoretical in Fig. 2.22(b). The dark portions represent alumina phase and white ones are zirconia. Sintering effects are observed to be homogeneous from the uniformly distributed grains. The rate of grain growth during the hold time after flash-effect is calculated, it

shows higher rate of growth under the flash-sintering compared to that by the conventional procedure.

2.3.5.3 Sintering of Circular SOFC cell

Another effort in the experimental arrangement for electric field assisted sintering of Ytria-stabilized zirconia (YSZ) electrolyte thin film. It is not exactly flash-sintering but the experimental-arrangement seems worth for discussion. In the arrangement, anode-electrolyte tape-casted layer is pre-sintered at 1300°C for 2h to remove binder and to give a mechanical strength. This structure is placed over an alumina tube and fixed with silver adhesive (Fig. 2.23). LSM cathode is deposited by screen printing followed with silver paste as other electrode for electrical connection. During the electric field application, current flows from central portion to outward direction. A voltage of 16V was applied while the furnace was heated with 5°C/min. The microstructure of different stages of the electrolyte showed that with the assistance of electric field a dense electrolyte layer can be prepared in shorter time. The grains were observed to be of smaller size than those produced with conventional-sintering.

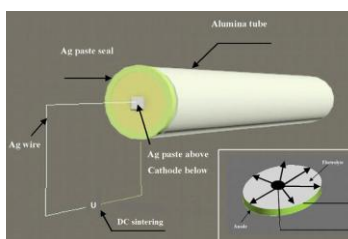


Figure 2.23: Schematic of the sample arrangement

2.4 Solid Oxide Fuel Cell (SOFC)

SOFC is an energy conversion device which produces electricity directly from a chemical reaction. It consists of two electrodes where the electrochemical reactions take place and an electrolyte which joins the two electrodes and transports oxygen from cathode to anode side. Hydrogen is used as the basic fuel and oxygen is needed to complete the reaction. All the three components are solid ceramic oxides and

arranged in the way shown in Fig. 2.24 and the involving reactions are presented in Fig. 2.25. Reaction starts at cathode where electron from outer circuit combines with oxygen and reduces it into oxygen ion. These are transported at the electrode anode interface through electrolyte and combines with hydrogen to release electrons. The basic requirements about these electrodes on the basis of their functions are briefly mentioned below.

Cathode: This electrode faces the oxidizing atmosphere and creates an environment for oxygen reduction, utilizing electron from outer circuit. The reaction takes place catalytically at the triple phase boundary (vacuum, cathode and electrolyte). For this reason, electrode is made porous to allow gas flow to electrolyte, should possess some ionic conductivity as well to increase the TPB area. LSM is the widely used cathode in intermediate temperature-SOFC. Sometimes a composite with ion conducting phase such as YSZ or GDC is preferred.

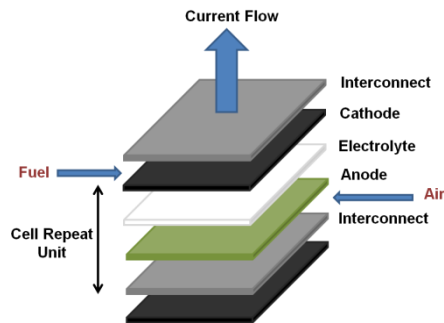


Figure 2.24: Schematic of component arrangement in planar SOFC

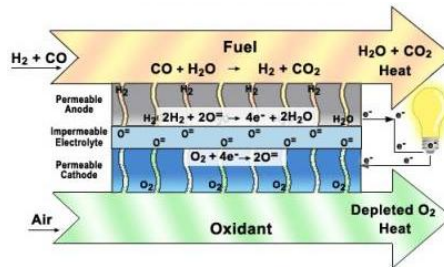


Figure 2.25: Operating concept of a SOFC

Anode: This is the electrode where hydrogen fuel enters. Therefore it should be stable in reducing atmosphere. Like cathode, the reaction preferably occurs at anode electrolyte interface. Anode should be porous to allow fuel to reach to the interface and should possess ionic and electronic conductivity. Ni based anode is preferred and to match with thermal expansion coefficient and providing ionic conductivity a composite with YSZ is widely applied for anode.

Electrolyte: In order to stop the interference between direct oxygen and hydrogen reaction, a dense electrolyte layer is inserted between the two. Electrolyte should be ion-conducting as it has to allow oxygen ion to pass through, and with no electronic conductivity because electrons is for ionizing oxygen at cathode electrolyte interface. It should also be as thin as possible to minimize resistive losses in the cell.

Interconnect and coating: Interconnect takes the electron generated in the electro-chemical reaction and allow to flow through the rest of the circuit and back to cathode. It should possess therefore high electrical conductivity and for the same reason metal is the first choice for Intermediate and low temperature SOFC. A coating is needed to protect the cell from Cr-poisoning and to metal from high temperature oxidation. Mostly Mn-Co based spinels are employed.

2.5 Manganese Cobaltite (Mn, Co)O₃

Mixed oxides of cobalt and manganese with a spinel structure are a key compound in the field of electronics (as negative temperature coefficient thermistors [85–87] in microelectronic), electro catalysis (for the oxidation of NO and CO [88,89], reduction of oxygen [90], and nitrogen oxide [91]), magnetic sensor [92–94] and energy (protective coating [29] in SOFC due to electrical characteristics). Other benefits are element abundance and low cost. Out of many applications, its use and development for protective coating application is discussed in further sections.

2.5.1 Application as Interconnect Coating in SOFC: MnCo₂O₄

High temperature-SOFC interconnect material lanthanum chromate was considered as the first option for coating on metallic Crofer [95,96]. Later on diffusion of

Cr towards the cell led to Cr-poisoning and degradation of cell performance [32]. Therefore in the search for material with no-Cr or least Cr-diffusion, number of ceramic oxides specially, spinel and perovskite were examined for their high conductivity, thermal expansion coefficient (TEC) and stability with metallic interconnect and cell's other component [33,99]. Some of the perovskite of such study are LSCr: (La, Sr)CrO₃, LSC: (La, Sr)CoO₃, LSM: (La, Sr)MnO₃ and LSF [97]: (La, Sr)FeO₃ etc and some of the spinels are (Co, Mn)₃O₄, (Cu, Mn)₃O₄, (Mn, Cr)₂O₄, (Ni, Mn)₃O₄ and (Ni, Fe)₃O₄ etc [12,76,77]. From the conductivity and TEC match spinels were found as a better choice. And specially, Mn-based oxide received great attention for the formation of conducting spinel layers with Cr at the interface as also depicted in Fig. 2.26. Because of strong diffusion of Mn from coating into metal and also from Crofer metal bulk (containing some % of Mn) to surface a comparatively conductive bi-layer based on Mn, Co, Cr spinel forms at the interface. These layers protect the metal from oxidation and the cell from Cr poisoning without deteriorating the conductivity of interconnect-coating structure [30].

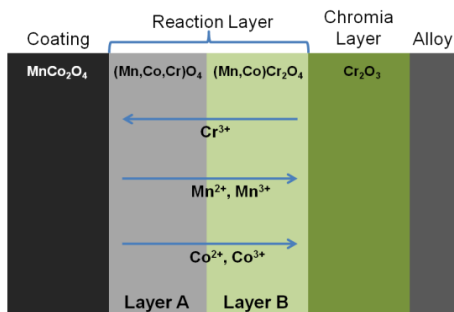


Figure 2.26: Reaction layers from reaction between (Mn, Co)₃O₄ and Cr₂O₃ [30].

In Mn-Co based oxide, a number of compositions are tested for conductivity and thermal expansion coefficient (TEC) for match with chromia and other components [30]. The properties of these spinels for different ratios of Mn and Co are reported. For the two oxides MnCo₂O₄ and Mn₂CoO₄ even the conductivity is similar but there is large difference of TEC. For equally distributed concentrations, TEC was found close to SOFC materials' requirement of 11-12 x 10⁻⁶ /°C. Compositions conta-

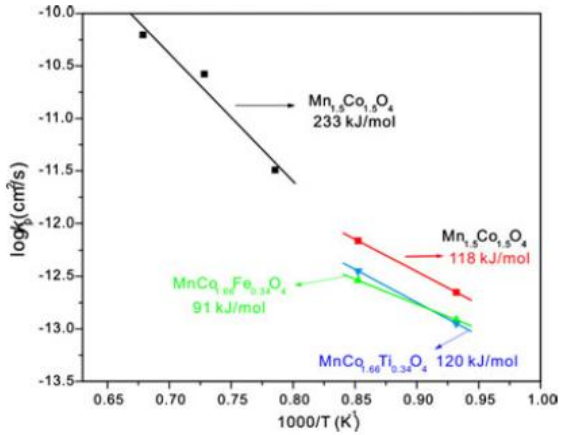


Figure 2.27: Temperature dependence of parabolic rate constant for reaction between $\text{Mn}_{1.5}\text{Co}_{1.5}\text{O}_4$ and Cr_2O_3 [30].

ining Fe and Ti also possess the requisite TEC. The importance of addition of these elements is related with the diffusion of Cr from metal to interlayer and to the coating (Fig. 2.27). The chromium gradient in the Cr-containing intermediate layer was steeper with Fe and Ti doping, which suggests that the growth rate of the intermediate layer was also decreased, which would improve the long-term stability of the interconnect and thus the cell. Also, Fe or Ti additions changes the transport properties of $(\text{Mn},\text{Co})_3\text{O}_4$ since the Co/Mn ratio in the reaction layer was still higher than that in the original spinel, but lower than that without Fe or Ti additions.

2.5.2 Crystal Structure and Electrical Conductivity

MnCo_2O_4 possess face centered cubic normal-spinel structure with the ionic arrangement as $\text{Co}^{2+}[\text{Co}^{2+}, \text{Co}^{3+}, \text{Mn}^{3+}, \text{Mn}^{4+}]_4\text{O}_4$ [100]. The representation outside the ‘[]’ shows the presence of Co is at tetrahedral site. Those within the bracket show the presence of doubly mixed valancy of Co and Mn at the octahedral sites which continuously undergo oxidation/reduction at any temperature showing two step transformations for $\text{Co}^{2+}/\text{Co}^{3+}$ and $\text{Mn}^{3+}/\text{Mn}^{4+}$ in thermo-gravimetric data. These transformations are also responsible for the characteristic conductivity-temperature plot of the spinel. The hopping of Co and Mn ions of octahedral site between their different oxidation states [41] are thermally activated giving semiconducting nature of the

conductivity. Its conductivity is reported to be in the range of 60-100 S/cm at 800°C [9]. Conductivity of MnCo_2O_4 sample sintered to higher temperature of 1300°C is lower than that of sintered at 1200°C. Such decrease of conductivity is associated with some irreversibility of Co^{3+} to Co^{2+} transition in polaron hopping which forms Co-O phase. This phase is semiconducting but of lower conductivity which decreases the conductivity of the sample with sintering temperature [101].

2.6 (La, Sr)(Co, Fe)O₃ based Oxides

Lanthanum and transition metals based perovskites have attracted much attention due to their striking mixed ionic and electronic conductivity (MIEC) which are easily tailor-able by the substitution of A-site La by alkaline earth metals [8,102,103] and B-site cations by Zn [104,105], Ni [104–108] or any doubly ionized transition metal ions [35,36,109]. These oxides are of practical interest for a wide variety of applications in catalysis e.g. as active catalysts for oxidation or reduction of pollutant gases [5,6], as electrode materials in solid oxide fuel cells [109] or materials for technological chemical sensors for the detection of humidity, alcohol, gases [110] etc and as oxygen permeating membranes [111–116]. Development of promising (La, Sr) (Co,Fe)O₃ (LSCF) for cathodic application in SOFC is discussed in next sections.

2.6.1 Application as SOFC cathode: (La, Sr)(Co, Fe)O₃

In the SOFC the oxide have to serve for the reduction and transportation of gaseous oxygen to the adjacent YSZ electrolyte. (La, Sr)MnO₃ (LSM) is currently state of the art cathode material for intermediate temperature SOFC (700-800°C). The efforts for producing efficient and cost effective SOFC suggests lowering of operating temperature to 600°C and below, and the search of materials for the lower temperature operation, with properties that can compete with that of current state of art SOFC materials. In this direction, Gd-doped ceria (GDC) [51] and Sr- and Mg-doped lanthanum gallate (LSGM) are ready to replace the well-accepted YSZ solid electrolyte due to higher ionic conductivity with lower activation energy.

Studies show that La-Co based cathode exhibits interesting electrical and electro-catalytic properties, combined with good ionic conductivity which might exceed

the conductivity of well known ion conductor 8YSZ even [8]. With the advance of research in this direction, LSCF based oxide with mixed ions at A and B-sites is found to show superior properties for catalytic activity for oxygen reduction [109]. The oxygen self-diffusion coefficient of LSCF is 2.6×10^{-9} cm²/s at 500°C, which is superior in performance to that of LSM which has a oxygen self-diffusion coefficient of 10^{-12} cm²/s at 1000°C [109]. The measured current densities of cells consisting of La_{1-x}-ySr_xCo_{0.2}Fe_{0.8}O_{3-δ} cathode, CGO electrolyte, and a NiO–YSZ anode were as high as 1.76 A/cm² at 800°C and 0.7 V, which is about twice the current density of cells with LSM/YSZ cathodes.

(La, Sr)(Co, Fe)O₃ is developed for cathodic application by changing A- and B-site elemental ratio in order to reach requisite properties of conductivities and TEC. Table 2.4 shows the ionic and electronic conductivities of different LSCF compositions. For all compositions, conductivity is higher than that of 8YSZ. Ionic conductivity in Table 2.4 increases with the increase of Sr and/or Co content. Ionic conduction is related to the concentration and mobility of oxygen vacancies which forms at higher temperature. The vacancy concentration is estimated from stoichiometry data. The non-stoichiometry increases with the increase of Sr content, and further with Co content.

Table 2.4: Ionic and electronic conductivity, activation energy for ionic conductivity of different LSCF compositions [8]

Composition	Conductivity (Ω-cm) ⁻¹		Activation energy for ionic conductivity (eV)
	Electronic	Ionic	
LSCF-6428	252	0.23	1.30
LSCF-4628	219	0.40	0.95
LSCF-2828	120	0.62	0.85
LSCF-2882	310	0.87	0.66

The electronic conductivity increases with the increase of Co content (Table 2.4). The conductivity of LSCF, at any temperature, is a coupled response of oxygen vacancy formed at A-site and polaron hopping at B-site in ABO₃ perovskite type structure [36]. The replacement of La³⁺ at A-site by doubly ionized Sr²⁺ brings about the oxidation of B-site cation (Co or Fe, preferably Fe) into its higher valence state for charge compensation and/or the formation of oxygen vacancies (p-type carrier). The

electro-neutrality leads to following charge balance reaction, $[Sr'_{La}] = [B_B] + 2[V_O^{\cdot-}]$. It explains that when a divalent Sr-acceptor is substituted for trivalent La, electro-neutrality requires that the effective negative charge of the Sr-cations be compensated by an increase in valence of some of the B-site cations (electronic compensation) and/or the formation of oxygen vacancies (ionic compensation). Therefore, electronic compensation results in an increase in the average valence of the transition metal cations, while ionic compensation reduces the oxygen stoichiometry. It is reported that electronic compensation mostly occurs through the oxidation of Fe, and therefore conductivity increases with the increase of Co by its hopping activity [35,36].

TEC has comparatively higher dependence on Co than on Sr-content. In terms of crystal structure, rhombohedral phase always has higher TEC value. There is a significant increase in TEC with temperature which is associated with the formation of oxygen vacancies and can be attributed to: 1) the repulsion force arising between those mutually exposed cations when oxygen ions are extracted from the lattice, 2) the increase in cation size due to the reduction of the Fe and Co ions from higher to lower valences [35,36]. TEC of different composition is shown in the Table 2.5.

Table 2.5: TEC and electrical conductivity of different LSCF compositions namely $La_{1-x}Sr_xCo_{0.2}Fe_{0.8}O_3$, $x:0.0-0.4, 0.6$ [36] and $La_{0.8}Sr_{0.2}Co_{1-y}Fe_yO_3$, $x:0.0, 0.1, 0.4, 0.6, 0.8-1.0$ [35]

LSCF (mol)	Temp. Range (°C)	TEC ($\times 10^{-6}/^{\circ}\text{C}$)	Crystal structure	LSCF (mol)	Temp. Range (°C)	TEC ($\times 10^{-6}/^{\circ}\text{C}$)
x=0.0	100-500	13.1	Ortho	y=0	100-900	19.7
0.0	600-900	17.5	Ortho>rhombo	0.1	100-900	20.1
0.1	300-900	16.0	Rhombo	0.4	100-900	20.0
0.2	100-800	15.4	Rhombo	0.6	100-900	17.6
0.3	100-700	14.6	Rhombo	0.8	100-800	15.4
0.4	100-600	15.3	Rhombo	0.9	200-900	14.5
0.6	100-400	16.8	Rhombo	1.0	300-900	12.6

2.6.2 Crystal Structure and Electrical Conductivity

The $La_{0.6}Sr_{0.4}Fe_{0.2}Fe_{0.8}O_3$ is most popularly chosen for the cathode application for it sufficiently high ionic and electronic conductivity [35–37]. It crystallizes into rhombohedral structure where Fe and Co forms BO_6 octahedra in distorted cubic

structure with A-ions sitting at the corners of cube edges with 12 co-ordination. Its thermal expansion coefficient is reported to be close to $15.4 \times 10^{-6} \text{ K}^{-1}$, little higher than the requirement range $\pm 20\%$ of that of other cell component materials. It is made less severe by forming it A-site deficient which is observed to have lower TEC [117].

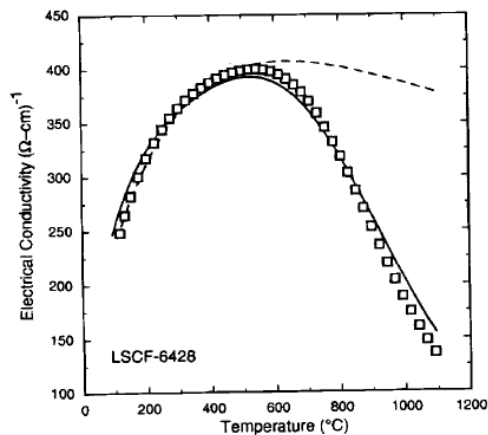


Figure 2.28: Electrical conductivity of $\text{L}_{0.6}\text{Sr}_{0.4}\text{Co}_{0.2}\text{Fe}_{0.8}\text{O}_3$ as a function of temperature [8]

The electrical conductivity has a peculiar behavior as shown in Fig. 2.28 [74,92]; it first increases with temperature up to 550°C , and then shows metallic kind of decreasing response. The initial increase in conductivity is from B-site hopping of polarons, mostly Co. In such hopping, the charge dis-proportionate, where (2Co^{3+} to Co^{2+} and Co^{4+}) transition (providing n- and p-type carriers) is responsible for its large control over conductivity; Fe oxidizes mostly for balancing the electro-neutrality. After 550°C the conductivity is dominated by oxygen compensation factor as the ionic content of materials decreases. The decrease in conductivity is associated with a weight loss which loses p-type carrier because of the stabilization of B site cation into lower valance state. The weight loss and decrease in conductivity is extended to a larger range of temperature. The decrease at higher temperature is with the hopping activity and stabilization of Co or Fe into lower states losing both type of carriers, p- and n-type.

Chapter III

Experimental Methods: Materials, Equipments and Characterizations

3.1 Materials

3.1.1 MnCo₂O₄ and (La, Sr)(Co, Fe)O₃ Powders

In the present work, commercial powders of Fe-doped MnCo₂O₄ (MCO) and La_{0.6}Sr_{0.4}Co_{0.2}Fe_{0.8}O₄ (LSCF) were chosen for the study. Particle size and surface area of powders supplied with the analyses are,

	Average Particle Size	Surface Area, cm ² /g
MnCo ₂ O ₄	~1.17 μm	4.22
LSCF	~500-600 nm	6.00

Particle size and phase of these powders are confirmed by SEM-EDS and XRD in preliminary characterizations, and shown in Figs. 3.1, 3.2 and 3.3. MnCo₂O₄ particles have irregular and faceted kind of morphology with average size of 1.17 μm (Fig. 3.1(a)). Energy dispersive x-ray spectra (EDS) of the powder recorded by under the accelerating voltage of 20 kV (Fig. 3.2) shows excitation peaks of Mn, Co and Fe placed between 5.5-8.0 keV. The wt% of each element observed from EDS quantitative measurement matches closely with the calculated concentrations, Mn: 31.85 wt%, Co:64.92 wt%, Fe:4.24 wt% (atomic weights of Mn: 54.94, Co: 58.93, Fe: 55.85) in MnCo_{1.9}Fe_{0.1} composition. XRD peak positions and relative intensities of Fig. 3.2, matches with JCPDS file number 023-1237 and that of MnCo₂O₄ reported in [9] confirming the manganese cobaltite cubic spinel phase. On the other side, LSCF has smaller and spherical particles with average size of 500-600 nm (Fig. 3.1(b)). EDS spectra and elemental concentration (Fig. 3.3) closely matches with calculated concentrations of La: 47.67, Sr: 20.04, Fe: 25.55, Co: 6.74 wt% (atomic weights of La: 138.91, Sr: 87.62, Co: 58.93) in La_{0.6}Sr_{0.4}Co_{0.2}Fe_{0.8} composition. XRD pattern for peak position and relative peak intensities represents the rhombohedral perovskite phase closely matched with the peaks from JCPDS file number 049-0285 (Fig. 3.3).

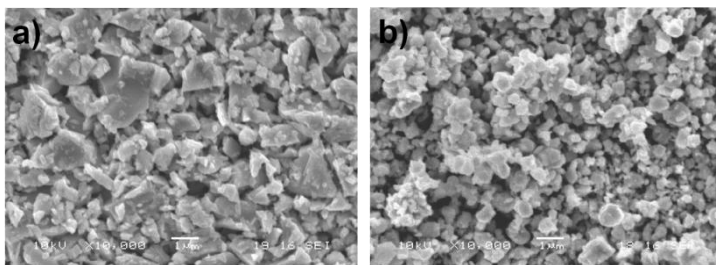


Figure 3.1: Microstructure of as-received a) Fe-doped MnCo_2O_4 and b) LSCF powders

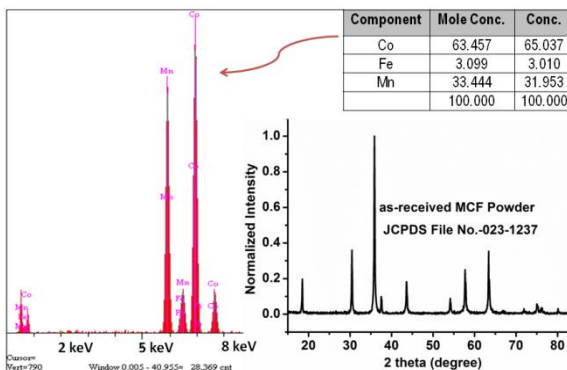


Figure 3.2: EDS spectrum with elemental concentration and XRD pattern of as-received Fe-doped MnCo_2O_4 powder

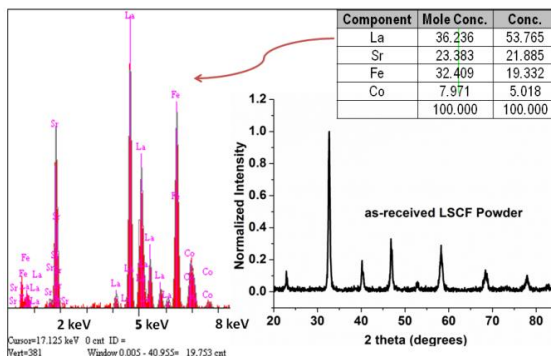


Figure 3.3: EDS spectrum with elemental concentration and XRD pattern of as-received LSCF powder

3.1.2 Binder

B-1000 (DURAMAX) organic based binder was used in order to provide sufficient strength to powder compacts for sintering experiments. B-1000 is an aqueous emulsion with 55% of solid binder having glass transition temperature -26°C . Its degradation starts at 300°C and complete removal occurs up to 600°C at the heating rate of $20^{\circ}\text{C}/\text{min}$. A minimal amount of ~ 3 weight % was chosen for making pellets with sufficient green density and handle-ability.

3.2 Sample Preparation

Powders were mixed homogeneously with 3 wt% B-1000 binder in aqueous media using agate-mortar and dried at 90°C overnight. Dried powders were pressed into dog bone shaped pellet by applying uni-axial load of about 165 MPa for successive flash-sintering and other experiments. The dimension of such a pellet is shown by a sketch in Fig. 3.4. The region between the holes (of dimension $\sim 21 \times 3 \text{ mm}^2$ from the top view) is made as the gauge section for the electric field sintering experiment.

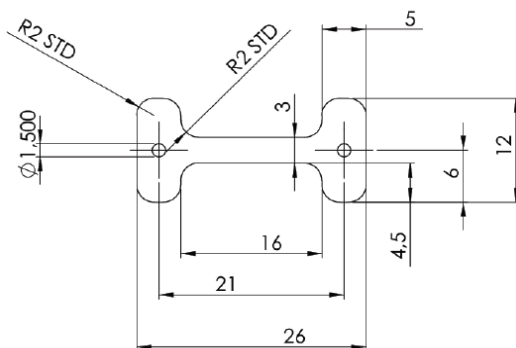


Fig. 3.4: Sketch of dog bone sample used for sintering experiments, numbers is in mm.

The LSCF/GDC composite powders containing different amounts of GDC (60/40, 50/50 and 40/60, LSCF/GDC weight ratio) are prepared by ball milling for 24 h in aqueous media, and afterwards dried overnight. Dog-bone shaped pellets were

prepared for the sintering experiment in the same way as described above for LSCF and MnCo_2O_4 . Green density of pellets was calculated from mass by volume (= area x thickness; area 161 mm^2 calculated by design software). The green densities of both the samples were in the range of 59-61 % of the theoretical density.

3.3 Flash-sintering Experiment

3.3.1 Experimental-arrangement

Flash-sintering on dog bone shaped sample was performed under constant electric fields in a four-point type electrical arrangement within a muffle furnace which was heated with a constant rate of $5^\circ\text{C}/\text{min}$. Schematic of experimental set up is shown in Fig. 3.5. The sample was hanged within the furnace, in an electrical circuitry, with the help of 0.5 mm thick platinum wires which were taken out from the furnace and were connected to the other electrical component such as power supply,

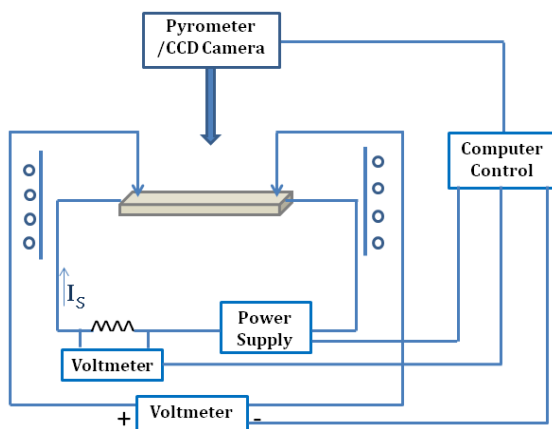


Figure 3.5: Schematic of flash-sintering experimental set-up

multimeter, shunt etc. Power supplies and multi-meters are connected with computer for voltage control and current/voltage data monitoring. During the experiment, the electric current in the measurement set-up was set to a fixed maximum value to avoid any kind of thermal/electrical runaway in the sample and to protect the connect-

ing wire and the sample from excessive heating. A hold time of 60 s was given at the maximum current density which is considered as the period of flash-sintering. Conventionally sintered samples were produced for comparing the microstructure, were treated for 60 s hold time for the close comparison; these were produced at different temperatures with 5°C/min heating rate. A CCD camera was focused on the sample during flash-sintering to record the shrinkage; it was set to record images every second. Images were processed for shrinkage data using either of, ImageJ or MATLAB, software. In some experiments when recording specimen temperature, a pyrometer in place of CCD camera was focused on the sample.

Flash-sintering of MnCo_2O_4 was performed on pre-sintered (at 900°C for 1 h: 67% dense) samples employing the electric field of 2.5-17.5 V/cm starting from 80-100°C, and limiting the maximum current to 1.4-1.6 A/mm². Pre-sintering is performed in order to remove the binder for avoiding any fluctuation in the power dissipation which may occur for binder degradation activity. It also allowed easier handling for successive flash-sintering experiments. Lanthanum strontium cobaltite (LSC) slurry and silver paste dried at 250°C for 20-30 min were used to reduce the contact resistance. Pictures of green and dense MnCo_2O_4 sample, sample arrangement for electric field experiment, and during flash-sintering are depicted in Fig. 3.6.



Figure 3.6: a) Green and sintered MnCo_2O_4 pellets, b) the actual sample arrangement, sample hanged with the help of Pt-wires and c) during flash-sintering

Flash-sintering on LSCF was performed using electric fields in the range of 2.5-12.5 V/cm and maximum current density of 1.50 A/mm² applied from the starting temperature of ~20°C. Here also, a hold of 60 s, unless mentioned, was given at the maximum current values. In the electrical circuitry, silver paste was used to reduce the contact resistance between the sample and the connecting wires, dried at 250-

260°C for 30 min. After drying, the furnace was brought down to room temperature (20-25°C) and heated again for flash-sintering experiments with constant rate. Such treatment was also found to be useful to avoid any fluctuation in the power dissipation associated to binder degradation (Duramax B-1000). Flash-sintering of LSCF samples containing different amounts of GDC (60:40, 50:50, 40:60, LSCF:GDC weight ratio) was performed under 7.5-20.0 V/cm in constant heating rate experiments; current density of 0.59 A/mm² was chosen for 5050 and 4060 composition whereas comparatively higher current density of 0.9 A/cm² were set for 6040 compositions as for being more conductive 0.59 A/mm² was found very low for sufficient heating.

Details of instruments used for flash-sintering experiments are given below:

3.3.2 Power Supply: Sorensen XG6025

XG6025 power supply was used for applying electric field. It can provide maximum 60 V in constant voltage mode and maximum 25 A in constant current mode, both with a resolution up to two decimal points. The power supply can be controlled manually or by computer programming through analog or an RS232-USB channel.

3.3.3 Multi-meters: Keithley 2000 and 2100 Digital Multimeter

Either of 2000 and 2100 model Keithley multimeters were used for measuring voltage and current. These multimeters can record current up to 3 A, and voltage up to 1000 V with precision of 6¹/₂ decimal place. For recording current higher than 3A (e.g. during flash-sintering experiments), keithley was used in voltage mode for measuring drop across a shunt of value 0.002 Ω. Data was recorded automatically using VISA-USB interface adapter for Keithley 2100 model and GPIB-USB for 2000.

3.3.4 Pyrometer

In flash-sintering rapid increase in conductivity raises specimen temperature to a value much higher than the furnace temperature. Therefore, the local temperature

is entirely different from the onset temperature mentioned from furnace LED-display-reading or thermocouple. In order to analyze flash-sintering and to compare from conventional-sintering, specimen temperature was recorded using an 'Ultimax Infra-red Thermometer, UX-20/600-3000°C' pyrometer during sintering and electrical conductivity experiments. Prior to the measurements, pyrometer was calibrated up to 1150°C (with no field applied) using sintered specimens of same powders that were used for sintering experiments. For calibration thick disc shaped (12 mm diameter) specimens were used; a hole was drilled at the cylindrical surface of the disc to keep a thermocouple (S-type) in the close contact of sample surface; pyrometer was focused on the flat circular surface. From the measurements, emissivity of MnCo_2O_4 is averaged to be 0.98 and that of LSCF is 0.93 over 800-1150°C.

3.3.5 Data Collection

Flash-effect for being a transient event, voltage, current and specimen temperature data were recorded automatically every ~0.15-0.20 s to increase the reliability, using data acquisition devices and MATLAB for interfacing as mentioned below:

3.3.5.1 Interface environment and language

MATLAB software provides an interactive background for numerical computation, analysis and visualization of data and programming. It provides an environment for interface between computer and different devices such as power supply, multimeter and pyrometer etc. It is equipped with data acquisition (DAQ) toolbox which provides functions for connecting MATLAB to data acquisition hardware such as USB, GPIB, VISA devices from National Instruments, Agilent and other vendors.

3.3.5.2 Data Acquisition Hardware used

- RJ45 - RS232 card, for power supply
- GPIB (General Purpose Interface Bus)-USB, for Keithley 2000 multimeter
- VISA-USB, for Keithley 2100 multimeter
- NI-DAQ (NI: National Instruments), for pyrometer

Some of commands for creating these objects for communication in MATLAB are:

Commands	Comments
serial	Create serial port object e.g. obj=serial('COM1'); %% the device is connected at COM 1 USB port in the computer
fopen	Connect interface object to instrument
fclose	Disconnect interface object from instrument
fprintf	Write text to instrument
fscanf	Read data from instrument, and format as text
delete	Remove instrument objects from memory
instrhwinfo	Information about available hardware
visa	Create visa object e.g. vu = visa('agilent', 'USB::0x1234::125::A22-5::INSTR') VISA-USB object connected to a USB instrument with manufacturer ID 0x1234, model code 125, and serial number A22-5
analoginput	Create the analog input object e.g. AI1 = analoginput('nidaq','Dev1'); %% for a National Instruments board
addchannel	add the hardware channels e.g. addchannel(AI1,0:3); %% (channels 0-3)

3.4 Sample Characterization Techniques

3.4.1 Dilatometry

Dilatometers serve for highly precise measurement of dimensional change of a body which occurs as a result of any physical or chemical process as a function of temperature. Conventional sintering of samples (with no electric field) was observed by recording linear shrinkage in a Linseis L75 dilatometer (Linseis GmbH, Bolzano, Italy). Bar-shaped samples made by the same way as for flash-sintering were heated up to 1500°C (or up to complete shrinkage) at 5°C/min in air. A correction curve that accounts for changes in sample support and sample push rod during such heating is determined using an alumina standard under the same experimental conditions.

3.4.2 X-ray Diffractometry

X-ray diffraction is a versatile, non-destructive analytical technique for identification and quantitative determination of the crystalline/amorphous phases present in solid materials and powders. The XRD technique is based on the interaction between x-ray and the three dimensional distribution of atoms in space, the crystal lattice.

Such interaction provides a set of diffraction peaks arranged at different angles, Θ , considered with respect to the sample plane. Each peak corresponds to diffraction from atoms of a specific set of planes, separated from one another by a distance, d (Bragg diffraction, $n\lambda = 2d\sin\Theta$). Therefore, position and relative intensities of peaks is a signature of materials. The details of crystalline nature such as lattice parameter, crystallite size etc. of powders and produced samples are calculated from the collected diffraction pattern.

3.4.2.1 Calculation of phase concentrations

The amount of CoO phase in sintered $MnCo_2O_4$ sample is calculated from the internal standard method [118], briefly discussed here. Quantitative analysis by XRD is based on the fact that the intensity of the diffraction pattern of a particular phase in a mixture of phases depends on the concentration of that phase in the mixture. The relation between intensity and concentration is generally not linear, since the diffracted intensity depends markedly on the absorption coefficient of the mixture and this itself varies with the concentration. Out of the different methods discussed in [118], the internal standard method is used here for calculating the concentration of constituent phases. In this method a diffraction peak of the phase being determined is compared with the peak of a standard substance mixed with the sample in known proportions. Suppose we wish to determine the amount of phase A in a mixture of phases. A known amount of test composite sample containing phase/sample A is mixed with a known amount of a standard substance (S) to form a new composite sample. If a XRD pattern is now obtained for the new composite sample, the ratio of intensity of a particular peak of phase A to that of composite is given by [118],

$$\frac{I_A}{I_S} = K w_A \quad (3.1)$$

where w_A is the weight fraction of phase A in the composite and K is a constant. Thus the intensity ratio of a peak of phase A and a peak of the standard sample S is therefore a linear function of w_A . This new composite contains the w_S , weight fraction of standard sample. A calibration curve can be prepared from measurements on

a set of synthetic samples, containing known concentrations of A and a constant concentration of a suitable standard, S . Once the calibration curve is established, the concentration of A in an unknown sample is obtained simply by measuring the ratio I_A/I_S for a composite sample containing the unknown and the same proportion of standard as was used in the calibration. This internal standard method has been used in our work.

X-ray diffractograms of raw powders, conventionally- and flash-sintered samples were collected from Rigaku D-Max diffractometer (Rigaku, Tokyo, Japan) in the Bragg-Brentano configuration using $\text{CuK}\alpha$ radiation operating at tube voltage of 40 kV and tube current of 30 mA. The scanning range was 10-90° with a step rate of 0.05° and acquisition time of 5 s per point. Peaks were identified by JCPDS (Joint Committee on Powder Diffraction Standards) database.

3.4.3 Scanning Electron Microscopy- Energy Dispersion X-ray Spectroscopy

The scanning electron microscope (SEM) has become one of the most widely utilized instruments for materials characterization. SEM uses a focused beam of high-energy electrons to generate a variety of signals at the surface of solid specimen. These signals include secondary electrons (that produce SEM images), backscattered electrons (BSE produce high resolution compositional map of a sample), diffracted backscattered electrons (EBSD that are used to determine crystal structures and orientations of minerals), photons (characteristic X-rays that are used for elemental analysis), visible light, and heat. Secondary electrons and backscattered electrons are commonly used for imaging samples: secondary electrons are most valuable for showing morphology and topography on samples and backscattered electrons are most valuable for illustrating contrasts in composition in multi-phase samples.

Microstructure of raw powders, conventionally and flash-sintered samples was examined by JEOL JSM-5500 scanning electron microscopy (SEM) attached with energy dispersive x-ray spectroscopy (EDXS or EDS). Images were taken at accel-

erating voltage of 10-20 kV under the magnification x1000- x10000. EDS analyses are observed at accelerating voltage of 20 kV, spot size 38 μm and working distance of 20 mm. Grain size of the samples were estimated from linear intercept method.

3.4.4 Electrical conductivity

The flash-effect which involves fast conductivity increase and sintering was investigated through the property of electrical conductivity controlled under electric field (I-V characteristics) and temperature. The measurement was performed in 4-point type arrangement using the same set of instruments those were used for the flash-sintering. For electrical conductivity sintered specimens were considered as they do not undergo any dimensional change and furnish reliable conductivity values. For observing the conductivity against the temperature, furnace was heated with 5°C/min while applying constant fields. For I-V curves, choice of increasing rate of electric field was limited to the experimental constraint of resolution of power supply (voltage can be set up to 2 decimal point in manual control) and the maximum field was to protect the connecting wires and the specimens from excessive heating since no maximum limit of the current was set.

In case of MnCo_2O_4 , conductivity with respect to temperature was recorded on 1050 and 1300°C-sintered specimens, heated up at the rate of 5°C/min while applying a field of ~ 0.25 V/cm. The two sintering temperatures were chosen as to observe the difference in the conductivity behaviors since MnCo_2O_4 is not a stable phase; it reduces to secondary phase at higher temperatures which affects the conductivity [1,2]. After confirming the effect of sintering temperature on conductivity behavior, electrical conductivity under electric field (I-V characteristics) was recorded on 1300°C-sintered MnCo_2O_4 specimens at constant furnace temperatures ranging from 200-700°C in the steps of 100°C. The field was increased with a rate of 8 mV/cm-s up to approximately 7.0 V/cm. To investigate further, the electric field was varied up and down in a continuous cycle at these temperatures (200-700°C) with simultaneous recording of specimen temperature using pyrometer.

In case of LSCF, electrical conductivity under electric field and temperature are recorded in following two ways:

- 1) On green specimen under constant field (5.0 and 7.5 V/cm) and variable temperature in the same way as in the flash-sintering tests: only the time (and furnace temperature) of the measurement was extended to larger values to record the material conductivity after the flash-effect.
- 2) On 1300°C-sintered specimen
 - Under constant electric field (0.1-1.7 V/cm), varying the temperature
 - At constant temperature (18, and 100-500°C) varying the electric field. Electric field was increased with a rate of ~7 mV/cm-s up to ~1.7 V/cm.

For being highly conductive, electric field was chosen to be smaller than those that can create flash-effect in LSCF. Its high conductivity generates a lot of current in dense specimen, even with a small voltage, which causes excessive heating of wires and sample in our experiments arrangement and thereby puts a constraint on the choice of voltage. For the same reason, the conductivity behavior during and after flash-effect was analyzed in sintering experiment, on green specimen.

Electrical conductivity of LSCF/GDC composites is recorded on dense specimens (at 1300°C for 2 h) under electric field and temperature in the same as for LSCF.

3.4.5 Thermogravimetry (TG)/Differential Thermal Analyzer (DTA)

Thermo gravimetric (TG) is a technique in which the change in mass of a substance is measured as a function of temperature, while the substance is subjected to a controlled temperature programme. Controlled temperature programme means

- heating and/or cooling at a linear rate
- isothermal measurements
- combinations of heating, cooling and isothermal stages

Mass of a sample can vary for any physical and chemical processes occurring upon increasing the temperature. TG analysis provide information about physical phenomena, such as second-order phase transitions including vaporization, absorption, adsorption and desorption, and likewise, about chemical phenomena including dehydration, decomposition and solid state reactions (e.g. oxidation or reduction). Differential thermal analysis (DTA) is a thermal technique in which temperature of sample (T_S) is compared with the thermally inert material or furnace temperature (T_f) as the sample is heated or cooled at a uniform rate. The temperature changes in the sample, which lead to the absorption or evolution of heat, can be detected relative to inert reference. Temperature of the sample changes due to phase change reactions, crystallization, melting, sublimation, vaporization, dehydration, reduction, oxidation etc. Generally phase transition, dehydration, reduction and some decomposition are exothermic. By using ($T_S - T_f$) differential method, a small temperature changes can be easily detected, while the peak area is proportional to the enthalpy changes ($\pm\Delta H$) and sample mass.

Thermo-gravimetric data for MnCo_2O_4 and LSCF powder samples were collected using NETZSCH Gerätebau STA 409 thermo-balance, combined with differential thermal analyzer. The ability to perform these complementary measurements simultaneously aids in the characterization of materials and provides better verification and interpretation of results. The measurements were performed at constant rate of 2-40°C/min up to 1500°C in air. Prior to the experiment, the powders were treated at 1300°C for 1 h in order to remove any volatile substance. Pure alumina powder was used as a reference in alumina crucible.

Chapter IV

Results and Discussions

Part of this chapter has been published in:

1) Anshu Gaur, Vincenzo M Sglavo,

“Flash-sintering of MnCo_2O_4 and its Relation to Phase Stability”

Journal of European Ceramic Society, volume 34 (2014) pages 2391-2400

2) Anshu Gaur, Vincenzo M Sglavo,

“Flash-sintering of $(\text{La}, \text{Sr})(\text{Co}, \text{Fe})\text{O}_3$ and its Possible Mechanism”,

Journal of Materials Science (2014)

4.1 Flash-sintering of MnCo_2O_4

4.1.1 Flash-sintering

4.1.1.1 Power dissipation and Shrinkage

The variation of power dissipation of 67%-dense pre-sintered MnCo_2O_4 sample as a function of furnace temperature, taken under different applied electric fields, are presented in Fig. 4.1(a); power dissipation is calculated from the product of applied electric field and the current density through the sample. It is clearly shown that the electric field has strong influence on the power dissipation behavior of the sample. At relatively low applied field (2.5 V/cm) the power dissipation shows almost linear dependence on the furnace temperature up to 550°C, which reflects the usual (increasing) conductivity behavior of MnCo_2O_4 [9,119]. For fields greater than 5 V/cm the linear dependence occurs with slightly higher slopes up to an onset temperature

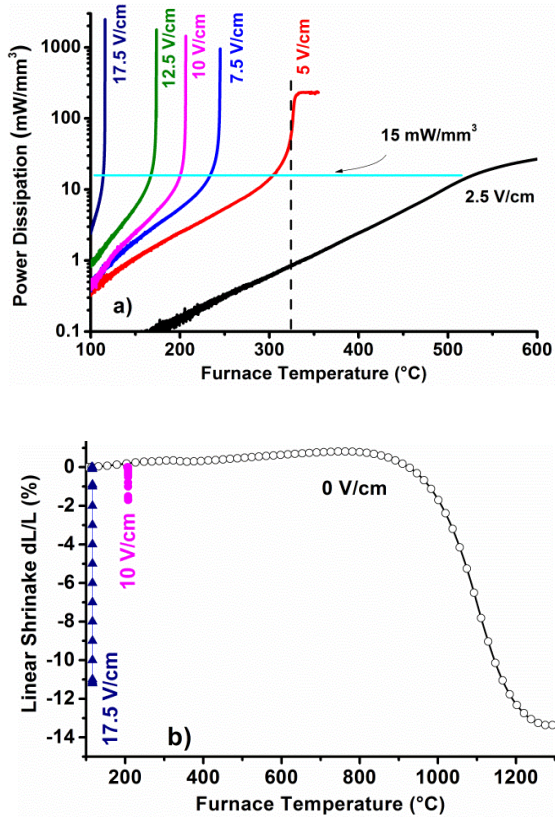


Figure 4.1: a) Power dissipation and b) shrinkage of 67%- dense pre-sintered MnCo₂O₄ samples as function of furnace temperature under different applied electric fields.

beyond which a sudden rise in power dissipation is observed. The higher slope of the power dissipation represents higher rate of conductivity increase and can be associated to the Joule effect whereas sudden rise in the power dissipation curve, after the almost-linear part, is the sign of flash-sintering [20,27]. Such increase occurs so abruptly that it can not be associated to be derived from thermal effect. However, corresponding to such flash-effect of power dissipation quick shrinkage occurs as shown in Fig. 4.1(b) for 10.0 and 17.5 V/cm. The sintering is shown to happen at the similar fast rate and the level of shrinkage under 17.5 V/cm is higher than that at 10.0 V/cm. These shrinkages are occurred at 120 and 210°C furnace temperatures which

are far lower than that required without electric field (0 V/cm case in Fig. 4.1(b)). Again from Fig. 4.1(a), it is observed that the initiation of such flash-sintering behavior for MnCo_2O_4 is commenced under 5 V/cm and 320°C threshold field and threshold furnace temperature, respectively; the power dissipation at the onset of the effect was $\sim 15 \text{ mW/mm}^3$. At relatively higher fields, the dissipation plots show similar sudden increase behavior at lower temperatures but commencing at the same power level. The observation of threshold field is in agreement with previous works on MnCo_2O_4 whereas the deviation of threshold temperature of 475°C from the reported literature [27] by $\sim 155^\circ\text{C}$ is expected to be due to the difference in the initial density of the samples.

4.1.1.2 Flash-parameter: Relation with density

As a matter of fact, flash-effect depends on the conductivity of the material and it is described by the combination of electric field and temperature [9,120]; the density of the sample has therefore a significant role on flash-parameters. The variation of onset furnace temperature as a function of electric field for different density samples (green: 60%, pre-sintered: 67%, sintered at 1300°C: full density) are presented in Fig. 4.2. The abrupt change that occurs during flash-sintering is observed in all samples, whether it is tightly-packed sintered or loosely-held green sample. According to such observation and previous works [21,81], the flash-effect of rapid increase in the conductivity and quick sintering is suggested to be an intrinsic property of the material, not simply connected to resistive heating (during rapid increase of current) at particle-particle contacts in the green sample; it is equally evident in dense samples also. In other words, it is proposed that every material could show specific flash-effect. Samples with different densities show the same threshold field of about 5 V/cm; but the onset temperatures at the same applied field changes with the density of the samples. The onset temperature difference of about 120°C between green and fully dense sample was observed at 10 V/cm. In general, the conductivity of the materials is a coupled response of bulk of the particle and inter-particle connectivity in the sample [2,8]. The constant threshold field observed for different density samples suggests that the conductivity of the spinel dominantly comes from the bulk prop-

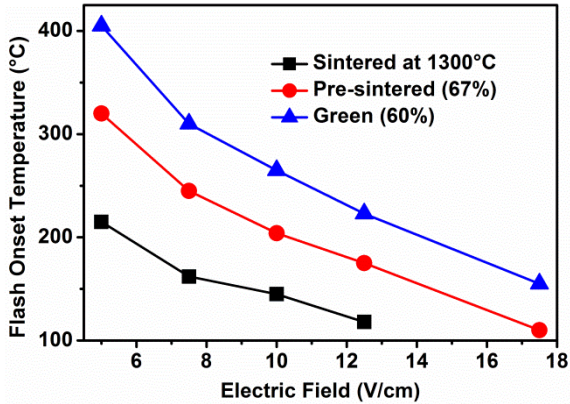


Figure 4.2: Variation of flash onset temperature with electric field for different density samples (Green-60%, Pre-sintered-67% and sintered at 1300°C)

ties and even a small channel through particle-particle connection can provide such conductivity that does not significantly affect the flash-parameter. On the other hand the deviation in the onset temperatures is expected to be associated to the difference in the inter-particle connectivity in the samples. Similar observation on the conductivity of MnCo_2O_4 has been previously reported where inter-particle connections lead to enhanced conductivity of the material [9]. The pre-sintered sample with 67% density, shown in the Fig. 4.2, shows flash-sintering at much lower furnace temperatures, at about 120-250°C, under 7.5-17.5 V/cm field. The processing temperature, here, is therefore 1000-1100°C lower than conventional heat treatment requirement of 1300°C (Fig. 4.1(b)). From this result we propose that MnCo_2O_4 material can be sintered by the flash-effect at 120-250°C without the requirement of high electric fields.

4.1.1.3 Specimen Temperature

The evolution of the 67%-dense pre-sintered sample under flash-sintering is here analyzed. The specimen temperature (T_s) measured by pyrometer during flash-sintering, along with the details of the applied field and power dissipation across the samples, is listed in the Table. 4.1. The amount of power dissipation observed for MnCo_2O_4 spinel reported in Fig. 4.1 as well as in the Table is substantially high com-

pared to those required for the flash-sintering of other low-conductive materials [20,24,26]. Further, increase of 50-75°C in specimen temperature involves with 250-300 mW/mm³ increase in power dissipation. Such high power dissipation values are

Table 4.1: Flash sintering parameter of 67% dense MnCo₂O₄ sample treated to different electric field (V= 95-99 mm³)

Sample Name*	Furnace Temp (°C)	E-Field (V/cm)	Maximum Current Density (A/mm ²)	Maximum Power Dissipation (mW/mm ³)	Specimen Temp (°C)
-	320	5.0	0.48 (material's limit)	240	<900
FS925	250	7.5	1.25 (material's limit)	960	925
FS975	210	10.0	1.40	1445	975
FS1050	170	12.5	1.40	1800	1050
FS1100	145	15.0	1.40	2160	1100
FS1160	120	17.5	1.40	2475	1160
FS1320	120	17.5	1.60	2830	1320

directly related to the low activation energy and higher conductivity of MnCo₂O₄. The change in specimen temperature during flash-sintering as a function of time for the 67%- dense pre-sintered MnCo₂O₄ sample under the electric field of 10 V/cm is presented in Fig. 4.3. The variation of power dissipation (solid line) with time is also included in the same figure in order to correlate the two behaviors. The power dissipation curve is the magnified part of 10 V/cm curve presented in Fig. 4.1(a) (pink line). It is shown to have anomalous effect at 210°C furnace temperature. A sudden increase in power dissipation from a minimum of 15 mW/mm³ to a maximum of 1445 mW/mm³ is observed within a short interval of time (~ 5 s). Afterwards drop in the power dissipation is due to the maximum current limit specified in the measurement set up, where the power supply switches from constant voltage to constant current control. The decrease in the power dissipation in such constant current region is a sign of conductivity increase [21]. After the power dissipation decrease, a steady state value is reached at longer hold time, indicating the saturation of conductivity through the sample. Similar to power dissipation, the specimen temperature exhibits sharp increase with time and reaches to ~975°C under 10.0 V/. Such increase in the specimen temperature is the outcome of Joule effect, occurred for large increase in

the power dissipation or the conductivity at very low furnace temperature (210°C). The observation is manifested in the time lag (~2-3 s) between the two curves, where the specimen temperature follows the power dissipation trend. The reliability of such

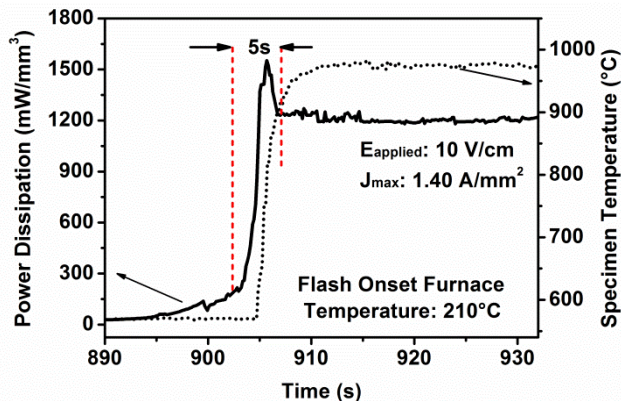


Figure 4.3: Power dissipation and specimen temperature as functions of time for FS975 sample, flash-sintered under 10 V/cm.

observation under fast effect is in that in order to record the power dissipation and temperature, clocks were matched and data are recorded every 0.17-0.20 s (approximately 10-15 data in 2-3 s). Under such change, specimen achieves the maximum temperature in the stabilization region, just before the steady state power dissipation. This increase in local temperature, during the (unstable) growth of power dissipation, facilitates the flash-sintering of the sample. At higher applied fields, relatively higher local temperature is achieved in the same time interval, which involves comparatively more drastic changes in power dissipation and specimen temperature (Table 4.1). Similar observation of flash-sintering during the stabilization of power dissipation, in the short time interval between the peak and the constant value, is reported for zirconia [21].

4.1.2 Microstructure Evolution

The extent of sintering was analyzed by the SEM for the samples subjected to various applied fields. The micrographs of 67%- dense pre-sintered MnCo_2O_4 sample

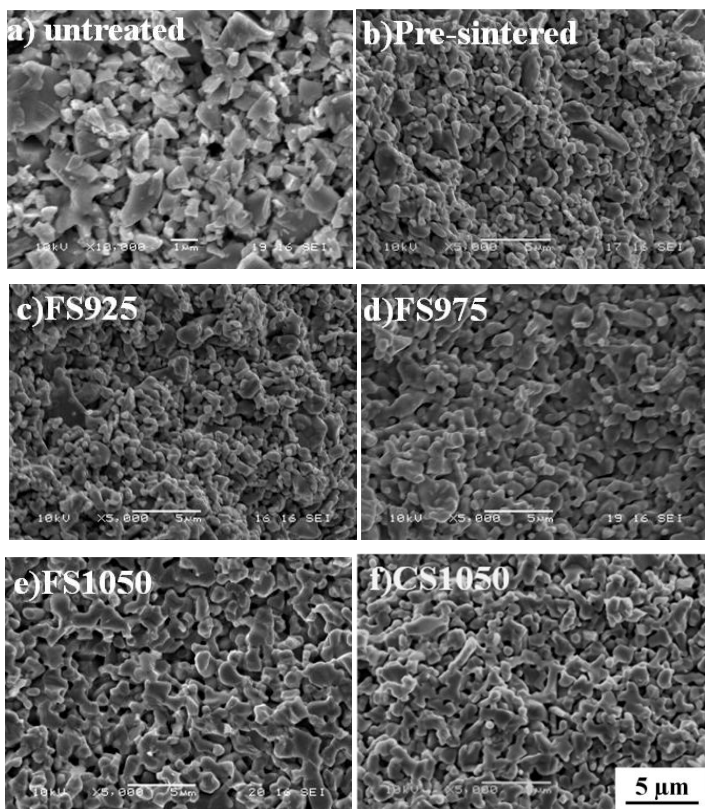


Figure 4.4: SEM micrograph of a) untreated, b) pre-sintered, flash-sintered sample namely c) FS925, d) FS975, e) FS1050, and conventionally-sintered MnCo_2O_4 sample, f) CS1050 presented for comparison. FS samples are produced under $7.5\text{-}12.5\text{ V cm}^{-1}$ at furnace temperatures of $120\text{-}250^\circ\text{C}$.

subjected to different applied electric field ($7.5\text{-}17.5\text{ V/cm}$) which in return produces different local temperatures are shown in Fig. 4.4. The details of field applied, furnace temperature and power dissipation are provided in Table 4.1. The microstructure of conventionally-sintered (CS) samples at similar temperatures is also compared. In this case, the furnace temperature is considered as the specimen temperature. The CS samples are sintered with a heating rate of 5°C/min , with hold time of 60 s and furnace temperature is measured by keeping the furnace thermocouple close to the sample surface for attaining the good correlation with FS samples. Sam-

ple are here labeled with prefix FS for flash-sintered and CS for conventionally-sintered, followed by the specimen temperature (Table 4.1).

The first two figures 4.4(a) and 4.4(b) show the difference in the microstructure of pre-sintered sample from untreated one, pre-sintered samples have been taken for flash-sintering experiments. The microstructure of FS925 sample (Fig. 4.4(c)) shows close resemblance to that of pre-sintered sample in Fig. 4.4(b), which suggests that the microstructure is not affected by the flash-effect observed at such low field and the specimen temperature. The microstructure of FS975 specimen (Fig. 4.4(d)) shows an incipient stage of grain growth, which became well pronounced in FS1050 sample (Fig. 4.4(e)). The grain morphology of CS sample sintered at 1050°C (Fig. 4.4(e)) exactly replicates that of FS1050 (Fig. 4.4(f)). Nevertheless, the extent of porosity estimated by image-binarisation [122] using MATLAB software considering two threshold values, 0.20 and 0.15, are shown in Fig. 4.5. It suggests that the FS sample has comparatively higher porous nature. The higher porosity in FS samples is expected to be associated to flash-sintering effect (rapid Joule heating). At higher temperature, a sudden change in the morphology is observed for FS1100 (Fig. 4.6(g)): the micrograph shows that the grains are substantially larger and grain to

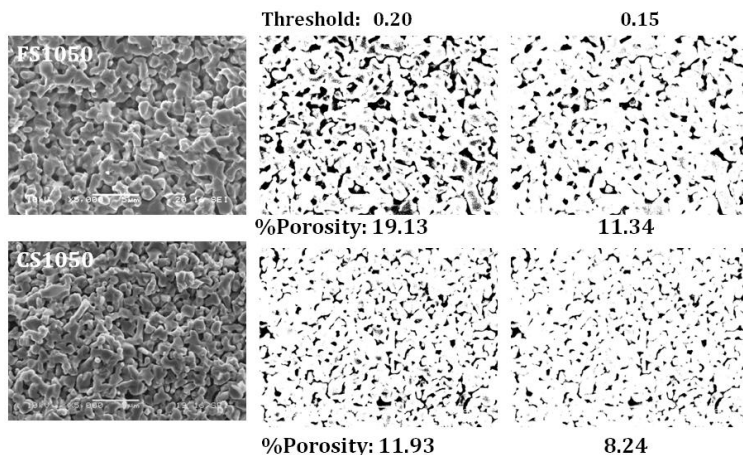


Figure 4.5: Porosity evaluation of FS1050 and CS1050 samples from image binarisation using MATLAB under different threshold values

grain connections are developed with reduced porosity. Conversely, the CS1100 sample (Fig. 4.6(h)) shows poor morphology with lower grain size and higher porosity compared to its counterpart of FS1100 (Fig. 4.6(g)). Similar observations are found for further higher temperature treated samples. A fully connected grain structure with average grain size of about $\sim 8 \mu\text{m}$ and without open porosity is observed for FS1160 sample (Fig. 4.6(i)). The CS sample produced at the same temperature (1160°C) possesses smaller grains with average grain size of $\sim 5 \mu\text{m}$ (Fig. 4.6(j)). The morphology of FS sample sintered at 1320°C (Fig. 4.6(k)) shows melted-like appearance

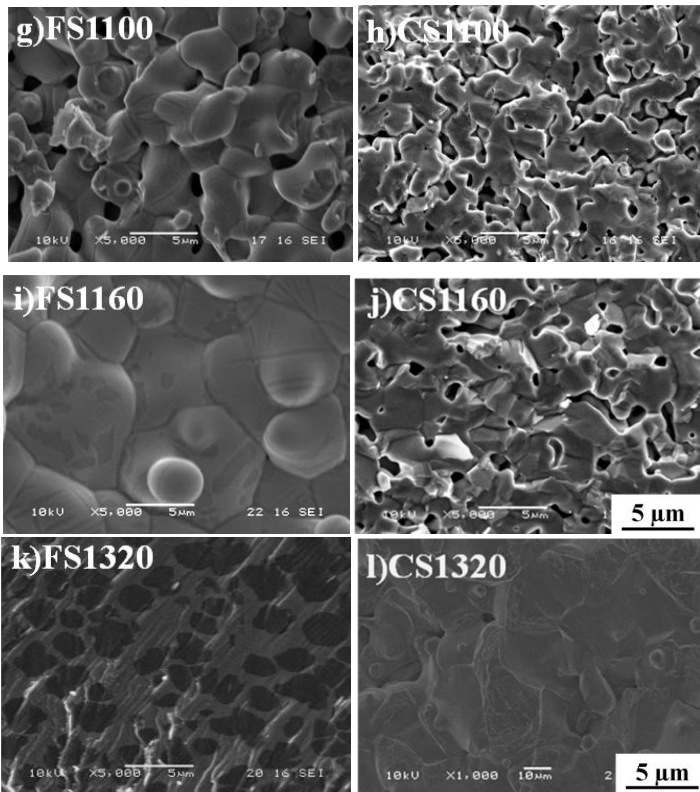


Figure 4.6: SEM micrograph of MnCo_2O_4 samples, flash-sintered namely g) FS1100, i) FS1160 and k) FS1320, and conventionally-sintered, h) CS1100, j) CS1160 and l) CS1320 presented for comparison. FS samples are produced under $12.5\text{-}17.5\text{V cm}^{-1}$ at furnace temperatures of $120\text{-}250^\circ\text{C}$.

without clear visibility of grain boundary in contrast to large grains of CS1320 (Fig. 4.6(l)). Black spots in Fig. 4.6(k) represent regions with higher Co concentration as detected by EDS; such regions originate from the reduction of MnCo_2O_4 to CoO [9] which will be discussed in the next section.

From SEM analysis, we conclude that the electric field sintering has a strong effect on the microstructure of the specimen at high temperatures. The FS sample microstructure sintered at lower temperatures (up to 1000-1050°C) has close resemblance with that of its counterpart of CS with slight change in the porosity; FS samples are more porous. It is inferred that the strong flash-effect and fast change in specimen temperature (Fig. 2) is not the only requirement for the flash-sintering (with additional sintering over CS) of MnCo_2O_5 . However, a fully dense morphology with interconnected grain structure is observed at higher temperature (in excess of 1100°C). This observation is dissimilar to that made on FS zirconia, where relatively higher shrinkage is reported over the conventional sintering at temperatures from 950-1600°C [80]. In addition, MnCo_2O_4 forms relatively larger grains in flash-sintering, the fast heating and sintering effect does not retard the grain-growth kinetics. It is again dissimilar from previous findings on zirconia [72], SrTiO_3 [40] and GDC [78] where similar or smaller grain size, is reported under flash-sintering. Flash-sintering was previously thought to inhibit grain growth due to lower processing time (and temperature) but from the results obtained on MnCo_2O_4 this can not be a general statement.

4.1.3 Spinel Phase-Stability Analysis

The phase composition of 67%-dense pre-sintered MnCo_2O_4 sample under flash- and conventional-sintering at different temperature was analyzed by X-ray diffraction (XRD). The XRD patterns are shown in Fig. 4.7. The pattern of FS975 sample (Fig. 4.7(a)) shows sharp diffraction pattern which exactly coincides with that of the raw powder. The XRD pattern was identified as belonging to the cubic spinel phase of MnCo_2O_4 (JCPDS File No: 023-1237). The spinel diffraction pattern is well preserved at higher sintering temperatures up to 1050°C, i.e. in FS975 and FS1050

respectively. At further higher sintering temperatures, a sharp peak centered around $2\theta=42.01^\circ$ and a small peak appearing as right shoulder of the (311) reflection of MnCo_2O_4 phase are observed. These new set of peaks are identified as belonging to the face centered cubic structure of CoO according to JCPDS file No: 065-2902. The intensity of the CoO phase pattern is observed to increase with sintering temperature along with the suppression of original MnCo_2O_4 phase pattern (Fig. 4.7(a)). In general, the intensities ratio of the two different phases is proportional to the weight fraction of the substances [118,123]:

$$\frac{I_{\text{CoO}}}{I_{\text{MnCo}_2\text{O}_4}} = \frac{w_{\text{CoO}}}{w_{\text{MnCo}_2\text{O}_4}} \quad (4.1)$$

where $I_{\text{MnCo}_2\text{O}_4}$ and I_{CoO} are the intensity of strong XRD reflection of MnCo_2O_4 and CoO, respectively, while $w_{\text{MnCo}_2\text{O}_4}$ and w_{CoO} are the weight fractions of MnCo_2O_4 and CoO, respectively. The ratio of the area (integrated intensity) under the strong peaks of (200) CoO and (311) MnCo_2O_4 is calculated and its variation as function of specimen temperature is shown in the Fig. 4.8. The (311) reflection of MnCo_2O_4 at $2\theta = 36^\circ$ shows a right shoulder at $2\theta = 36.5^\circ$ of (111) reflection of CoO phase. The strong peak at $2\theta = 36^\circ$ is de-convoluted into two peaks centered at 36° and 36.5° and then the area under the (311) peak is evaluated. The increase in the intensity ratio is a measure of the growth of CoO or of the suppression of MnCo_2O_4 . Fig. 4.8 shows a systematic increasing trend of the intensity ratio with the temperature above 1050°C . This is also evident from the peak intensities variation in Fig. 4.7(a). Conversely, CS samples are mono-phasic up to much higher temperatures. The set of XRD diffraction pattern presented in Fig. 4.7(b) for CS samples shows that the single phase of MnCo_2O_4 is preserved up to 1100°C . A weak CoO pattern is observed for CS1160, whose intensity increases for higher sintering temperature as in sample CS1320. The ratio of the peak intensity presented in the inset of Fig. 4.8 shows that the curve deviates from its counterpart of FS samples. The FS samples show sudden increase in the peak intensity ratio at 1100°C . A comparison between FS and CS spectra shows greatly enhanced cobalt oxide peaks intensity for FS samples. The two treatments (FS and CS) are performed for the same sintering time of 60 s with

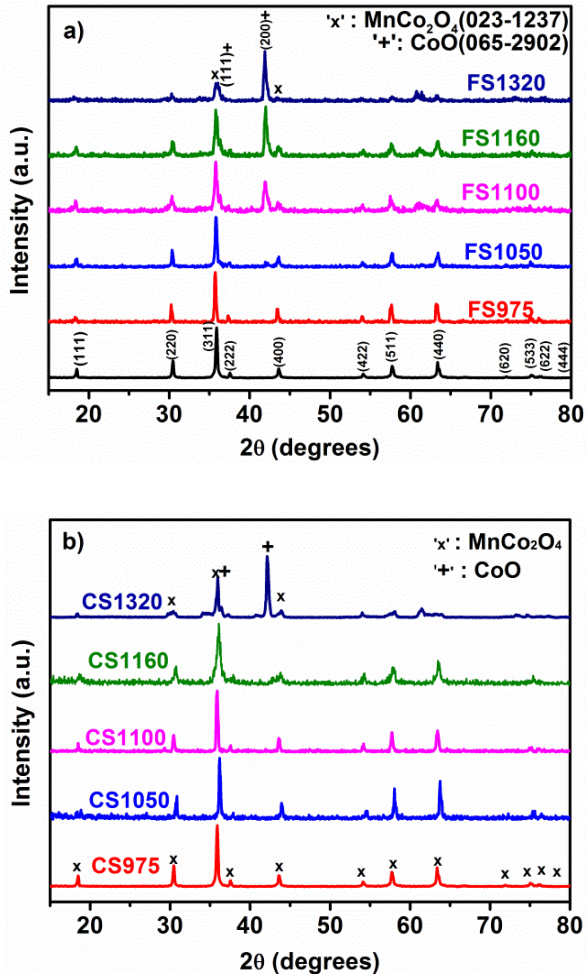


Figure 4.7: XRD of flash-sintered samples namely a) FS975, FS1050, FS1100, FS1150 and FS1320 along with as-observed MnCo₂O₄ powder, and conventionally-sintered samples b) CS975, CS1050, CS1100, CS1160 and CS1320.

CS at the heating rate of 5°C/min and FS at 9600°C/min (160°C/s) or more. From XRD study we conclude that the spinel phase is stable up to specimen temperatures of 1050°C in flash-sintering and 1160°C in conventional-sintering. Both conventional sintering and electric field assisted flash-sintering shows the formation of secondary

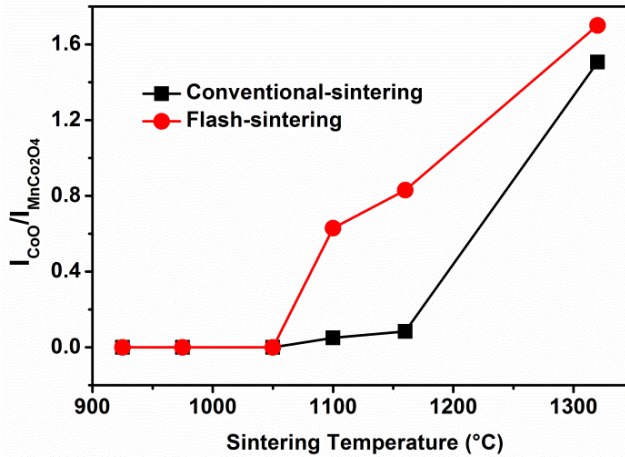


Figure 4.8: The weight fraction of CoO and MnCo₂O₄ for flash- and conventionally-sintered MnCo₂O₄ samples as functions of sintering temperature.

phase at higher specimen temperatures. However, the flash-sintering shows CoO phase concentration higher than its counterpart at all corresponding sintering temperatures. The observations from XRD are found in correlation with SEM results where flash-sintering is found to enhance over conventional at temperatures of 1100°C and higher. From this study we conclude that the microstructural-growth and phase-decomposition are shared processes and the sintering might have derived through the actions involved in the phase decomposition.

4.1.4 Electrical Conductivity of MnCo₂O₄

Flash-sintering phenomenon starts with an abrupt increase in the conductivity, subsequent Joule heating followed by mass-diffusions which eventually leads to sintering. The reason of such rapid increase of conductivity under applied electric fields greater than the threshold value is still not clear. Therefore, to investigate the details of flash-effect in MnCo₂O₄, we carried out electrical conductivity and I-V measurements on green and sintered samples applying fields of the range that may cause flash-effect.

4.1.4.1 On green specimen: I-V relation of flash-effect

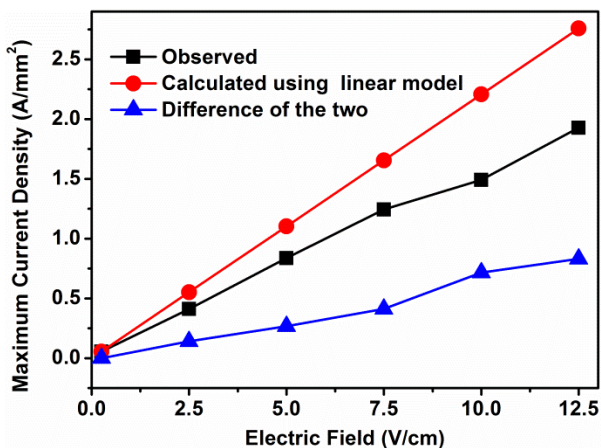


Figure 4.9: Maximum current density observed under different electric fields: flash-sintering.

In order to make I-V relation of the flash-effect, maximum current (without any control over the current under the flash-effect) is recorded at different electric fields (0.25-12.5 V/cm) and is presented in Fig. 4.9 (data represented in black square symbol). These are the currents (for fields 5.0-12.5 V/cm) which came after strong non-linear increase in the conductivity. Each point in the graph represents the extent of the field to generate the charge carriers. A hypothetical linear current-voltage response has also been made at the same electric fields (from the current-voltage relation recorded at 1200°C for 0.25 V/cm) to show the deviation from linear behavior (data represented in red-circular symbol). Difference in two responses (plotted in blue-triangular symbol) is found to increase with the increase of the field. The current observed in flash-effect, which is the representation of generated carriers, do not increase in linear proportion, but decline with electric-field showing large difference at higher electric fields. This behavior corresponds to stabilization of flash-effect and might be related to the conductivity property of the spinel [2,18].

4.1.4.2 Effect of Sintering Temperature on Conductivity

The conductivity of MnCo_2O_4 spinel sintered at 1050°C and 1300°C for 2 h was measured in an experimental arrangement similar to that used for flash-sintering and the results are compared in Fig. 4.10. The samples are subjected to sintering to avoid stimulated effects due to dimensional-changes and porosity. Measurement for two densities is performed to confirm the conductivity behavior of sintered MnCo_2O_4

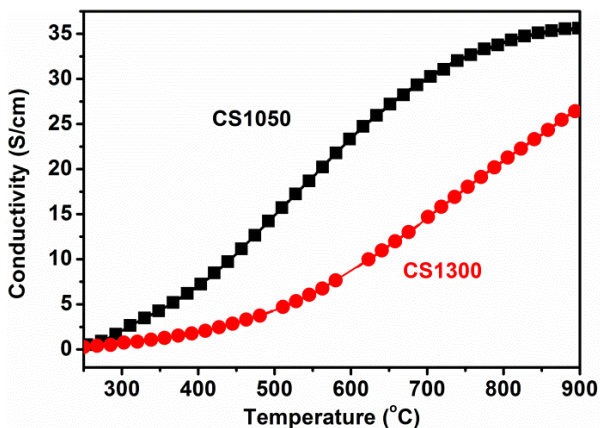


Figure 4.10: Electrical conductivity of MnCo_2O_4 , conventionally sintered at 1050°C and 1300°C for 1 h, as functions of temperature

samples which will be used further for investigating electric field effect on conductivity. From Fig. 4.10, one can observe that the conductivity of both samples increases with temperature. The conductivity is lower for the sample sintered at higher temperature of 1300°C with no appreciable change in the semiconducting behavior. The decrease in the conductivity is expected to be due to the formation of low-conductive secondary CoO phase [101] as it is clear from the XRD analysis. Yi et al. reported the growth of similar low conductive phase when MnCo_2O_4 is sintered at higher temperature [9]. The conductivity of MnCo_2O_4 sample sintered at 1300°C (Fig. 4.10) is lower than that reported in previous works on Mn-Co oxide [9,30], this probably being related to contact resistance and different experimental arrangement. However, in the present investigation, we are interested on the variation of conductivity with temperature. With the observation that the high temperature sintering does not affect the

conductivity behavior of MnCo_2O_4 , we carried out conductivity and current-voltage measurements on fully dense MnCo_2O_4 samples sintered at 1300°C , discussed in further sections.

4.1.4.3 On dense Specimen

4.1.4.3.1 Conductivity versus Temperature: Effect of electric field

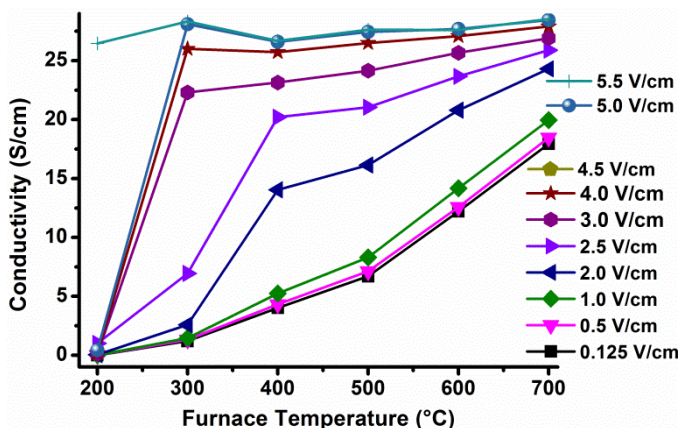


Figure 4.11: Conductivity of MnCo_2O_4 as functions of temperature, observed under different electric fields (0.125-5.5 V/cm). ~ 5 V/cm causes flash-effect in MnCo_2O_4 sample (Fig. 4.2).

The conductivity of 1300°C -sintered MnCo_2O_4 sample as function of temperature observed under different electric field (0.125-5.5 V/cm) is compared in Fig. 4.11. Under smaller electric field of 0.125-0.5 V/cm, the conductivity shows a smooth increase with temperature having overlapped data points for different fields. It represents the usual conductivity trend of MnCo_2O_4 (as shown in Fig. 4.10) and suggests that the conductivity is invariable with respect to the electric field (ohmic behavior). In other words, field is small enough to perturb the material system and therefore conductivity increases in an ohmic way. The conductivity of MnCo_2O_4 is governed by small polaron hopping. In the mathematical form, the temperature dependence of conductivity is reported by Arrhenius relation, as,

$$\sigma = \frac{A}{T} \exp\left(-\frac{E_a}{RT}\right) \quad (4.2)$$

where A is material's constant and depends on the carrier concentration, E_a is the activation energy, R gas constant ($= 8.314 \text{ J/mol-K} = 5.189 \times 10^{-19} \text{ eV/mol-K}$) and T absolute temperature. Using this equation activation energy is calculated from the slope of $\log_e(\sigma \cdot T)$ versus $1/T$ graph and is shown in the Fig. 4.12. The activation energy of MnCo_2O_4 is calculated to be 0.37 eV under $0.125\text{-}0.5 \text{ V/cm}$ which is higher than the reported ones [119,124]; it is associated with the different experimental arrangement. However, from the Fig. 4.12, a linear relation exist between $\log_e(\sigma \cdot T)$ and $1000/T$ which confirms that the MnCo_2O_4 conduction mechanism comes from thermally activated hopping of small polarons between $\text{Co}^{2+}/\text{Co}^{3+}$ and $\text{Mn}^{3+}/\text{Mn}^{4+}$ pairs [41,100], and whose temperature dependence is given by Eq. 4.1.

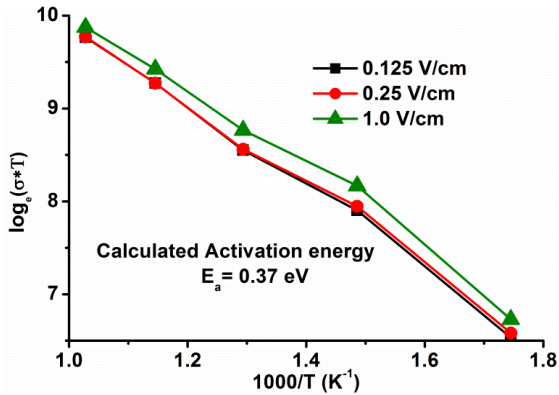


Figure 4.12: Arrhenius plot of the low-field conductivity as a function of temperature.

Again from the Fig. 4.11, some deviations in the conductivity are observed for 1 V/cm case; the same is visible in Arrhenius plot as a linear response but with smaller slope; such change can be associated with Joule effect. With further increase of electric field, the conductivity starts showing jump-kind of behavior at lower-side of temperatures. Conductivity after such jump follows smooth increasing behavior with temperature which seems following the usual tendency of the material. Additionally, the temperature of such a jump found to move towards lower values with the in-

crease of electric field. For 3-5 V/cm, it occurs at 300°C and for 5.5 V/cm at 200°C only. Correlating with Fig. 4.2, the field close to 5 V/cm can cause flash-effect in dense MnCo₂O₄ sample and the same we observe here. The strong impact of electric field on the conductivity for 5.5 V/cm case, unlike for low field cases, does not seem to derive from Joule effect since it occurred all of a sudden at starting temperature of 200°C. Therefore, for the considered range, electric field has strong influence on the conductivity versus temperature curves and the dependences vary from ohmic (field independent) to non-ohmic (field dependent) within a short range of electric field i.e. 0.125-5.5 V/cm.

4.1.4.3.2 Conductivity versus Electric field: Effect of Temperature

Smooth-to-rapid effect of electric field is clearly observable in the current-voltage behavior. I-V characteristics of 1300°C-sintered MnCo₂O₄ samples measured at different furnace temperatures (200-700°C) are compared in Fig. 4.13(a). The electric field is applied at an increasing rate of $\sim 8 \text{ mV cm}^{-1} \text{ s}^{-1}$. From the curve it is observed that the furnace temperature has significant influence on the I-V behavior of MnCo₂O₄ sample. At 200°C, the current grows linearly up to 5.18 V/cm but with very small current density compared to that recorded at higher temperatures. As the field reaches 5.18 V/cm the current density increases at faster rate having appearance of a flash-like effect. The increasing rate of the current was so fast that at the same time the field decreased down showing backward flow in the I-V characteristics (Fig. 4.13(a)). A comparison with the Fig. 4.2 for the sample sintered at 1300°C suggests that there is a close match between the temperature and field values for flash-effect, (210°C, 5.0 V/cm) and (200°C, 5.18 V/cm), where one measurement is performed in constant-field experiment and the other at constant-temperature. Such observation represents the consistency of flash-effect, and invariability of the material's property to respond under the electric field. Fig. 4.13(a) shows that the flash characteristic nature of MnCo₂O₄ in I-V curve gradually reduces to smooth behavior at higher temperatures. For temperature of 300°C, the current shows a linear dependence on the voltage with slightly higher slope and sudden increase at 2.1 V/cm, which is much earlier than it was at 200°C. However, the extent of current density

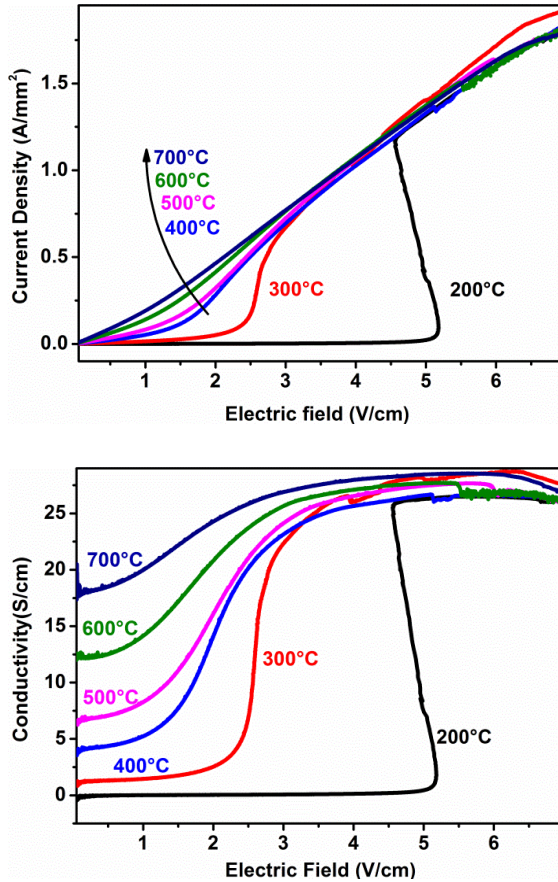


Figure 4.13: I-V characteristics of 1300°C-sintered MnCo₂O₄, recorded at 200-700°C furnace temperatures, presented as a) current density and b) conductivity as functions of electric field.

increase at flash-effect field is relatively lower than that obtained at 200°C. At further higher furnace temperature, such flash effect is not observed and the I-V behavior is almost linear at 400-700°C temperatures with a not-significant non-linearity (in 1-2 V/cm field range). A similar observation is recorded from Fig. 4.1(a), where furnace temperatures higher than 200°C belong to the FAST regime, the material showing a smooth current increase. For all furnace temperatures, after the non-linear changes (either strong or moderate) the current increases linearly with the field.

The variation in the conductivity of MnCo_2O_4 samples sintered at 1300°C as a function of the applied electric field is shown in the Fig. 4.13(b). The flash-effect corresponding to increased conductivity is clear here. The conductivity reflects the same trend of I-V curve (Fig. 4.13(a)) and shows flash-like abrupt behavior at 200°C . It is observed that the conductivity increases in a non-linear manner with the applied field at all temperatures; the initial values at any temperature represent the conductivities by thermal-activation. The conductivity trend under electric field looks to be the same as observed under temperature (Fig. 4.11). However, the non-linearity feature varies with the furnace temperature. At 200°C , the conductivity is relatively very low, and almost constant until a critical field is reached, at which the spinel undergoes to a strong non-linear increase (flash-effect). The effect is so fast, and occurs at very low temperature that it is not expected to come from Joule-effect. For temperatures in excess of 200°C , the non-linear feature is comparatively modest but starts occurring at lower field-values. The highest temperature of 700°C and the lower $500\text{-}600^\circ\text{C}$ which are free from flash-like rapid effect (following from Fig. 4.2), the non-linearity of the conductivity might be associated with the Joule heating (also discussed in the next section). Therefore, all graphs show a systematic change from strong to moderate non-linear behavior from 200 to 700°C . Under different degree of non-linearity with the electric field, all curves seem to reach a common stable value. Similar temperature dependent consistent effect of electric field on conductivity is observed in YMnO_3 and other materials also [125,126].

4.1.4.3.3 Role of thermal-effect (Joule heating)

The discussions on the conductivity and flash-effect are extended considering the measurement of specimen temperature. The variation of specimen temperature (solid line) and current density (dotted line) with electric field for 1300°C -sintered MnCo_2O_4 sample recorded at different furnace temperatures are presented as functions of time in Fig. 4.14. In order to correlate the low- and high- temperature behavior, case of 200 and 600°C are arranged in one graph (Fig. 4.14(a)). Both, the specimen temperature and current density are interrelated and are observed to follow abrupt and gradual changes with time/electric field at 200°C and 600°C furnace

temperature, respectively (Fig. 4.14(a)). At 200°C, the specimen temperature rises abruptly to more than 900°C following the trend of the current density; afterwards, beyond the flash-effect, it increases almost linearly with the applied field. The changes are smoother at furnace temperature of 600°C. In any case, the specimen temperature rises above the furnace temperature by Joule heating. Close observation of 200°C curve in the inset of Fig. 4.14(a) shows that there is a time lag of 2-3 s between the two parameters and therefore suggests that it is the increase in the condu-

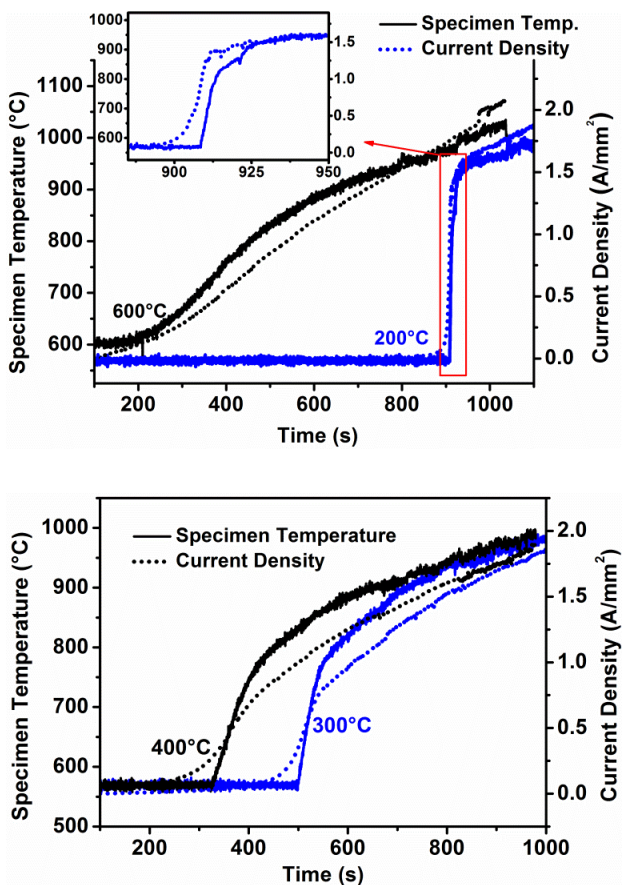


Figure 4.14: Current density and specimen temperature of MnCo_2O_4 samples sintered at 1300°C as functions of time recorded at a) 200 and 600°C, b) 300 and 400°C.

ctivity which drives the Joule-effect (also evident in Fig. 4.3). The same explanation is not applicable to 600°C case where conductivity and temperature changes are comparatively smooth. Therefore, the increase of conductivity is associated to come from thermal effects. For the cases of 300°C and 400°C in Fig. 4.14(b) which belong to the FAST regime from electric field assisted sintering description, we observe the same sign of rapid-effect and Joule-heating which is clearly visible in 200°C case; however, the changes are intermediate to 200- and 600°C-cases. Such sign of changes at 300-400°C clearly represent the stronger competence of electric field against temperature for increasing the conductivity compared to 600°C-case and the same is lesser compared to 200°C-case. Correlating the effect of temperature on conductivity versus electric field curves, it is observed that a smooth cross over occur between 'conductivity derived thermal-effect' and 'thermal effect activated conductivity'. In other words, a smooth crossover occurs between the capabilities of electric field and temperature for increasing the conductivity. Such effect of electric field on conductivity which depends upon the temperature, can be associated for the case of MnCo_2O_4 to Poole Frankel effect (for 500-600°C), electric field assisted tunneling (for 300-400°C) and direct tunneling by electric field (for 200°C) [127,128]. In the discussion of electric field assisted sintering, this cross over defines the two regime of sintering, flash associated to direct tunneling effect and FAST to Poole Frankel effect. Therefore, the conductivity results and its correlation from the reported effect follow from the competitive role of the two parameters; the electric field is more likely to have stronger influence on conductivity of Mn-Co spinel at lower temperatures which is observed to be involved with sintering of green specimen.

4.1.4.3.4 Hysteretic Behavior

The effect of electric field on the electrical conductivity of MnCo_2O_4 is further investigated under cyclic variation of field. Figure 4.15 shows I-V curve during cyclic change in the electric field (0.0-4.5-0.0 V/cm) recorded at 300°C. On reversing the voltage, the conductivity/current density does not decrease in a fast manner as it was happened during voltage increase and therefore it does not follow the same path but shows increased values in the form of hysteresis loop. Such kind of behavior was

observed at other temperatures also. Residual conductivity is observed with MgO doped alumina also [24] which is proposed to be the result of newly nucleated charged species during flash-effect.

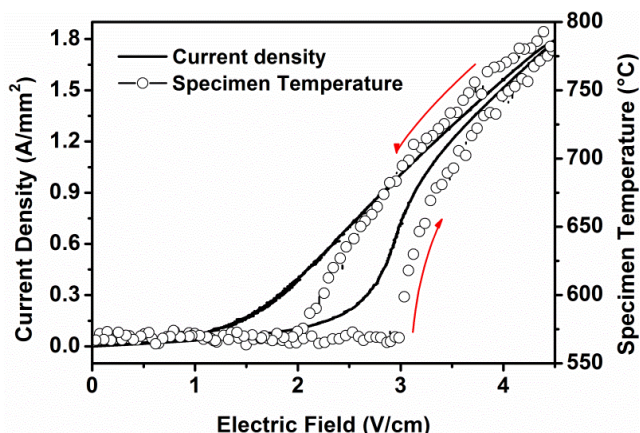


Figure 4.15: Hysteretic behavior of conductivity and specimen temperature of 1300°C-sintered MnCo_2O_4 measured at 300°C as function of electric field.

This residual occurrence of conductivity was better analyzed by the simultaneous sample temperature measurement. Hysteretic behavior was observed with sample temperature also. Temperature and conductivity found to follow each other. During reverse cycle, drop in temperature with field was rather smoother than that during forward cycle. Temperature did not decrease all of sudden, but continued to decrease gradually. Changes in sample temperature and conductivity are correlated. It is clear that during forward path Joule effect comes after sudden increase in the conductivity; a small time lag is involved between power dissipation and sample temperature (Fig. 4.15). So, electric field generated flash effect drives Joule heating and at the start of reverse cycle, local temperature starts with higher values. These temperatures are sufficient to support the higher conductivity of the spinel, and the stronger thermal effect weakens the role of electric field. It was somewhat like during forward cycle, local temperature is increased by sudden increase in conductivity by electric field effect. During reverse cycle, same temperature preserves the high conductivity state, giving rise to residual value when voltage is made lower to onset

value. The conductivity variation at 300°C is not as fast as it is at 200°C but still shows residual values.

From the quantitative comparison of the conductivity values in Figs. 4.10, 4.11 and 4.13(b), one can derive interesting correlation between the intrinsic conductivity and the conductivity under flash-effect. The conductivities (of 27.5-28.7 S/cm) after strong or modest flash-like-effect shows match with that (29.5 S/cm) recorded at 1000°C under purely thermal effect in Fig. 4.10. The specimen temperature after such flash-effect is observed to be approximately 1000°C and therefore in both cases similar conductivity is attained. Here, it is worth mentioning that conductivities shown in Fig. 4.10 are purely based on thermal effects, whereas in Figs. 4.11 and 4.13(b) it is assisted with the additional effects of electric-field. Electric field and temperature show a competitive behavior for increasing the conductivity. From the smooth crossover of electric field to temperature dependence, we suggest that the conductivity under electric field follows the same mechanism which is involved during its thermal activation i.e. small polaron hopping. Similar kind of temperature dependent ohmic to non-ohmic crossover is reported for YMnO_3 and Eu-O-N based ceramics [125,129] and is also observable on some non-ceramics [126,130,131]. All these have a common point of polaron-hopping based conduction mechanism; such thing could be a starting point to understand the sintering effect (molecular/ionic transitions) of electric field. The increase in conductivity is associated with the generation of charge carriers and the increasing rate depends on the temperature and the applied electric field. On the basis of presented results and after confirming the role of electric field, we made an attempt to understand the mechanism involved in the generation of charge carriers in terms of ionic/molecular transitions which causes increase in conductivity and eventually may lead to sintering of the spinel oxide.

4.1.5 Discussion

4.1.5.1 Electric field dependent (Polaron-hopping) Conductivity: Literature Review

This section is based on the literature review of electric field dependence on conductivity specially, based on polaron hopping which provides a support to our experimental observations of the electric field enhanced/derived conductivity and conclusions regarding the ionic transitions for flash-sintering during such a situation. There are sufficient number of literature discussing carrier transport in semiconductors under weak-moderate-strong electric field [29,30,31]. Also, there is particular subset discussing only about those based on polaron hopping conduction mechanism. Hopping is major transport mechanism in systems with strong localization such as carriers in disordered systems [134,135], as well as small polarons in crystal [125,136].

Application of electric field can stimulate the emission of charge carriers which is trapped in a localized state. The emission depends upon the strength of electric field and can be described by Poole-Frankel effect, phonon/electric field assisted tunneling and the direct tunneling as shown by a schematic diagram in Fig. 4.16 [132,137]. It depicts three situations of carrier emission in an applied electric field. The Poole-Frankel effect, applicable to lower electric fields, describes the increase of the thermal emission rate of carriers in an external electric field due to the lowering of the barrier associated with their Coulomb potential. In this situation the dependence of electric field is described by

$$\sigma \propto C \left[\exp \left\{ - \left(\frac{\varphi - \beta E^{1/2}}{kT} \right) \right\} \right] \quad (4.2)$$

where C is a constant, k is Boltzmann constant, T absolute temperature, φ barrier height, β barrier lowering coefficient given by $\beta = \left(e^3 / \pi \epsilon_r \epsilon_0 \right)^{1/2}$. In this case, $\log_e \sigma$ increases as a square root of the electric field. The Poole-Frankel theory is true for smaller/intermediate range of electric fields where field acts for lowering of barrier height and thermal excitation of carriers aid itself to cross the barrier (thermal excitation of electric field).

At high electric field, the conduction is mostly described by the theory of electric field assisted tunneling; it is similar to the phenomenon of phonon assisted tunneling, with the difference that the part of the energy is provided by the electric field. In this case dependence is given by square of the electric field as [127,132],

$$\sigma \propto \exp\left(\frac{(eE)^2 \tau^3}{3m^* h}\right) \quad (4.3)$$

where is the τ is tunneling time and m^* the effective carrier mass. Under higher electric field, the tunneling probability increase by the lowering of potential barrier height due to coulomb potential of charged particle. This is a crossover point where conductivity is majorly derived from electric field effect. At sufficiently higher electric field, a crossover occurs where charged particle can directly go to one trapping site to another with the help of energy provided by electric field (direct tunneling). This situation is different from Poole effect in the role of electric field.

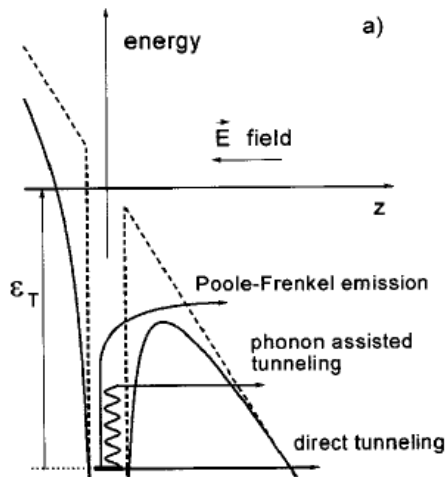


Figure 4.16: Potential barrier for the emission of an electron from a deep-level defect in external electric field [127].

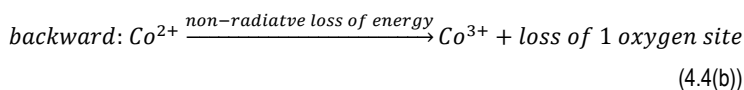
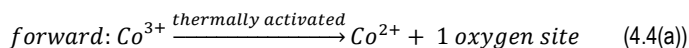
Compared to the present observations on electric conductivity, the case of 300 and 400°C for enhanced conductivity can be associated with the electric field assist-

ed tunneling whereas the sudden increase of conductivity at 200°C resembles more to the direct excitation effect of electric field. Though the fields used for MnCo₂O₄ looks to be quite small but for conductive system it can be sufficient. One example of Poole-Frankel effect is reported for La-Fe based perovskite involving fields less than 10 V/cm [137].

4.1.5.2 Flash-sintering Mechanism

The mechanism of unusually fast flash-sintering is a topic of discussion. Materials of different properties, conducting-insulating, oxides-non-oxides are reported to show flash-effect. In all these materials, the electric field affects the conductivity of material in an unusually non-ohmic manner which becomes the starting point of flash-sintering. The flash-effect, therefore, involves two separate kinds of particle motions, 1) of lighter electrons which lead to increase in conductivity and 2) heavier ions which results to sintering. The movement of both the particles should be in the way that electro-neutrality and stoichiometry of the materials phase is maintained. The phase analysis of sintered samples by XRD confirms the stability of phase under flash-sintering unless the phase reduction is inherent property of the material. So, any mechanism should be able to account for the increased rate of the two. Based on the observations made here on electrical conductivity, we try to analyze the mechanism of conduction of MnCo₂O₄ in order to elucidate the 'rather unclear' flash-sintering phenomenon.

The conductivity of MnCo₂O₄ spinel [2,6] is governed by the hopping of electrons or oxidation states between Co³⁺/Co²⁺ and Mn⁴⁺/Mn³⁺ pairs [4,7]. These hopping states are bidirectional and are responsible for the relatively high conductivity of the spinel. Transitions related to cobalt states are described as:



These transitions are thermally activated [119,124]. As temperature increases, the number of such transition also increases and therefore the conductivity becomes higher [119,124]. At higher temperatures, the hopping transition occurs more frequently in one direction and hence the conductivity increase becomes slower. As a consequence, a weight loss corresponding to oxygen deficiency takes place and this behavior is well observed in thermo-gravimetry (TG) analysis [100]. The TG response of MnCo_2O_4 spinel is shown in Fig. 4.16, the measurements having been made at three different heating rates, 2, 5 and $40^\circ\text{C}/\text{min}$. TG curve shows a two-step weight loss; the first at 1080°C – 1320°C , the second between 1320°C and above 1500°C . The first weight loss corresponds to $\text{Co}^{3+}/\text{Co}^{2+}$ while the second is associated to $\text{Mn}^{4+}/\text{Mn}^{3+}$ [100]. It is observed that the onset temperature for each weight loss is independent from heating rates; however, the extent of weight loss decreases at

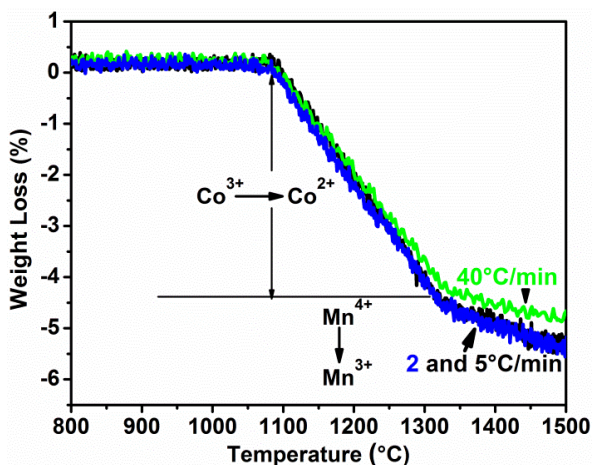


Figure 4.16: Weight loss as a function of temperature for MnCo_2O_4 at three different heating rates, 2, 5 and $40^\circ\text{C}/\text{min}$.

higher heating rates. On the basis of this observation, we expect that the same onset temperature and weight losses decrease takes place during high heating rates of flash-sintering. It is interesting to correlate the observations drawn from TG curve with that of the Co-oxide phase recorded in XRD analysis (Fig 4.7). The convention-

ally-sintered (CS) samples heat treated up to 1050°C do not show Co-oxide phase, but at higher temperatures there is an increasing formation of CoO. These weight loss and phase structure are reported to be reversible and can be achieved back if cooling rate is very slow (2°C/min or less) [100]. However, at fast heating/cooling rates as in flash-sintered (FS) samples, the possibility of retaining the transformations decreases. Therefore, the weight loss and the CoO phase formations remain in the sample after the flash-effect. This is well evident from the XRD analysis of FS samples, where the prominent CoO phase is observed much earlier than CS samples.

Moreover, the hopping mechanism leads to the formation and annihilation of ionic-sites as discussed in Eq. 2 which are expected to be used for mass-diffusion. In the context of sintering, there is the possibility of two effects to occur with such exploitable sites: 1) backward transition Co^{2+} - Co^{3+} which reduces the generated ionic-sites and 2) maintenance of the Co^{2+} state which increases the life of ionic-site. The TG and XRD analyses suggest that these effects depend on the sintering temperature. At temperatures below 1080°C, the two transitions are equally probable and there will be no ionic-sites available for mass diffusion; this state is unfavorable for sintering to occur. As a consequence to equal probability, no weight loss and no Co-oxide are detected in TG and XRD study respectively. At temperature higher than 1080°C, the formation of ionic-sites is more favored than its counterpart of annihilation which gives rise to weight loss and phase separation. The lower probability for backward transition increases the life of ionic-sites (Eq. 4.4) which in return facilitates the mass diffusion and eventually leads to the sintering. The transition related to Mn is not discussed here as it falls out of the sintering temperature range for spinels (Fig. 4.16). By extending the ideas drawn from conventional sintering and the results observed in our present work, we made an attempt to understand the mechanism of flash-sintering for the MnCo_2O_4 material. The major observations found in this work are as follows.

1. SEM images show dense grain growth by electric field (in addition to thermal) when local temperature is greater than 1050°C. XRD analysis shows that the ex-

tent of new phase formation is more extensive in FS compared to CS samples treated to similar times. The phase decomposition and shrinkage occur concurrently in flash-sintering.

2. Systematic changes and close match of conductivities at higher temperature, where one is associated to purely thermal effect and the other dominantly by electric field, suggest sharing the same conductivity mechanism.

In case of flash-sintered FS925, FS975 and FS1050 samples, fast increase in conductivity produces avalanche of ionic-sites along with the increase in the specimen temperature due to the interaction of electric field. As the temperature in these cases is lower than 1080°C, the material shows incompetence for the utilization of generated sites because of equally probable Co^{2+} - Co^{3+} transition. Hence, the microstructure is not improved (over CS) and stable-phase is observed in XRD spectra. For the samples FS1100, FS1160 and FS1320, an abrupt increase in the conductivity brings the specimen temperature to more than 1080°C along with the generations of ionic-sites. As these temperatures are high enough, some of Co^{2+} states are stabilized increasing the life of O-site. Out of many oxygen sites, some result in the oxygen loss and some acts as site for diffusion. Faster sintering kinetics at temperatures in excess to 1100°C causes ions/mass to utilize now-stable oxygen sites for diffusion and hence sintering occurs. A significantly dense microstructure produced at 1100°C and 1160°C supports such argument. From this study we conclude that the minimum temperature required for conventional sintering is above 1080°C and we are able to attain the required conditions at 120-150°C furnace temperature under the applied electric field of 15.0-17.5 V/cm.

4.1.6 Summary

In summary, we have demonstrated the flash-sintering of MnCo_2O_4 spinel at furnace temperature of 120-250°C under the electrical field of 7.5-17.5 V/cm and current density of 1.40-1.60 A/mm². It has been shown that the furnace temperature, at which the flash-effect observes, can be reduced by increasing the density of the sample. We have also demonstrated that in flash-sintering power dissipation occurs at first, followed by Joule heating, which eventually leads to increase in local temper-

ature. SEM analysis shows that the microstructure of the flash-sintered sample changes to dense and pore-free morphology at specimen temperature greater than 1080°C. From XRD analysis, it is found that MnCo_2O_4 phase decomposes by significant amounts for samples treated to 1100°C and higher temperatures. The concentration of secondary phase was found higher for flash sintered samples compared to that of conventionally-sintered at the same time. Consistent changes in I-V behavior at different temperatures and close match of conductivities resulting from thermal and electric effect suggested that flash-effect is assisted by the mechanism of usual conductivity phenomenon. Correlating the sintering results, a mechanism of flash-sintering in MnCo_2O_4 spinel is proposed: the flash-sintering is accompanied through the natural ionic rearrangements, which occur during conductivity increase. Sintering is found to be drastically accelerated by utilizing these ionic sites when the specimen temperature is above 1080°C. In addition, the work clarifies the extent of local temperature required for sintering which is important to know for the protective coating application.

4.2 Flash-sintering of $\text{La}_{0.6}\text{Sr}_{0.4}\text{Co}_{0.2}\text{Fe}_{0.8}\text{O}_3$ (LSCF)

4.2.1 Flash-sintering

4.2.1.1 Power Dissipation and Shrinkage

Linear shrinkage and corresponding power dissipation (i.e. product of the applied electric field and the current density through the sample) of LSCF samples subjected to different electric field (2.5-12.5 V/cm) as functions of furnace temperature are shown in Figure 1. It is observed in Figure 1(a) that there is rapid decrease in sample dimension (shown by vertical drops) for fields greater than 2.5 V/cm. Such rapid effect occurred under minimum electric field of 5 V/cm and at 210°C furnace temperature. For higher fields the sintering-effect occurred at lower temperatures and surprisingly at 25°C under 12.5 V/cm. The shrinkage of Figure 1(a) is the subsequent outcome of fast increase in the power dissipation and specimen temperature (Figure 1(b) and 2(a)); the increase of power dissipation with temperature accounts for increase in the conductivity. For 2.5 V/cm, power dissipation or conductivity increases in a gradual manner without showing any rapid change up to 900°C; the sample is not associated to any dimension variation. Under higher fields, the power dissipation increases with higher slope, ultimately leading to flash-sintering effect. Under these observations, 5 V/cm is suggested to be the threshold field for LSCF and 210°C the threshold furnace temperature which discriminate the two regimes of electric field effect typically called “flash” and “FAST” [3, 8]. Under the rapid flash-effect, the degree of shrinkage is controlled by the electric field and the current density [80]. Here the maximum current density was set to a fixed maximum of 1.55 A/mm², the electric field being therefore the controlling parameter. For this control, a systematic increase in the shrinkage (Figure 1(a)) and correspondingly, a systematic drop in power dissipation (inset of Figure 1(b)) are observed with electric field at the end of 60 s hold time. Power dissipations of 370, 440 and 548 mW/mm³ were recorded for 12.5, 10.0 and 7.5 V/cm, respectively; these end values reflect the conductivity increase by the electric field (material property) as well as by the sintering process (pore removal). Moreover, as a part of flash-sintering parameters, the minimum

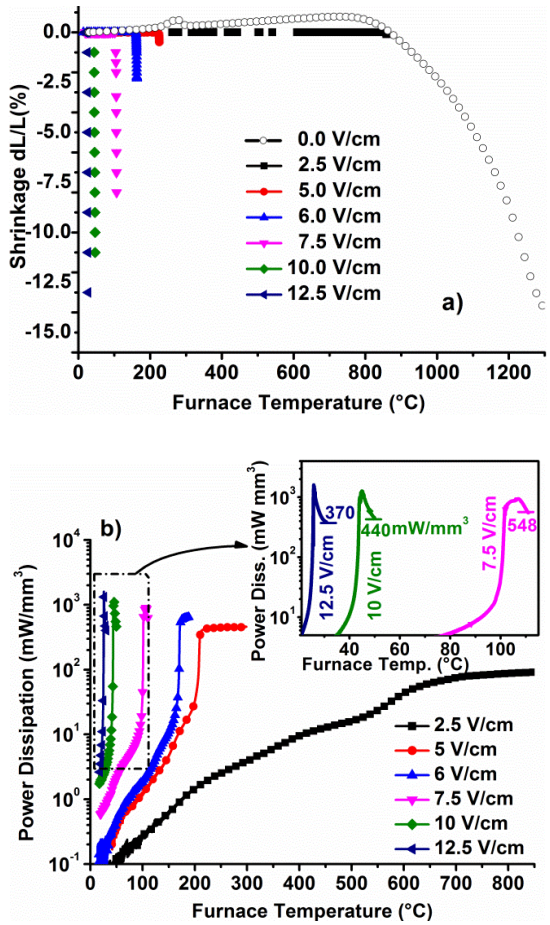


Figure 4.17: a) Shrinkage and b) power dissipation LSCF samples as functions of furnace temperature under 2.5-12.5 V/cm. Shrinkage with no electric field applied is also shown in 1(b). Inset shows the power dissipation value at the end of 60 s hold time for different electric fields.

power dissipation to see flash-effect in LSCF seems to attain a steady value in the range of 5-8 mW/mm^3 (10.0-12.5 V/cm) which is lower than that observed in other materials subjected to similar processing procedures [3, 4, 8].

It is shown in Figure 1(a) that the onset temperature for sintering under 0 V/cm (conventional treatment) is 850 $^{\circ}\text{C}$ and almost full shrinkage is reached at about

1300°C, and under 6.0-12.5 V/cm, the flash-sintering effect is observed at 25-170°C. Therefore, the two methods show a large gap of processing temperature. Such flash-sintering behavior for LSCF is associated with its semiconducting nature (up to 550°C [36]) and the required very low furnace temperatures is connected with its high conductivity.

4.2.1.2 Specimen Temperature

The sintering behavior was analyzed by monitoring the specimen temperature during flash-sintering. The parameters of flash-sintering-effect of LSCF samples under different electric fields are listed in Table 4.2. Under the employed electric fields (5.0-12.5 V/cm) and current densities (1.18-1.55 A/mm²), the maximum temperature was observed to be in the range of 900-1360°C which are achieved by the flash-effect at furnace temperatures as low as 25-210°C.

Table 4.2: Flash-sintering parameters of LSCF samples subjected to different electric fields

Electric Field, V/cm	Furnace Temp., °C	Max. Current Density, A/mm ²	Power Dissipation mW/mm ³		Specimen Temperature °C	
			Peak	Lowest	Peak	Lowest
12.5	25	1.55	1600	370	1360	705
10.0	45	1.55	1271	440	1280	750
7.5	100	1.55	940	548	1160	838
6.0	170	1.36	658	658	990	990
5.0	210	1.18	450	450	900	900

Regarding the behavior of such effect, power dissipation and specimen temperature of LSCF sample subjected to 10 V/cm as functions of furnace temperature are shown in Fig. 4.18(a). Under electric field at the onset of flash, power dissipation increases sharply for rapid increase in the conductivity until the maximum limit of the current is achieved (which was set in order to prevent thermal runaway); the value of power dissipation at this maximum current is reported as peak value in the Table 4.2. After this maximum, power dissipation starts decreasing for further increase in the conductivity. Unusually, this decrease is continuous and smooth in LSCF and continues during the 60 s hold time. The power dissipation at this stage is reported as the lowest in Table 4.2. Additionally as a consequence of such change in power dissipa-

tion, under 10 V/cm specimen temperature rises up to 1280°C in the same sharp manner (Figure 4.18(a)), followed by a continuous drop to sufficiently low temperature (about 750°C) at the end of 60 s.

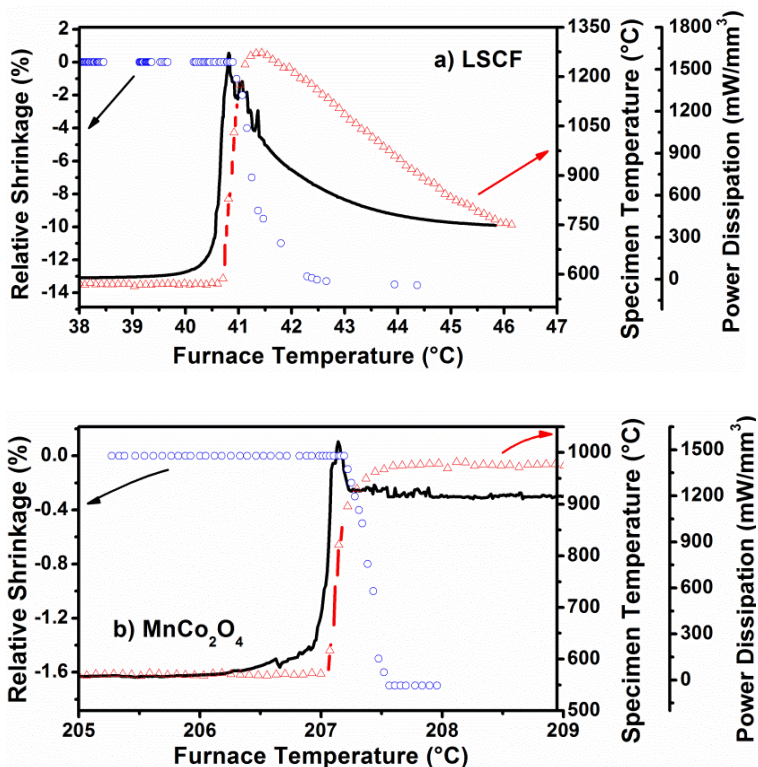


Figure 4.18: Evolution of power dissipation, shrinkage and specimen temperature of a) LSCF and b) MnCo_2O_4 samples subjected to 10 V/cm as functions of furnace temperature.

4.2.1.3 Comparison with MnCo_2O_4

Such continuous decrease of power dissipation and specimen temperature does not resemble the observation performed on MnCo_2O_4 shown in Figure 4.18(b). The comparison is made because the flash-effect is initiated with a conductivity increase; MnCo_2O_4 , as mentioned previously, is an electronically conducting material as like LSCF and its conductivity is controlled by similar type of mechanism. In case

of MnCo_2O_4 , the temperature follows the power dissipation, increasing sharply at flash-onset and decreasing after the peak for further increase in the conductivity; nevertheless, dissimilarly from LSCF, both parameters achieve a steady value within 5 s from flash-onset. The observed behaviors might be associated with the conductivity properties of LSCF [36] and MnCo_2O_4 [9]. Among the materials studied so far, weakly and ionically conducting zirconia is also shown to achieve quick steady state value [21].

4.2.1.4 Importance of Specimen Temperature and Electric field

Under the electric field derived conductivity and specimen temperature changes (Fig. 4.2(a)), shrinkage is observed to occur during early and mid duration of 60 s hold period when specimen temperature was recorded to be sufficiently high, in excess to 850°C (Fig. 4.18(a)). A large portion of the shrinkage occurs within 9-11 s after the peak when the temperature is close to its maximum. The continuous increase in the conductivity after the peak allows improving the densification with the help of temperature; no shrinkage was recorded when temperature went down to 800°C (Fig. 4.18(a)). This is further realized when the hold time is extended to 120 and 300 s; in this case, the conductivity continues to increase for significantly longer periods (Figs. 4.19 and 4.22) but without involving any shrinkage (or any improvement in the microstructure); it is because the temperature is lower than that required for densification. The present observation points out the importance of local temperature for flash-sintering and also suggests that quick increase in the conductivity, which is suggested as the cause of defect-generation, is not the only requirement. Conversely, in case of MnCo_2O_4 , sintering is mainly achieved during peak and stabilization regime when temperature achieves its maximum and conductivity is increasing (Fig. 4.18(b)); most of the shrinkage is observed in this 5 s short period. After this period, power dissipation and temperature attain a steady value and remain almost constant for the remaining period; the hold does not improve the microstructure by any significant degree after this initial period (of 5-6 s), because of quick stabilization of conductivity. In case of LSCF, the same is observed to be extended over a comparatively longer period of time (30-40 s) because of continuous increase in conduc-

tivity. Such observation indicates the importance of increase in conductivity during flash-sintering. The rapid sintering within 5 s of flash-effect is reported for zirconia also [80].

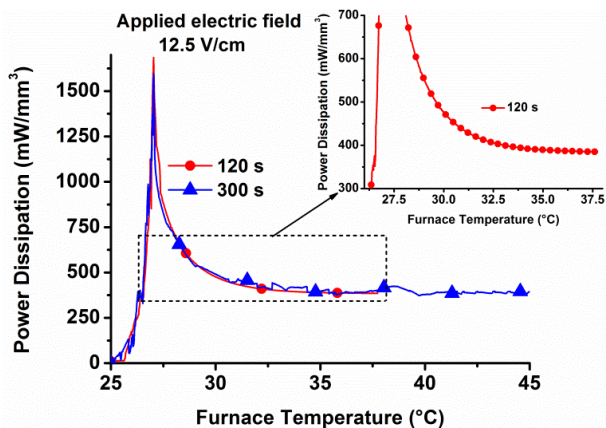


Figure 4.19: Power dissipation as function of specimen temperature showing stabilization.

The correlation between shrinkage, specimen temperature and conductivity implies that 1) in flash-sintering temperature has the same importance as in conventional process and 2) for ‘fast and enhanced’ sintering, the increase in conductivity is a necessary condition and is not the only requirement. From the first point, electric field does not seem to change the diffusion activation energy of ions and therefore quick sintering is pointed to be the result of increased defect-concentrations, it is suggested in literature also [24,28]. The increased defects concentration might be associated with electric field through rapid increase in the conductivity. This way, the observed power dissipation and temperature behaviors are associated with the conductivity property and sintering mechanism of the considered materials, LSCF and MnCo_2O_4 .

4.2.2 Microstructure Evolution

The extent of sintering under electric field was further examined by scanning electron microscopy. SEM micrographs of LSCF samples sintered under different

electric field are shown in Fig. 4.20. The microstructure of conventionally sintered samples is also shown for comparison. In order to better correlate the two sintering methods, samples are compared on the basis of specimen temperature and are labeled with prefix FS for flash-sintered and CS for conventionally-sintered, followed by the temperature. Electric field treated sample FS900 (Fig. 4.20(b)) does not show

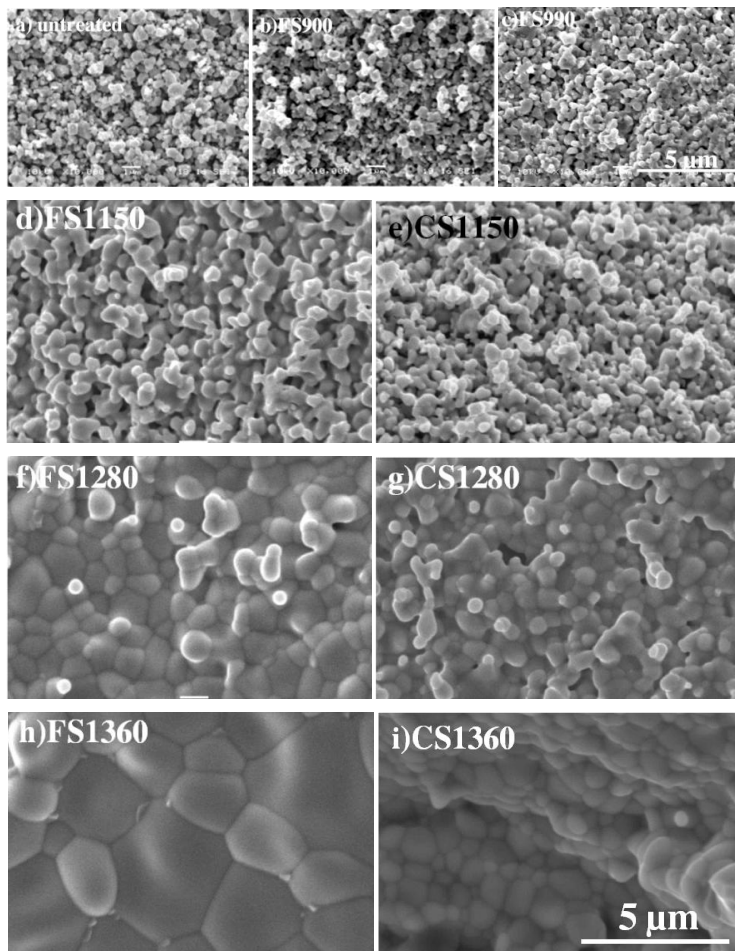


Figure 4.20: SEM images of LSCF samples, a) untreated and flash-sintered, subjected to (b) 5 V/cm, processed at 210°C, c) 6 V/cm at 170°C, d) 7.5 V/cm at 100°C, (f) 10.0 V/cm at 45°C (h) 12.5 V/cm at 25°C and conventionally sintered at (e) 1150°C, (g) 1280°C and (i) 1360°C.

any significant sintering effect in the microstructure compared to that of untreated sample (Fig. 4.20(a)). Improved microstructure with significant particle connectivity is observed for FS990 sample (Fig. 4.20(c)). Homogeneously distributed pores and particles structures are observed which might be as required for SOFC cathodic application [37]. It suggests that under the electric field assisted sintering with proper choice of parameter microstructure can be produced for porosity requirement as well. Sample FS1150 (Fig. 4.20(d)) subjected to 7.5 V/cm is not fully dense, but shows many inter-connected particles in a porous morphology. The evolution of morphology by fast-sintering (1 min of total treatment time) is observed to be more evident than in conventional-sintering (4.20(e)) where limited inter-particle connections are visible. Sample FS1280 (Fig. 4.20(f)) produced under 10.0 V/cm is well sintered with properly connected grains. Its complementary sample produced by CS shows almost similar grain morphology but with lower grain size (Fig. 4.20(i)). However, grains in flash-sintering are shown to be more tightly packed with each other. The microstructure evolved under electric field is observed to be homogeneous, and regular with field and temperature as observed in conventional-sintering. For the FS1360 sample (Fig. 4.20(h)) sintered under 12.5 V/cm, the grain size is increased significantly from $\sim 1 \mu\text{m}$ for 10 V/cm (Fig. 4.20(f)) to $\sim 4 \mu\text{m}$ (Fig. 4.20(h)). Its counterpart CS sample shows smaller grain size. The trend of increasing grain size with temperature is found for LSCF under electric field assisted flash- as well as conventional-sintering. Significant changes in the microstructure are observed by 2-3 V/cm increase of electric field which is again associated with conductivity property of LSCF; small increase (relatively) in electric fields results in a large increase in the conductivity and leads to significant changes in the specimen temperature and so the microstructure. Moreover, the effect of electric field on sintering is regular and homogeneous unlike to the observation on MnCo_2O_4 [8] where sintering is found to be enhanced over conventional for temperatures of 1100°C and higher, and not for lower temperatures.

4.2.3 Phase stability

XRD pattern of flash-sintered LSCF sample subjected to 12.5 V/cm which heated the specimen to 1280°C temperature is shown in Fig. 4.21. XRD pattern of

conventionally sintered at the same temperature of 1280°C, for 2h, and raw LSCF powder samples are also shown. All three patterns are congruent suggesting that flash-sintering, similar to conventional-sintering, does not produce any structural change in the LSCF sample. Peaks are matched with JCPDS file no. 049-0284 which corresponds to rhombohedral phase of the perovskite.

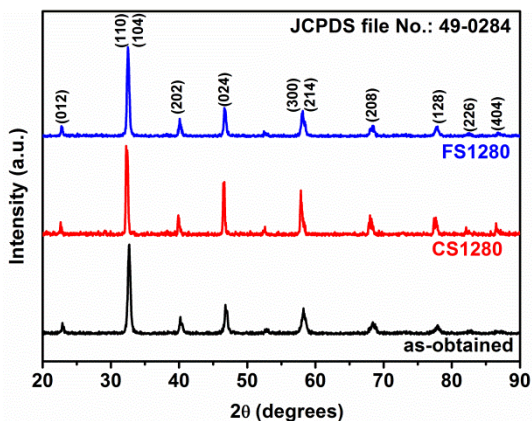


Figure 4.21: XRD pattern of LSCF samples, as received powder, conventionally sintered at 1280°C and flash-sintered under 10 V/cm to the same specimen temperature.

4.2.4 Electrical conductivity of LSCF

Like MnCo_2O_4 in earlier section, flash-effect of conductivity and sintering of LSCF is investigated by analyzing dependence of electrical conductivity on electric field and temperature.

4.2.4.1 On Green Specimen

The conductivity behavior during and after flash effect was analyzed in sintering experiment (on green specimen) similar to as reported in Fig. 4.17(a) by extending the time of measurement. The electrical conductivity of green LSCF sample under 5.0 and 7.5 V/cm, constant electric field, is shown in Fig. 4.22 reporting the evolution of power dissipation and specimen temperature as functions of furnace temperature.

LSCF undergoes to rapid increase in the power dissipation and specimen temperature in response to the electric field; the temperature rises sharply well above the furnace temperature in both cases. Out of the two, under 5 V/cm current at rapid increase of conductivity reaches to 1.18 A/mm², therefore, there is no peak like appearance as is observed for 7.5 V/cm case (Fig. 4.22(b)); in the set-up the current was limited to a maximum of 1.50 A/mm². Under 7.5 V/cm the

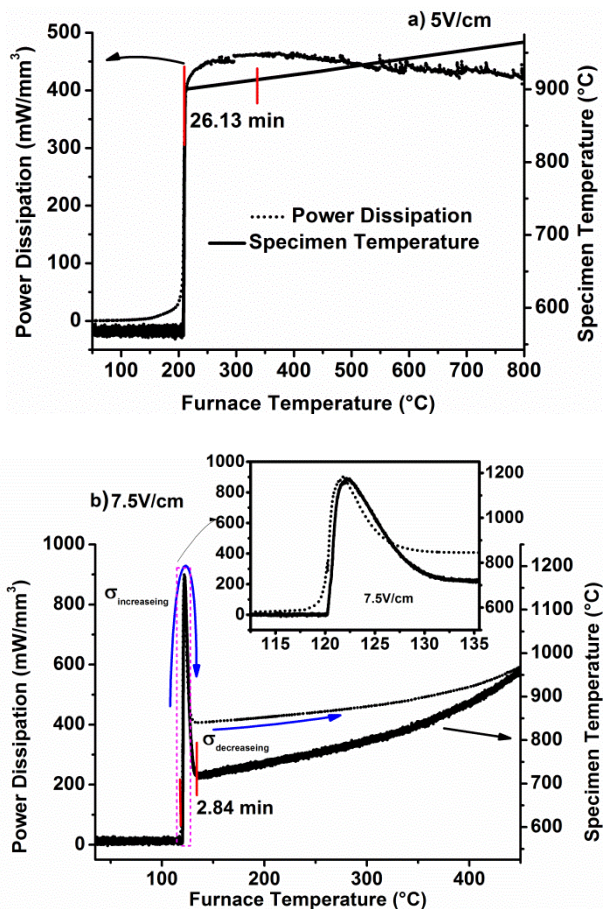


Figure 4.22: Power dissipation and specimen temperature for LSCF samples as functions of furnace temperature under constant electric fields: a) 5.0 V/cm and b) 7.5 V/cm. Current was limited to maximum of ~ 1.55 A/mm².

large increase in current causes the formation of power dissipation spikes. It is observed that the increasing tendency of conductivity after such flash-effect continues for significant periods (Fig. 4.22(a) and 4.22(b)). The beginning of this increasing tendency is shown to be responsible for flash-sintering in Fig. 4.2. With further increase of time, conductivity starts to decrease which is reflected as a decrease of power dissipation under 5.0 V/cm in Fig. 4.22(a) and an increase of power dissipation under 7.5 V/cm (Fig. 4.22(b)); the transition of increase-to-maximum-to-decrease under 7.5 V/cm is clearer in the inset of Fig. 4.22(b). A comparison of the time in which conductivity increases by flash-effect for the two electric fields suggests that the increasing tendency continues for a significantly longer period under lower field of 5.0 V/cm. The time and the maximum conductivity involved for such tendencies are (26.13 min, 465 mW/mm³) for 5 V/cm and (2.8 min, 905 mW/mm³) for 7.5 V/cm. Therefore, the power dissipation of LSCF under the two fields (although it looks different because of settings in the measurement set up) follows the same trend of rapid increase followed with a decrease. Such increase of conductivity for significantly large periods is dissimilar from the observations performed on MnCo₂O₄ [22] and zirconia [21], where the power dissipation is reported to attain a steady value within 5 s from the flash-onset. The trend of LSCF seems to reflect the traditional conductivity behavior observed with varying temperature [36].

4.2.4.2 On Dense Specimen

4.2.4.2.1 Conductivity versus Temperature: Effect of electric field

Electrical conductivity of sintered LSCF sample (at 1300°C for 2 h) subjected to different electric fields (0.1-1.5 V/cm) as a function of temperature is shown in Figs. 4.23 and 4.24. The conductivity in Fig. 4.23, which is observed under lower side of the considered electric field range, increases with the temperature till a maximum, from where it decreases. This is the usual conductivity behavior of LSCF [8,36]. The observed conductivities are lower than the reported; it is associated to the different experimental arrangement. The conductivity during increasing tendency is described by the small polaron-hopping [8,36] and its temperature dependence is given by Eq.

4.1. The linear relationship of $\log_e(\sigma \cdot T)$ versus $1/T$ curve in the inset confirms the said hopping mechanism [41]. The activation energy is calculated from the slope of the lowest field case i.e. 0.1 V/cm, and is found to be 0.09 eV which is lower than the reported 0.10 eV [8,36]. Such difference is associated with the Joule-heating effect which is also manifested in the maximum conductivity-temperature (Fig. 4.23). The conductivity attains the maximum in 300-400°C furnace temperature range which is significantly earlier than the reported i.e. at 550°C [8,36]; Joule effect justifies such difference.

Under relatively higher 0.4 V/cm the trend of conductivity is same but significant deviations at lower temperatures are observed. From Fig. 4.24, under 0.5-1.5 V/cm the conductivity starts with considerably higher values, 210-260 S/cm which are much higher than 80 S/cm recorded under 0.1 V/cm at the same temperature, and also with the maximum, 200 S/cm at 300-400°C (Fig. 4.23). The conductivity, after this high initial, drops down suddenly and afterwards follows the usual increasing-decreasing trend. Such high conductivities at 18°C which are the result of electric field effect are not usual. It could be associated with 'direct excitation effect' of electric field as reported for some hopping based materials [125,127,128]. Even though these 0.5-1.5 V/cm is quite small but for a conductive system like LSCF could be

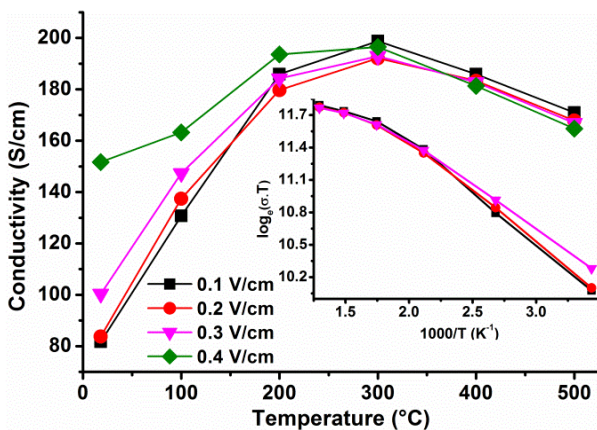


Figure 4.23: Electrical conductivity of sintered LSCF sample, measured under 0.1-0.4 V/cm, as a function of temperature. Inset shows the corresponding Arrhenius plot.

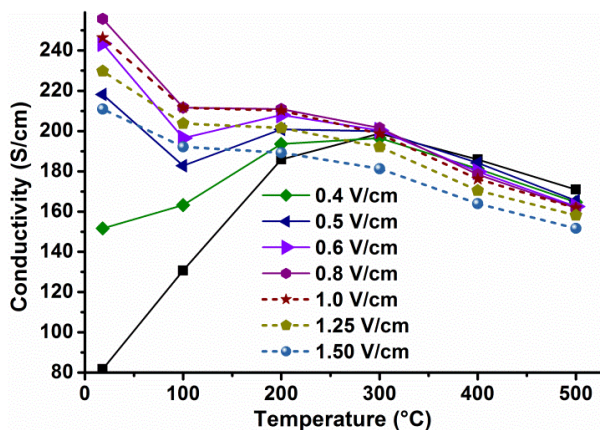


Figure 4.24: Electrical conductivity of sintered LSCF sample, measured under 0.4-1.5 V/cm, as a function of temperature.

enough for any stimulated interaction [22,137]. Under this supposition about increased behavior, the initial drop of conductivity is associated with the intervention of thermal effect on the field derived effect [22]. The rise in temperature after sudden increase in the conductivity is clearly seen in flash kind of effect (refer to Figure 2). It may diminish the role of the electric field for conductivity. Such competitiveness of electric field and temperature is observed on MnCo_2O_4 also [22]. Therefore, the electric field has strong influence on the conductivity versus temperature curves and for the same range of electric field the conductivity goes from ohmic to non-ohmic regime. These are the fields which do not involve with flash-kind of effect on green samples (Fig. 4.17) but still strongly affect the conductivity of LSCF. These sharp increases at unusual (lower) temperature can be the reason of flash-sintering effect, possibly, if the applied field is higher and working temperature is lower than 18°C .

4.2.4.2.2 Conductivity versus Electric field: Effect of Temperature

The electrical conductivity under electric field was further analyzed by current-voltage measurements. Figure 4.25 shows the conductivity of sintered LSCF (1300°C for 2 h) as a function of electric field taken at 18, 100-300°C furnace temperatures. The figure shows that the conductivity at the lowest temperature of 18°C

is not constant with electric field but increases sharply from 80 S/cm to 256 S/cm within a narrow range of field (up to 0.72 V/cm) and then decreases. This conductivity trend clearly matches with that observed with temperature (Figure 4.23) suggesting that electric field tunes the conductivity in the similar ways as temperature does. Similar tendency is observed during flash-sintering also (Figure 4.22). This increase at 18°C is, however, large and sharp but does not involve with flash-kind of effect. It is clear from the current density plot shown in the inset of the Fig. 4.25 which shows almost linear increase in current unlike to that in flash-effect. At 100-200-300°C, conductivity starts with successively higher values (132-169-187 S/cm) and changes

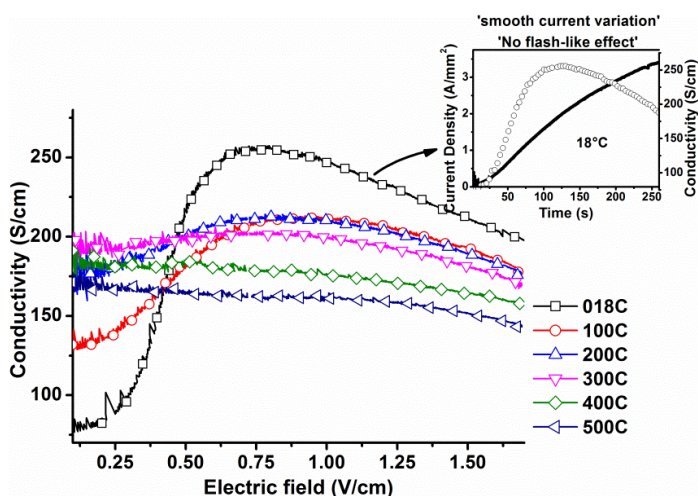


Figure 4.25: Dependence of the Conductivity on the electric field taken at different temperatures for 1300°C-sintered LSCF. The inset shows the smooth current increase at 18°C, for observed conductivities.

with field following the same trend as it is observed at 18°C. However, the change is appreciably gradual and eventually reaches a maximum (212-212-200 S/cm) which is much lower than that observed at 18°C (256 S/cm). At relatively higher temperature, 400 and 500°C, conductivity starts with 183 and 168 S/cm, respectively, and shows decreasing tendency only with the electric field. Conclusively, there is a systematic effect of temperature on the conductivity versus electric field. The semicon-

ducting trend of conductivity which is observable at 18°C can lead to the flash-sintering effect. Although these temperatures are not involved with as rapid increase of conductivity as in flash-sintering, but from systematic conductivity changes, the flash-effect on dense specimen can be extrapolated to occur at temperatures lower than ambient.

In order to confirm the role of the electric field, specimen temperature is recorded. The conductivity, during increasing trend, and the specimen temperature as a function of electric field are shown for 18°C case in Fig. 4.26. The initial measurement of temperature is restricted by pyrometer-use, but it is clear that increase in the conductivity is followed with smooth rise in the specimen temperature which goes sufficiently high from the furnace value. From the correlation, the maximum conductivity is observed at ~600°C, which is slightly higher than the reported, i.e. at 550°C.

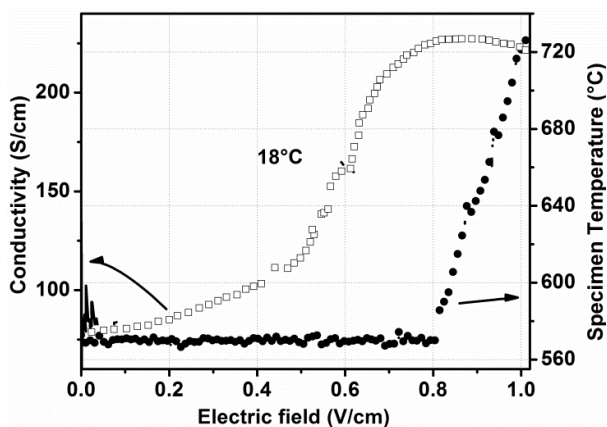


Figure 4.26: Conductivity and Specimen temperature as a function of electric field at 18°C furnace temperature (i.e. room temperature)

Similar to 18°C, conductivity trends at other temperatures are associated with smooth rise in local temperature. These observations suggest that the enhanced conductivity is the results of thermal excitation of charge carriers (similar to Poole-Frankel effect) [22,127]. But comparing the conductivity values (Fig. 4.24), the high conductivity at lowest temperature of 18°C suggests that enhanced conductivity is

not totally associated with thermal excitation. There is an additional effect, other than thermal, of electric field which probably works efficiently for conductivity of LSCF when the thermal effects are lower [22,127]. Such observation on the field enhanced conductivity can be associated with 'direct excitation (by electric field) or electric field assisted tunneling of charge carriers which is similar to rather known phenomenon of phonon assisted tunneling [127,133]. Unlike to random thermal activation, electric field may enhance the excitation of charge carriers to a large extent by its directional nature[138,139]. The directed effect of electric field is reported in different physical and chemical phenomenon involving movement of charged species [138,139]. The similar kind of observation on the I-V behavior is observed for relatively similar composition of (La, Sr)FeO₃ also which was associated with Poole-Frankel effect of electric field [127,137].

4.2.4.2.3 Comparison with MnCo₂O₄

The observation of electrical conductivity of LSCF is correlated with that of MnCo₂O₄. Figure 4.27 shows the electrical conductivity of sintered MnCo₂O₄ (1300°C for 1 h) at 200, 400 and 600°C. The corresponding specimen temperatures for 200 and 600°C are shown in Fig. 4.28. Similar type of electric field dependent

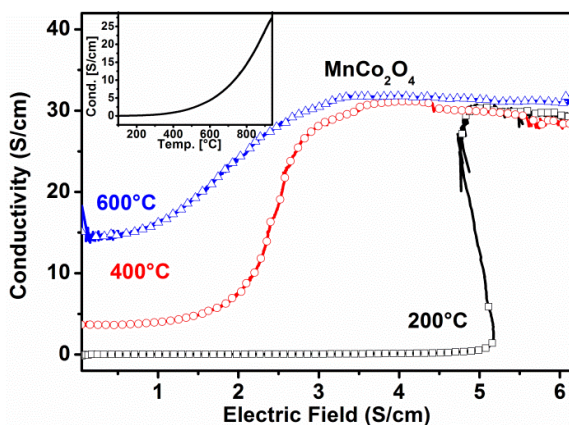


Figure 4.27: Electrical conductivity of sintered MnCo₂O₄ sample as a function of electric field observed at 200, 400 and 600°C. Inset shows the conductivity as a function of temperature.

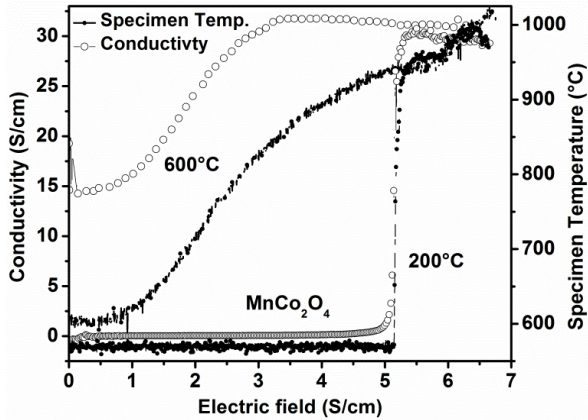


Figure 4.28: Electrical conductivity and specimen temperature as a function of electric field observed at 200 and 600°C.

conductivity is shown for MnCo_2O_4 and that resembles to the one recorded with temperature, shown in the inset of the Fig. 4.27. Consistent behavior from flash-like to FAST-like is clearly seen when temperature is increased. Curves show a nonlinear and semiconducting behavior with electric field. The degree of non-linearity varies with temperature and the one with stronger non-linearity at lower temperature of 200°C is reported to be responsible for flash-sintering [22]. This observation is in support of the proposition of onset of flash-effect at temperatures lower than ambient in LSCF because of its higher conductivity. The correlation with specimen temperature in Fig. 4.28 suggests that, at lower temperature increase in conductivity is very sharp which raises the specimen temperature as a subsequent step and therefore, this high conductivity is the direct excitation effect of electric field. At higher temperature the enhanced conductivity which is rather smooth comes from thermal excitation effect of electric field. A clear cross over between the role of electric field is reported for MnCo_2O_4 where a thermally enhanced conductivity turns to conductivity derived thermal effect at lower temperature. Conversely in LSCF, the considered temperatures do not involve with crossover behavior and the observed conductivity therefore is associated with electric field enhanced thermal excitation of charged carriers. Nevertheless, from consistent changes, electric field can be expected to cause the

same crossover phenomenon at 'more' lower temperatures which will enhance the conductivity by direct supplying the energy from electric field. Therefore, for both materials, LSCF and MnCo_2O_4 , undergo consistent changes and conductivity versus electric field curve resembles that recorded as a function of temperature. Such observations on conductivity could be a general property of electronically conducting material, more specifically of those based on polaron-hopping. The role of electric field for conductivity is better described, depending on the temperature, by Poole effect (higher temperature), electric field assisted tunneling (at intermediate temperatures) and then to direct tunneling (lower temperatures, responsible for flash-sintering effect). Similar kind of non-ohmic behavior of electrical conductivity is reported for $\text{La}_{1-x}\text{Sr}_x\text{FeO}_3$ perovskite [137] where the behavior is associated with Poole-Frankel effect (with 0-10 V). This composition of La-Fe based-perovskite is comparatively low-conducting with respect to the LSCF used in the present work.

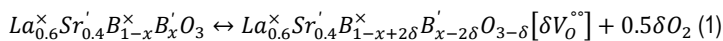
On the basis of presented conductivity results of LSCF and MnCo_2O_4 , one can now strongly point out that the electric field can tune the conductivity in a similar way as temperature does, but to different extent, depending on the processing temperature. Observing the systematic effect of electric field on conductivity we conclude that these stages of conductivity under electric field follow the usual mechanism of conduction i.e. small polaron hopping.

4.2.5 Discussion

4.2.5.1 Flash-sintering Mechanism

The present discussion aims to identify the cause of accelerated sintering in LSCF by investigating the source of defect centers that are believed to account for flash-sintering at/after an abrupt increase in the conductivity. Similar to MnCo_2O_4 , The discussion begins with understanding the conductivity of LSCF and proceeds by investigating the sintering mechanism. The fundamental results obtained on MnCo_2O_4 are considered in order to verify the proposed mechanism [41].

The conductivity of LSCF at any temperature is a coupled response of 1) oxygen vacancy formed at A-site and 2) polaron hopping at B-site in ABO₃ perovskite type structure [35,36]. The replacement of La³⁺ at A-site by doubly ionized Sr²⁺ brings about the oxidation of B-site cation (Co or Fe, preferably Fe) into its higher valence state for charge compensation (p-type carrier) and/or the formation of oxygen vacancies. From B-site, hopping of transition metal cations into their different oxidation states controls the conductivity. In such hopping, the charge dis-proportionate, where $2 \text{Co}^{3+} \rightarrow \text{Co}^{2+} + \text{Co}^{4+}$ transition (providing n- and p-type carriers) is responsible for its large conductivity. The relative importance of the two processes varies with temperature, this being responsible for the specific conductivity behavior [36]. The conductivity of LSCF, at first, increases (Fig. 4.23) by polaron-hopping mechanism with temperature, up to a characteristic maximum (~550°C [36]). Beyond 550°C, the conductivity continuously decreases up to 1200°C; such conductivity decrease is associated to an oxygen loss from the matrix, which is also regular and extended to higher temperatures [36]. The weight loss and the decrease in conductivity are initially dominated by changes occurring at A-site [140,141]. But above 770-780°C, these are occurred for misbalance in hopping probabilities which causes reduction of B-site cation; it brings about the loss of charge carriers (n- and p-type) thereby conductivity decrease; additionally it leads to the formation of negatively charged oxygen end which further results to the release of oxygen showing weight loss [8]. These reactions, at any place under the electronic and ionic compensation, are reported in the form of defect reaction (by using the Kröger-Vink notation) as [37,41]:



where 'B' is B-site cation, Fe or Co. The electro-neutrality condition is expressed as:

$$Sr_{La}' = [B_B^{\circ}] + 2[V_O^{\circ\circ}] \quad (2)$$

At sintering temperatures (in excess of 800-850°C), each thermally generated $V_O^{\circ\circ}$ is formed by reducing two B-site cations for ionic compensation. As an intermediate step for such reduction reaction, a charged species of $\{V_O^{\circ\circ} B_B'\}$ type forms, as

reported in Eq. 1 which can be involved in mass-diffusion for sintering in the similar way as suggested for MnCo_2O_4 [22]. Such formed defect structure can move as a whole or can act as a path for diffusion, causing the shrinkage of the structure. Under electric field, these defects structures are generated at a rapid rate, and can be quickly involved in sintering through the support of local temperature and field giving a flash-kind of response for shrinkage.

4.2.5.2 Role of Reduction Reaction: Correlation with MnCo_2O_4

Polaron hopping mechanism for conductivity is observed in MnCo_2O_4 as well. The hopping process in spinel forms, in a similar way as in LSCF, $\{V_O^{\circ\circ}Co'_{Co}\}$ and $\{V_O^{\circ\circ}Mn'_{Mn}\}$ kind of defect complex. Such defect complex is proposed to be utilized for ionic-diffusion and sintering [22]. However, one constraint is suggested about the exploitation of such defects for sintering. The hopping continuously involves with the formation and also, annihilation of such type of complex. The hopping (two-way transition) did not seem to be favorable for sintering unless there is a probability imbalance. MnCo_2O_4 spinel phase undergoes a reduction reaction via the reaction $\text{MnCo}_2\text{O}_4 \rightarrow (\text{Mn, Co})_3\text{O}_{4.5} + \text{CoO} + \text{O}_2$ at 1080°C . This reaction occurs for stabilization of forward reaction, or because of lower probability of backward reaction. Such kind of implication regarding the use of defect complex for sintering is made from the results of MnCo_2O_4 . The microstructure of MnCo_2O_4 is reported to be enhanced over conventional sintering when local temperature was in excess of 1080°C . For lower temperatures, the microstructure was poorer compared to that in conventional sintering [22]. Below 1080°C , the same defect complex is presumed as being more under the tendency to be absorbed into the lattice, not available for sintering, and is quickly neutralized by an equally probable oxidation reaction. From these observations on MnCo_2O_4 , it is confirmed that the (hopping) reaction, when involved with stable reduction increases the availability of defects complexes, formed during polaron-hopping, for sintering. The reduction reaction is detected with oxygen weight loss in TG and also as a secondary phase of CoO in XRD. In LSCF the reduction reaction is observed through weight loss only. A reduction reaction is associated with zirconia also which involves the formation of similar kind of defect complex. This reactions

causes blackening effect [83]. The same defect structure is suggested to be actively participating for diffusion in flash-sintering [81].

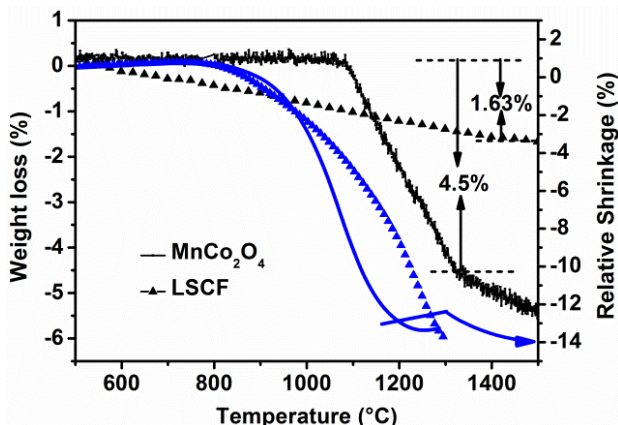


Figure 4.29: Weight loss as a function of temperature for LSCF and MnCo_2O_4 at $5^\circ\text{C}/\text{min}$.

Following from the role of the reaction associated with weight loss in flash-sintering, thermo-gravimetric plots of LSCF and MnCo_2O_4 recorded in air up to 1500°C with $2^\circ\text{C}/\text{min}$ are shown in Fig. 4.28. The dilatometric shrinkage plots are also shown for comparison. LSCF shows a weight loss of 1.9% within a large temperature range ($550\text{--}1500^\circ\text{C}$). On the other hand, MnCo_2O_4 shows a higher weight loss of 5% extended over a comparatively small range of temperature, $1080\text{--}1320^\circ\text{C}$. Sintering behavior can be estimated from such plots following the proposed mechanism. The comparison of associated temperature range for two materials points out the importance of 1080°C for enhanced-sintering of MnCo_2O_4 , conversely for LSCF all temperatures starting from sintering onset will result into enhanced sintering. From the comparison of amount of weight loss, the sintering will occur in comparatively slower degree for LSCF at any particular temperature because of smaller weight loss. These predictions from TG plot are well matched with the result observed and discussed. Even it was clear from the managing of the samples during flash-sintering; LSCF was easier to produce perhaps because of relatively slow sintering effect.

Therefore, sintering in LSCF (as well as in MnCo_2O_4), electronically conducting material is proposed to be mediated and enhanced by polaron-hopping which is usual mechanism of conduction in these materials.

4.2.5.3 Comparison with Reported System

Nucleation of paired defects (Frenkel-pair) is the most raised mechanism/theory of flash-sintering which can account for both, the instantaneous increase in the conductivity and shrinkage rate under applied electric field [9,26]. Here, electric field is suggested to be as possible cause for removal of ions from its lattice site creating vacancies-interstitials.

For the case of insulating materials, the charged carriers such as electrons are trapped into localized states. Random thermal fluctuations provide necessary energy to these electrons to get off such localized states, electron stays in this situation for a small period of time before it gets locked into localized state again. Poole-Frankel effect describes that in a sufficiently high electric field, electron does not need that much thermal energy. They gain energy from the electric field. Such effect is expected to be initiated by some local polarization of crystal lattice under electric field [24,142]. Another result on high electric field treated MgO sample shows higher concentration of vacancy and interstitials defects [28] and on the same basis, defect segregation and selective melting of grain boundaries is suggested for enhanced diffusion and rapid sintering under electric field. Such kind of observation or prediction by different groups may support the formation of paired-defects by thermal ionization under electric field in insulating materials.

In weakly conducting materials such as zirconia, under the similar range of voltage as used for flash-sintering, zirconia is reduced to zirconium causing blackening effect [83]. John et al correlated this electrolytic reduction with the observed flash-sintering effect [81] and proposed that the defects involved in the reduction of zirconia can be the reason for enhanced diffusion and sintering under electric field [7]. The

observation of zirconia is more close to the theory of flash-sintering proposed in the present work for electrically conducting materials.

In the electronically conducting materials, conduction is rather easy process; a large amount of charge carriers is generated under relatively small electric fields [36,137]. In our proposed flash-sintering mechanism of materials based on polaron hopping, the sintering is shown to be enhanced by involving a kind of reduction reaction which occurs during usual conductivity increase. The effect of electric field on hopping based conduction process is extensively discussed issue [23,24]. Under electric field larger than the threshold, the same reaction initiates at a very fast rate and leads to two almost simultaneous effect, conductivity and Joule-heating; both events have importance in sintering. The highly non-linear increase in the conductivity provides diffusion-able sites at a rapid rate; these are utilized for sintering when the temperature is sufficiently high. The large increase in the temperature or even conductivity in conducting materials diminishes the efforts of electric field, and such small fields could be inefficient for self-driving the ionic diffusion.

As a general idea about flash-sintering, only the initial mechanism for the nucleation of charge carriers (ions and electrons) seems to be different, and it could be general property of semiconducting nature materials, and not associated to ceramics only. The similar kind of electric field effect on conductivity is reported for different materials including those which are not ceramics [126,131,144].

4.2.6 Summary

The flash-sintering of LSCF has been demonstrated to occur at furnace temperatures as low as 25-100°C and in time as low as 1 min under electric field of 7.5-12.5 V cm⁻¹. This is mainly associated with the high electrical conductivity of the material. SEM microstructure suggests that sintering effect is homogenous and regular with electric field and local temperature unlike to MnCo₂O₄ where sintering is enhanced over conventional when temperature was greater than 1080°C [22]. Under the employed electric field and current densities, a series of microstructure from

porous to fully dense is produced, this allowing to tailor the cathodic material according to the specific application. The performed work clarifies the importance of temperature for diffusion/sintering and suggests the electric field to be more responsible for producing diffusion-able sites. Sintering is proposed to be enhanced through defect structures formed during reduction of B-site transition metal cations in polaron-hopping mechanism. The formed defect structures are found available for sintering when there is a second oxygen loss reaction which assures the stability of reduced states and also the defect complex. The proposed mechanism is verified by comparing the results of LSCF and that of previously reported MnCo_2O_4 . As ultimate conclusion, the very short sintering time (<1 min or 20-30 s), processing at 25-100°C and sintering, activated-mediated by usual phenomenon can lead to improved sintering results for microstructure and interfacial reaction in multilayer development.

4.3 Flash-sintering of LSCF/GDC Composites

4.3.1 Flash-sintering

4.3.1.1 Power Dissipation

Out of the three LSCF/GDC mixtures, the power dissipation of the composite with higher GDC content i.e. LSCFGDC4060 subjected to different electric fields (7.5-20.0 V/cm) as a function of furnace temperature is shown in the Fig. 4.30. The same, power dissipation versus temperature plot for pure LSCF and GDC phases are shown in Fig. 4.31 for comparison of sintering parameters. It is observed that composite similar to pure LSCF phase undergoes rapid increase in the power dissipation in response to the application of electric field. This instantaneous increase is the signature behavior of flash-sintering effect. The shrinkage is observed at these rapid increases at temperatures shown in Fig. 4.30. Compared to conventional treatment temperatures, composite with the help of electric field can be sintered at very low furnace temperatures in less than a minute. With no field applied, LSCFGDC4060 starts sintering at about 820°C and requires higher than 1400°C in

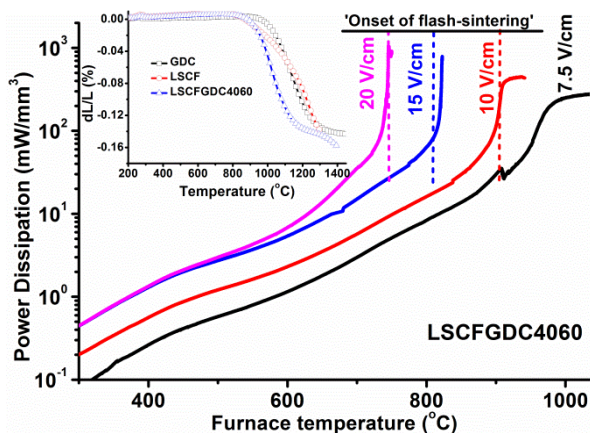


Figure 4.30: Power dissipation as a function of furnace temperature. Shrinkage profile of LSCFGDC4060 composite along with LSCF and GDC pure phases is shown in the inset

order to reach full density (inset of Fig. 4.30); it involves more than 100 min whereas in flash-sintering the sintering is achieved 740°C under 20 V/cm in 1 min of time (the extent of shrinkage is evaluated by SEM). In Fig. 4.30, power dissipation of composite, before flash-effect, increases in almost linear manner reflecting the continuous

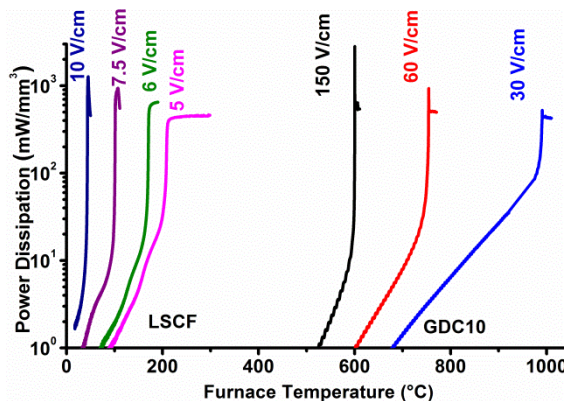


Figure 4.31: Power dissipation of pure phases, LSCF and GDC, as functions of furnace temperature observed under different electric field, showing difference in flash-parameter for the two compositions

increase of the conductivity with temperature. Slopes of this linear portion under different fields (7.5-15.0 V/cm) are almost constants over a wider range of temperatures, up to 800°C, compared to that of LSCF phase. The linear increase continues to higher temperatures for 7.5 V/cm, and until the flash-onset temperature of 905°C for 10.0 V/cm is reached where the flash occurs via a quick increase in the power dissipation. It subsequently leads to heating and sintering effect. The constant slope of the power dissipation at initial temperatures reflects the addition of low conductivity (and heat capacity) material GDC (Fig. 4.30). The first occurrence of flash under 10 V/cm and at 905°C suggest these to be threshold parameters for LSCFGDC4060 composition. Conversely, the flash-effect of conductivity in constituent phases, LSCF and GDC, starts occurring under 5 and 30 V/cm and at temperatures of 210°C and 1000°C respectively (Fig. 4.30). Substantially higher temperature for flash-onset is required in 4060 composite compared to pure LSCF phase.

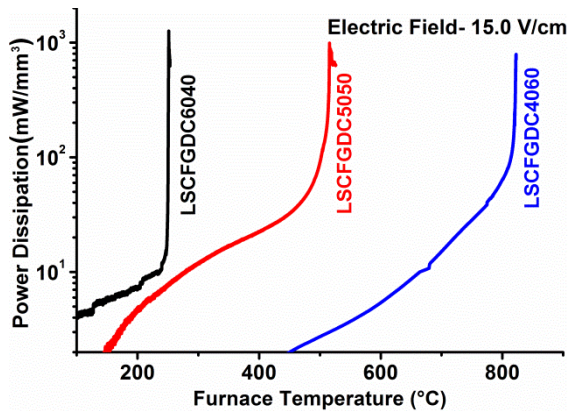


Figure 4.32: Power dissipation of LSCF/GDC composites with different weight ratios (60/40, 50/50 and 40/60) as functions of furnace temperature

The power dissipation of LSCF/GDC composites (60:40, 50:50, 40:60, LSCF:GDC weight ratio) under 15 V/cm as function of temperature is shown in Fig. 4.32. The flash-sintering parameters of the three compositions are mentioned in Table 1. All the compositions undergo rapid increase in the power dissipation which eventually leads to the rapid sintering effect. From the Fig. 4.32, composite containing higher LSCF sinters first at a furnace temperature of 240°C. With increase of GDC, sintering happens at higher temperature of 510 and 800°C. The curves show a significant and systematic increase in the onset temperature with GDC additions. Compared to LSCF, composites require higher electric fields (10-20 V/cm) and higher furnace temperatures for flash-sintering which is associated with the addition of low conductive GDC phase (right part of Fig. 4.31). Dominance of GDC in composites is reflected in gradual increase in power dissipation before the flash-onset which is clearly seen in higher GDC content composition.

In addition to the temperature and field, the threshold power dissipation which represents the minimum amount of energy required to drive the flash-effect is systematically increasing with the GDC content. The flash happens at 10-12 mW/mm³ for 60:40 compositions, it increased to 40 and 90 mW/mm³ for 50:50 and 40:60 compositions. The threshold value might be related to the mechanism of flash-effect. The

threshold value of power dissipation is found close to 10-15 mW/mm³ for all the compositions of conductivities ranging from conducting MnCo₂O₄ and insulating alumina. In case of LSCF, its value is found the lowest of all, less than 10 mW/mm³ (5-7 mW/mm³), and for GDC it is close to 10-12 mW/m³. In case of composite, this threshold value is found higher than that of LSCF and GDC. Therefore, flash-sintering of composite represents the versatility of the sintering scheme.

Table 4.3: Flash-sintering parameters of LSCF/GDC composites

Composition LSCF/GDC Wt %	Current Density A/mm ²	Electric field V/cm	Furnace Temperature °C
100/0	1.50	5.0-12.5	25-260
60/40	0.90	7.5-20.0	220-325
50/50	0.56	10.0-20.0	350-700
40/60	0.56	10.0-20.0	750-905
0/100	0.18-0.20	30.0-120	600-990

4.3.2 Microstructure Evolution

The backscattered electron mode micrographs of LSCF: GDC composites with weight ratios of 60:40, 50:50 and 40:60 subjected to 20 V/cm are shown in Fig. 4.33. The white phase corresponds to LSCF phase and black ones to GDC. Two phases are homogeneously grown and dispersed in all the three sintered sample. The microstructure form connected grain-network of each phase for all compositions. The grains are totally packed suggesting that under the chosen current densities, 20 V/cm is sufficient to reach full density at relatively lower processing temperatures. Well grown and homogeneous microstructures of composites under E-field suggest that the two phases are good compatible under the flash-sintering which starts with increase in the conductivity and leads to sintering. The choice of the current density is clearly realized to be an important parameter in controlling the microstructure of composites. Under the same current density of 0.59 A/mm², average grain size of 5050 composition is observed to be <1 μm and for 4060, it is relatively higher i.e. ~2.5 μm. Being more conductive, 5050 composite requires more current in order to have the same effect on the microstructure. It is clear from 6040 composition also which with a higher current density of 0.90 A/mm² shows grains larger than that of 5050, but still smaller than 4060 composite. Such observation shows the importance

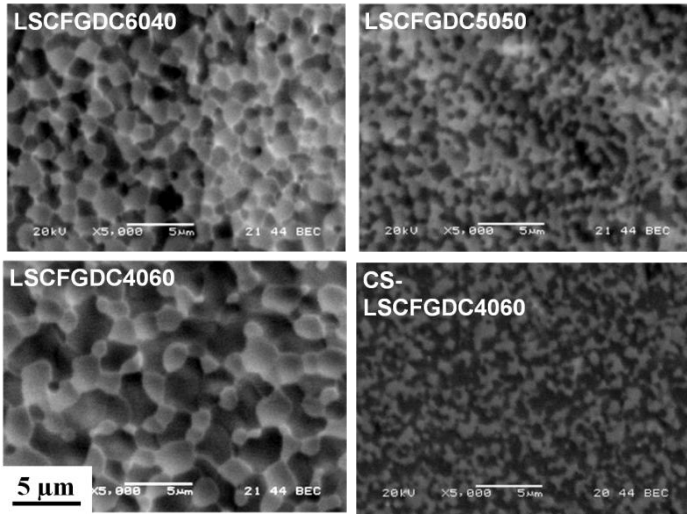


Figure 4.32: SEM micrograph of LSCF/GDC composite (60/40, 50/50 and 40/60 wt%) flash-sintered under 20 V/cm, and LSCFGDC4060 conventionally sintered at 1400°C.

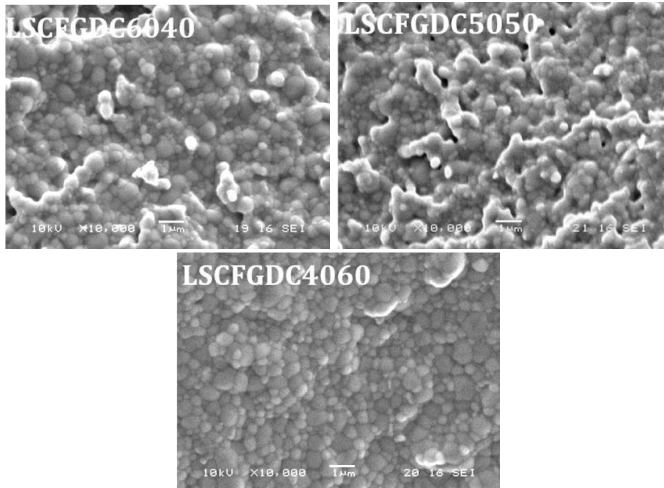


Figure 4.33: SEM micrograph of LSCF/GDC: 60/40, 50/50 and 40/60 wt% composites flash-sintered under 15 V/cm.

of current density in flash-sintering for different conductivity-compositions. Along with 20 V/cm, it is well observed for the samples produced under 15 and 10 V/cm fields

also, as shown in Fig. 4.33 and 4.34. Under the same field, compositions containing more LSCF require higher current to guarantee the same dense microstructure. 50/50 LSCF/GDC composite is slightly more porous than 40/60 one under 0.57 A/mm², whereas with higher current density (0.9 A/mm²) 60/40 LSCF/GDC composite is dense. It also suggests that with the proper choice of current density, porous morphology can also be produced for cathodic application. The microstructure of the composites appears sintered to larger areas with respect to pure LSCF which is related to the higher green density of the composites which provides more homogeneously distributed conductive environment around LSCF grains.

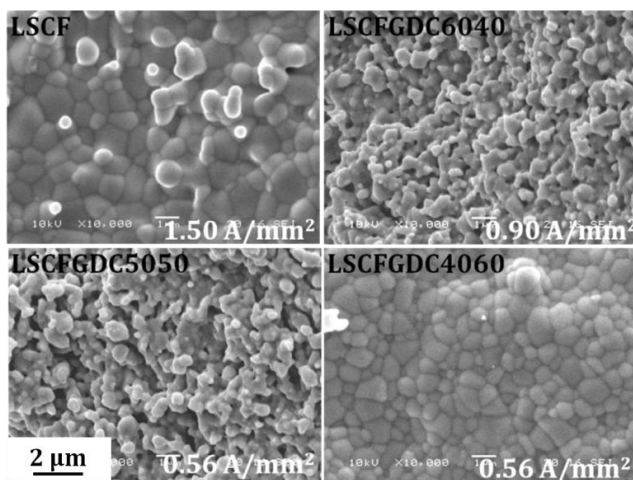


Figure 4.34: SEM micrograph of LSCF/GDC: 60/40, 50/50 and 40/60 wt% composites flash-sintered under 10 V/cm.

4.3.3 Phase-compatibility

Compatibility of the two phases under flash-sintering is analyzed by XRD. The pattern of LSCFGDC4060 sample flash-sintered under the highest field of 20 V/cm along with that of untreated LSCF, GDC10 and LSCFGDC4060 composite powders is shown in Fig. 4.35. In the pattern, there is no extra peak in the flash-sintered LSCFGDC4060 sample, other than that of constituent LSCF and GDC phase which confirms the compatibility of two phases under flash-sintering.

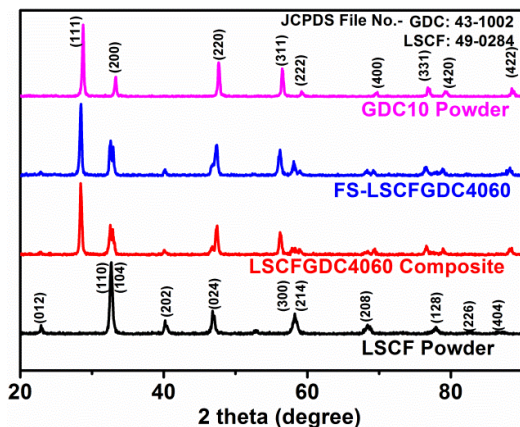


Figure 4.35: XRD pattern of flash-sintered LSCFGDC4060 composite, along with untreated composite and pure phase powders.

4.3.4 Electrical Conductivity of LSCFGDC4060

In the similar way as for LSCF, electric conductivity is analyzed under electric field and temperature, in order to compare/distinguish the flash-effect of composite from the pure LSCF phase.

4.3.4.1 Conductivity versus Temperature

The electrical conductivity of 1300°C-sintered LSCFGDC4060 composite (having highest GDC %) sample as a function of temperature is shown in Fig. 4.36. The conductivity of composite, observed under 0.25-0.5 V/cm, increases with temperature in a rather linear manner with respect to pure LSCF whose conductivity increases in a non-linear fashion (Fig. 4.23). For the obvious reason, the conductivity has decreased significantly, by almost one fourth with GDC addition. Under higher electric fields, the conductivity starts showing deviations, and a jump kind of behavior is observed under a minimum field of 1.75 V/cm. In case of LSCF, the same occurred at a minimum of 0.5 V/cm. The observed conductivity changes suggest that the by GDC10 addition, phase has become relatively inert against electric field. The conductivity changes of composite with respect to LSCF are associated with the flash-

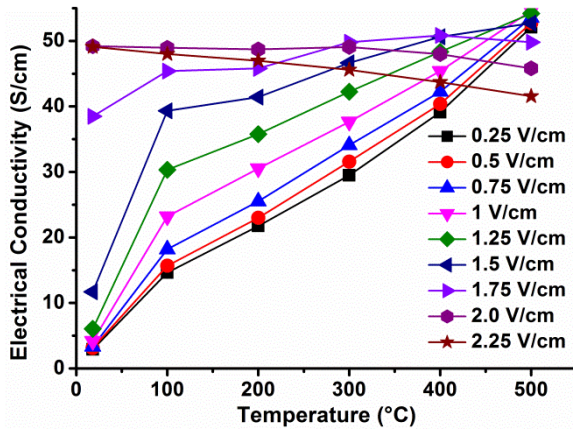


Figure 4.36: Electrical conductivity of LSCFGDC4060 composite as a function of temperature, measured under different electric fields.

sintering behavior. Rather linear behavior suggests that composite needs relatively higher field to cause a significant change in the conductivity. From the previous sections, it is clear that increase in conductivity is related with the generation of defects which facilitates sintering. Therefore, for composite sintering the required electric field spreads over a wider range. It is observed in microstructure also where change of microstructure from 10 to 20 V/cm is shown in Fig. 4.32 and 4.34, and for LSCF in Fig. 4.20 it is clearly shown that a small increase of field say, from 10 to 12.5 V/cm, causes significant changes the microstructure.

4.3.4.2 Conductivity versus Electric field

The electrical conductivity of 1300°C-sintered LSCFGDC4060 composite sample as a function of electric field, observed at different temperatures (18°C and 100-500°C) is shown Fig. 4.37. Systematic change in conductivity versus electric field curves with temperature is observed for composite as well. Being less conductive the conductivity trend at 18°C resembles to flash-kind of effect shown by current density plot in the inset figure. The current density increases in a rather faster manner compared to LSCF (Fig. 4.25) representing closeness to the electric field stimulated effect.

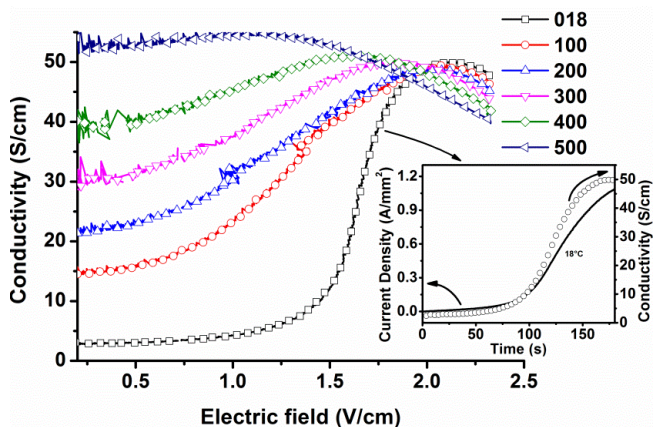


Figure 4.37: Electrical conductivity of 1300°C-sintered LSCFGDC4060 sample as a function of electric field observed at 18 and 100-500°C.

4.3.5 Summary

In this section, flash-sintering of LSCF/GDC composite with different weight ratios (40/60, 50/50 and 60/40) is reported. LSCF-GDC composite flash sinters at relatively higher temperature and under higher electric field. The sintering parameters increase systematically with respect to GDC addition. The sintering effect on grain morphology is found to be homogenous, which is a good observation for optimization of porosity under flash-effect. Current is observed to be an important parameter in controlling the microstructure and the porosity. The addition of GDC to LSCF increases homogeneity-isotropy in sintering. Electrical conductivity behavior of dense LSCFGDC4060 composition under electric field and temperature is reported in order to differentiate it with the pure LSCF phase. The sintering and conductivity results are correlated and suggested that addition of GDC makes the materials system relatively inert against electric field, so a higher field is required to bring significant sintering.

Chapter V

Conclusion and Future Perspective

In the present doctorate research work, the recently adopted electric field assisted flash-sintering technique is applied to two electrically conducting ceramics, MnCo_2O_4 and LSCF which are promisingly used in SOFC technology. Flash-sintering is extended to LSCF-GDC composites which are considered as improved cathode material compared to pure LSCF in SOFC. The motivation of the work is to understand the flash-sintering behavior of conducting-edge ceramics and to evaluate the effect of DC electric field on the electrical conductivity of two ceramics, in order to better formulate the phenomenon of flash-sintering for practical applications.

The conducting MnCo_2O_4 and LSCF samples are densified at very low processing temperatures, within a couple of seconds by employing a sufficiently high electric field. These materials in sharp contrast to weakly conducting materials like zirconia, GDC or alumina require relatively smaller electric fields and temperatures. It is shown that, 59% dense green MnCo_2O_4 samples are sintered at 220-310°C when subjected to 7.5-12.5 V/cm in a constant heating rate experiment, while 67% dense sample sinters at 170-250°C. Conversely LSCF, being more conductive, needs lower temperatures and surprisingly sinters at 25-100°C under similar fields, 7.5-12.5 V/cm. Composites show similar flash-sintering behavior, however, sinter under relatively higher electric field and at higher temperature. Such flash-sintering effect of the materials is associated with the semiconducting behavior and the requirement of very low temperature for LSCF and MnCo_2O_4 is associated with their high conductivity. The flash-effect of LSCF unlike to MnCo_2O_4 and other reported materials shows a continuous increase in the conductivity which lasts for significant period of time, more than 2 min which is unusual among the already discussed materials. Such observation is shown initially as an increase in the power dissipation and after the peak as continuous decrease of power dissipation. For MnCo_2O_4 the power dissipation or conductivity attains a steady value within 5 s after the flash-onset.

The pyrometric measurement of specimen temperature was fruitful in determining the sintering behavior. It confirms that flash-sintering occurs in the same temperature range as required during conventional sintering. For both oxide materials, a large extent of the sintering is achieved within a short interval of time, just as flash occurs and temperature reaches close to a sufficient maximum within 5-6 s duration of time. The shrinkage of LSCF sample is significantly improved, after this initial period, along with further increase of the conductivity. It was not the case with MnCo_2O_4 . Following the power dissipation, LSCF experiences continuous decrease in temperature. No shrinkage was observed when temperature under such decrease went down to 800°C , even though it is associated with a continuous increase in the conductivity. Such correlation between shrinkage, specimen temperature and conductivity implies that 1) in flash-sintering temperature has the same importance as in conventional process and 2) for fast and enhanced sintering, the increase in conductivity is a necessary condition and is not the only requirement. From the first point, electric field does not seem to change the diffusion activation energy of ions and therefore quick sintering is pointed to be the result of increased defect concentrations. The increased defects concentration might be associated with electric field through rapid increase in the conductivity. Therefore, the observed power dissipation and temperature behaviors are associated with the conductivity property and sintering mechanism of the considered materials, LSCF and MnCo_2O_4 .

The extent of sintering is confirmed through SEM analysis. Micro-structural observations suggest similar morphology and homogeneous grain growth compared to traditional sintering; with the proper choice of processing parameters (electric field and current density) during flash-sintering, dense/pore-free microstructure for MnCo_2O_4 coating or porous microstructure of LSCF for cathodic application can be obtained in very short time. The microstructure of flash-sintered MnCo_2O_4 evolves noticeably after specimen temperature reaches 1100°C . A clear difference in microstructure is observed before and after this temperature. The implication was made by comparing the microstructure with conventionally produced samples. The sintering was enhanced over its conventional counterpart only for temperatures higher than 1100°C . It was realized in the managing of flash-sintering experiment also; the ex-

periment and the samples were easy to handle for $<1100^{\circ}\text{C}$ but the samples were quickly affected (sintered) and broken if temperature was higher than this. No such temperature discrimination was observed for LSCF and its composite samples, in both, SEM microstructure and managing of experiments/samples. Micro-structural observation of LSCF and composites suggest that sintering effect is homogenous and regular with the electric field and the local temperature. Sintering is always found to be enhanced over its conventional counterpart. Current density is noted to be an important parameter for microstructure when dealing with different LSCF/GDC compositions. From XRD analysis, MnCo_2O_4 phase decomposes to CoO secondary phase by significant amounts for samples treated to 1100°C and higher temperatures. The concentration of CoO phase was found higher for flash-sintered samples compared to that of conventionally-sintered for the same time. The growth of microstructure is correlated with the phase stability or vice versa. The phases of LSCF and LSCF/GDC were well preserved in flash-sintering. The temperature observations about phase stability are in accordance with conventional sintering.

The effect of DC electric field on electrical conductivity of dense specimens is investigated in detail. Conductivity versus electric field curves of MnCo_2O_4 and LSCF (also of composites) changes in a consistent manner with temperatures. For the considered electric field range and the increasing rate, the conductivity is not constant at any temperature but changes substantially with electric field following materials specific trends. The conductivity of MnCo_2O_4 continuously increases with electric field whereas LSCF shows increasing tendency followed by a decrease. The conductivity increasing rate (degrees of non-linearity) is different at different temperatures. The conductivity of composites follows the trend of LSCF but with a rather linear manner which is associated with GDC addition. These observations suggest that electric field and temperature can affect the conductivity in, more or less, the same way, their relative competences vary with temperature (or vice versa). The measurement of specimen temperature elucidates the role of electric field at higher and low temperatures. In case of MnCo_2O_4 , at higher temperatures ($500\text{-}600^{\circ}\text{C}$), the conductivity and specimen temperature simultaneously increase in a systematic ways, suggesting that the enhanced conductivity is the result of increase in specimen

temperature by Joule-effect. At sufficiently low temperature of 200°C, it is clearly observed that electric field causes a rapid increase in the conductivity by its own impact in a situation when thermal effects are very low; the rise in the specimen temperature is subsequent effect of this conductivity increase. It is manifested in a time lag of 2-3 s between conductivity and temperature data and the reliability of this 'small time difference' observation lies in that the data were recorded at a speed of ~0.17s/each data. At intermediate temperatures (300-400°C) the conductivity increases are moderate, not as smooth as at higher temperature and not as drastic as at lower temperature. The effect is intermediate of electric field and temperature effect. So, a clear crossover between the roles of electric field for conductivity occurs. At one side conductivity increases thermally, rather gradually and at other side conductivity takes a direct sweep to higher values by electric field. In case of MnCo_2O_4 it occurs first when temperature is 200°C and electric field is 5.18 V/cm, referred as threshold values. This is also the point of (maximum) temperature and (minimum) electric field where first time flash-sintering effect starts.

The consistent change of conductivity is observed in LSCF as well its composites. LSCF presents a nice system with characteristics increasing-decreasing conductivity behavior which clearly displays the stimulated effect of electric field. Non-linear behavior suggests that the 1-2 V/cm is sufficient for LSCF to strongly interact with the material. The observed changes of conductivity in LSCF are associated with electric field derived increase in temperature. Being highly conductive flash-like effect is not visible in dense specimen at ambient temperature; it follows from the smooth increase in the current density with electric field/temperature. Conversely being less conductivity, increase in the conductivity of composite at similar temperatures has more closeness to the flash-effect. From the systematic changes, the results can be extrapolated to realize that in dense LSCF, the flash-effect will occur at lower temperatures and those higher than room temperature belongs to FAST regime. The electrical conductivity results clearly show that the electric field may act for conductivity in two ways, 1) by thermal excitation or Joule effect and 2) by direct excitation or energy transfer to charge carriers. Such electric field based effect from literatures

can be explained in terms of Poole effect (electric field enhanced thermal excitation), phonon/electric field assisted tunneling and direct tunneling.

- 1) At high temperature: Increased conductivity effect is better associated with electric field enhanced thermal excitation of charge carriers (Poole-Frankel effect)
- 2) At low temperature: Such effect is associated with 'direct excitation' of carriers where the energy is provided directly from the field (direct tunneling)
- 3) At intermediate temperatures: The conductivity behavior is explained as the outcome of Phonon/electric field assistance tunneling during thermal excitation of charge which increases the generation rate of carriers.

From the systematic ohmic to non-ohmic changes, sudden increase in the conductivity during flash-effect is suggested to follow the usual small polaron hopping mechanism and therefore, sintering is proposed to be accelerated by utilizing defect complexes formed during this hopping. A correlation between the microstructure, phase structure and the conductivity, suggest a constraint about the utilization of defect complex for sintering. In hopping, the forward reduction reaction results into generation of defect complex whereas the backward oxidation reaction of oxidation acts for annihilation. These transitions are thermally activated and occur at the same rate, up to a certain temperature. The formation of such defect complex is favorable for sintering only when the reduction reaction is stable and there is probability imbalance between two reactions. Such a situation probably assures the availability of defect complexes for any other cause such as sintering. For equally probable transitions, the defect complex is more under the tendency of oxidation reaction. It is realized from the case of MnCo_2O_4 . In this, the sintering is found to be enhanced over conventional sintering only when the temperature is higher than 1080°C . Before this temperature, the relatively poorer microstructure is associated as the result of sintering from rapid thermal effect. This reduction reaction is visible in MnCo_2O_4 in the form of CoO phase and oxygen weight loss. Similar kind of reduction reaction associated with polaron hopping is involved in LSCF also. It is visible only in the form of weight loss which is comparatively smaller and gradual, associated to LSCF for all sintering

temperatures. For this reason sintering is enhanced for all considered temperature and gradual weight loss supports the observed comparatively slow sintering behavior of LSCF.

As a final conclusive statement, the flash-sintering in polaron hopping conduction mechanism-based materials occurs by the movement of 'reduced' transition metal cations following the usual mechanism. Such kind of situation is available at all sintering temperature for LSCF and above 1080°C for MnCo_2O_4 .

Future Perspective

The present thesis reports the detailed analysis on the flash-sintering behavior of MnCo_2O_4 and LSCF electro-ceramics. The work reaches to insight of the flash-effect where role of electric field (thermal and/or direct excitation) for increasing the conductivity and the sintering rate is better realized. It helps to understand the evolution of microstructure and phase with electric field/temperature which is fundamental to know for any application.

Regarding the use of this sintering scheme, the phase-stability and sintering of electrically conductive systems, especially those based on polaron hopping conduction mechanism, is interrelated. Therefore, MnCo_2O_4 like materials for which high temperature phase loss is a sintering issue, careful control of treatment time can provide an optimal level of porosity and phase stability. Work remains on sintering the materials in the form of coating on planar substrate or in other geometrical arrangement. For cathode, it is shown that a series of microstructure from porous to fully dense can be achieved by proper control of electrical parameters and time. In a further move, flash-sintering can be used for sintering multilayer structure. Flash-sintering is a conductivity based phenomenon, so depending upon the conductivity of anode, electrolyte and cathode a selective flash-sintering would be a future work. For the sintering of such multilayer' in a parallel circuit type of electrical arrangement, the conductive phases would tend to decrease the drop and would draw more currents through it. Their relative thickness may play a role in controlling the sintering effect.

References

- [1] Colombo P, Mera G, Riedel R, Sorarù GD. Polymer-derived ceramics: 40 years of research and innovation in advanced ceramics. *J Am Ceram Soc* 2010;93:1805–37.
- [2] Yordanov SP, Ivanov I, Carapanov CP. Dielectric properties of the ferroelectric Bi₂Ti₂O₇ ceramics. *J Phys D Appl Phys* 1998;31:800–6.
- [3] Manicone PF, Rossi Iommetti P, Raffaelli L. An overview of zirconia ceramics: basic properties and clinical applications. *J Dent* 2007;35:819–26.
- [4] Eom J-H, Kim Y-W, Raju S. Processing and properties of macroporous silicon carbide ceramics: A review. *J Asian Ceram Soc* 2013;1:220–42.
- [5] Yokokawa H, Sakai N, Horita T, Yamaji K. Recent Developments in Solid Oxide Fuel Cell Materials. *Fuel Cells* 2001;1:117–31.
- [6] Agarwal D C. *Technology Advanced Ceramics*. IIT Kanpur, India 2000.
- [7] Badwal SPS, Ciacchi FT. Oxygen-ion conducting electrolyte materials for solid oxide fuel cells. *Ionics (Kiel)* 2000;6:1–21.
- [8] Stevenson JW, Armstrong TR, Carneim RD, Pederson LR, Weber WJ. Electrochemical Properties of La_{1-x}M_xCo_{1-y}Fe_yO₃- Mixed Conducting Perovskites (M = Sr, Ba, Ca). *J Electrochem Soc* 1996;143:2722–9.
- [9] Yi E-J, Yoon M-Y, Moon J-W, Hwang H-J. Fabrication of a MnCo₂O₄ /gadolinia-doped ceria (GDC) dual-phase composite membrane for oxygen separation. *J Korean Ceram Soc* 2010;47:199–204.
- [10] Auerkari P. *Mechanical and physical properties of engineering alumina ceramics* 1996.
- [11] Clarke DR, Oechsner M, Padture NP. Thermal-barrier coatings for more efficient gas-turbine engines. *MRS Bull* 2012;37:891–8.
- [12] Krogstad J a., Krämer S, Lipkin DM, Johnson C a., Mitchell DRG, Cairney JM, et al. Phase Stability of t'-Zirconia-Based Thermal Barrier Coatings: Mechanistic Insights. *J Am Ceram Soc* 2011;94:168–77.

- [13] Shimoda K, Eiza N, Park J-S, Hinoki T, Kohyama A, Kondo S. High-Temperature Mechanical Property Improvements of SiC Ceramics by NITE Process. *Mater Trans* 2006;47:1204–8.
- [14] Piconi C, Maccauro G. Zirconia as a ceramic biomaterial. *Biomaterials* 1999;20:1–25.
- [15] Okada M, Furuzono T. Hydroxylapatite nanoparticles: fabrication methods and medical applications. *Sci Technol Adv Mater* 2012;13:064103.
- [16] Liu B, Lun D. Current application of β -tricalcium phosphate composites in orthopaedics. *Orthop Surg* 2012;4:139–44.
- [17] Šponer P, Urban K, Kučera T, Kohout A, Brtková J, Knížek J. The use of interconnected β -tricalcium phosphate as bone substitute after curettage of benign bone tumours. *Eur J Orthop Surg Traumatol* 2010;21:235–41.
- [18] Huijsmans J. Ceramics in solid oxide fuel cells. *Curr Opin Solid State Mater Sci* 2001;5:317–23.
- [19] Minh N. Solid oxide fuel cell technology-features and applications. *Solid State Ionics* 2004;174:271–7.
- [20] Cologna M, Prette ALG, Raj R. Flash-sintering of cubic yttria-stabilized zirconia at 750°C for possible use in SOFC manufacturing. *J Am Ceram Soc* 2011;94:316–9.
- [21] Raj R. Joule heating during flash-sintering. *J Eur Ceram Soc* 2012;32:2293–301.
- [22] Gaur A, Sglavo VM. Flash-Sintering of MnCo_2O_4 and its relation to Phase Stability. *J Eur Ceram Soc* 2014;34:2391–400.
- [23] Francis JSC, Cologna M, Montinaro D, Raj R. Flash sintering of anode–electrolyte multilayers for SOFC applications. *Am Ceram Soc* 2013;96:1352–4.
- [24] Cologna M, Francis JSC, Raj R. Field assisted and flash sintering of alumina and its relationship to conductivity and MgO-doping. *J Eur Ceram Soc* 2011;31:2827–37.
- [25] Jha SK, Raj R. The Effect of electric field on sintering and electrical conductivity of titania. *J Am Ceram Soc* 2013;97:527–34.

- [26] Zapata-Solvas E, Bonilla S, Wilshaw PR, Todd RI. Preliminary investigation of flash sintering of SiC. *J Eur Ceram Soc* 2013;33:2811–6.
- [27] Prette ALG, Cologna M, Sglavo V, Raj R. Flash-sintering of Co_2MnO_4 spinel for solid oxide fuel cell applications. *J Power Sources* 2011;196:2061–5.
- [28] Narayan J. A new mechanism for field-assisted processing and flash sintering of materials. *Scr Mater* 2013;69:107–11.
- [29] Yang Z, Xia G, Li X, Stevenson J. $(\text{Mn},\text{Co})_3\text{O}_4$ spinel coatings on ferritic stainless steels for SOFC interconnect applications. *Int J Hydrogen Energy* 2007;32:3648–54.
- [30] Wang K, Liu Y, Fergus JW. Interactions Between SOFC Interconnect Coating Materials and Chromia. *J Am Ceram Soc* 2011;94:4490–5.
- [31] Fergus J. Effect of cathode and electrolyte transport properties on chromium poisoning in solid oxide fuel cells. *Int J Hydrogen Energy* 2007;32:3664–71.
- [32] Bentzen JJ, HÄ,gh JVT, Barfod R, Hagen. Chromium poisoning of LSM/YSZ and LSCF/CGO composite cathodes. *Fuel Cells* 2009;9:823–32.
- [33] Ebrahimifar H, Zandrahimi M, Habibifar H. Improved electrical conductivity of coated ferritic stainless steel used in SOFC as interconnect at 700°C. *2010;2:519–26.*
- [34] Fergus JW. Metallic interconnects for solid oxide fuel cells. *Mater Sci Eng A* 2005;397:271–83.
- [35] L.-W. Tai, M. M. Nasrallah, Anderson HU, Sparlin DM, Sehlin SR. Structure and electrical properties of $\text{La}_{1-x}\text{Sr}_x\text{Co}_{1-y}\text{Fe}_y\text{O}_3$. Part 1. The system $\text{La}_{0.8}\text{Sr}_{0.2}\text{Co}_{1-y}\text{Fe}_y\text{O}_3$. *Solid State Ionics* 1995;76:259–71.
- [36] Tai L-W, Nasrallah MM, Anderson HU, Sparlin DM, Sehlin SR. Structure and electrical properties of $\text{La}_{1-x}\text{Sr}_x\text{Co}_{1-y}\text{Fe}_y\text{O}_3$. Part 2. The system $\text{La}_{1-x}\text{Sr}_x\text{Co}_{0.2}\text{Fe}_{0.8}\text{O}_3$. *Solid State Ionics* 1995;76:255–71.
- [37] Leng Y, Chan S, Liu Q. Development of LSCF–GDC composite cathodes for low-temperature solid oxide fuel cells with thin film GDC electrolyte. *Int J Hydrogen Energy* 2008;33:3808–17.

- [38] Figueiredo FM, Labrincha JA. Reactions between a zirconia-based electrolyte electrode materials. *Solid State Ionics* 1997;101-103:343–9.
- [39] Kawada T, Yokokawa H, Dokiya M. Ceria-zirconia composite electrolyte for solid oxide fuel cells. *J Electroceramics* 1997:155–64.
- [40] Karakuscu A, Cologna M, Yarotski D, Won J, Francis JSC, Raj R, et al. Defect structure of flash-sintered strontium titanate. *J Am Ceram Soc* 2012;95:2531–6.
- [41] Massarotti V, Capsoni D, Bini M, Chiodelli G, Azzoni CB, Mozzati MC, et al. Electric and Magnetic Properties of LiMn_2O_4 - and Li_2MnO_3 -Type Oxides. *J Solid State Chem* 1997;100:94–100.
- [42] Tanaka H, Yamamoto A, Shimoyama J, Ogino H, Kishio K. Strongly connected ex situ MgB_2 polycrystalline bulks fabricated by solid-state self-sintering. *Supercond Sci Technol* 2012;25:115022.
- [43] Forrester JS, Goodshaw HJ, Kisi EH, Suaning GJ, Zobec JS. Effect of Mechanical Milling on the Sintering Behaviour of Alumina 2008:47–52.
- [44] Indrakanti SS, Nesterenko VF, Maple MB, Frederick NA. Hot isostatic pressing of bulk magnesium diboride : mechanical and superconducting properties n.d.
- [45] Yang Z, Xia G, Simner SP, Stevenson JW. Thermal growth and performance of manganese cobaltite spinel protection layers on ferritic stainless steel SOFC interconnects. *J Electrochem Soc* 2005;152:A1896.
- [46] Asgharzadeh H, Ehsani N. Densification and microstructural evolutions during reaction sintering of SiC-Si-C powder compacts. *ISRN Mater Sci* 2011;2011:1–7.
- [47] Rahaman MN. *Sintering of Ceramics*. CRC Press; 2014.
- [48] Matsui K, Ohmichi N, Ohgai M, Enomoto N, Hojo J. Sintering kinetics at constant rates of heating: Effect of Al_2O_3 on the initial sintering stage of fine zirconia powder. *J Am Ceram Soc* 2005;88:3346–52.
- [49] Rhamdhani MA, Soepriyanto S, Ramelan A, Barliansyah A. Determination of mechanism and grain growth kinetics of MgO doped Al_2O_3 . *J Trop Med* 2005;12:148–58.

- [50] Hua B, Pu J, Gong W, Zhang J, Lu F, Jian L. Cyclic oxidation of Mn–Co spinel coated SUS 430 alloy in the cathodic atmosphere of solid oxide fuel cells. *J Power Sources* 2008;185:419–22.
- [51] Wang S, Kobayashi T, Dokiya M, Hashimoto T. Electrical and Ionic Conductivity of Gd-Doped Ceria. *J Electrochem Soc* 2000;147:3606.
- [52] Groza JR, Zavaliangos A. Sintering activation by external electrical field. *Mater Sci Eng A* 2000;287:171–7.
- [53] Knibbe R, Drennan J, Dicks a., Love J. Effect of alumina additions on the anode|electrolyte interface in solid oxide fuel cells. *J Power Sources* 2008;179:511–9.
- [54] Rajeswari K, Reddy R, Hareesh US, Saha BP, Johnson R. Micro structural control of stabilized Zirconia ceramics (8YSZ) through modified conventional sintering methodologies. *Sci Sinter* 2010;42:91–7.
- [55] Xiao C-J, Chi Z-H, Li F-Y, Feng S-M, Jin C-Q, Wang X-H, et al. prepared by high pressure assisted sintering. *Chinese Phys Socety* 2007;16:3125–8.
- [56] Stanciu LA, Kodash VY, Groza JR. Effects of heating rate on densification and grain growth powders 2001;32:2633–8.
- [57] Weerasinghe HC, Sirimanne PM, Franks GV, Simon GP, Cheng YB. Low temperature chemically sintered nano-crystalline TiO₂ electrodes for flexible dye-sensitized solar cells. *J Photochem Photobiol A Chem* 2010;213:30–6.
- [58] Taktak R, Baklouti S, Bouaziz J. Effect of binders on microstructural and mechanical properties of sintered alumina. *Mater Charact* 2011;62:912–6.
- [59] Takekawa J. Effect of binder composition on debinding and sintering processes of injection molded Fe–8Ni mixed powders. *J Mater Res* 2011;11:1127–32.
- [60] He Y, Winnubst A, Verweij H, Burggraaf A. Improvement of mechanical properties of zirconia-toughened alumina by sinter forging. *J Mater Sci* 1994;29:5868–74.
- [61] He YJ, Winnubst J, Verweij H, Burggraaf. J. Sinter forging of zirconia toughened alumina. *J Mater Sci* 1994;29:6505–12.

- [62] Ekimov E a., Sadykov R a., Gierlotka S, Presz a., Tatyanyin E V., Slesarev VN, et al. A High-Pressure Cell for High-Temperature Experiments in a Toroid-Type Chamber. *Instruments Exp Tech* 2004;47:276–8.
- [63] Kusonmaz N. High Pressure Sintering of Nano-Size γ -Al₂O₃. *Intech* 2013;57–71.
- [64] Khvostantsev LG, Sidorov VA, Tsiok OB. High pressure toroid cell: Applications in planetary and material sciences 1984.
- [65] Gallas MR, Rosa a. R, Costa TH, Jornada J a. H Da. High pressure compaction of nanosize ceramic powders. *J Mater Res* 2011;12:764–8.
- [66] Costa TMH, Gallas R, Benvenuti E V. Study of nanocrystalline γ -Al₂O₃ produced by high-pressure compaction 1999:4278–84.
- [67] Lee H-K, Kim K-M, Park M-K, Kang W-H. Microwave-assisted sintering of amorphous powders. *J Korean Ceram Soc* 2011;48:14–9.
- [68] Ck CRO. Electro-discharge consolidation of nanocrystalline Nb – Al powders produced by mechanical alloying n.d.;3:241–6.
- [69] Groza JR, Zavaliangos A. Nanostructured bulk solids by field activated sintering. *Rev Adv Mater Sci* 2003;5:24–33.
- [70] Downs JA, Sglavo VM. Electric field assisted sintering of cubic zirconia at 390°C. *J Am Ceram Soc* 2013;96:1342–4.
- [71] Khanra AK, Patra S, Godkhindi MM. Electrical discharge machining studies on reactive sintered FeAl. *Bull Mater Sci* 2006;29:277–80.
- [72] Cologna M, Rashkova B, Raj R. Flash sintering of nanograin zirconia in <5 s at 850°C. *J Am Ceram Soc* 2010;93:3556–9.
- [73] Ghosh S, Chokshi AH, Lee P, Raj R. A huge effect of weak dc electrical fields on grain growth in zirconia. *J Am Ceram Soc* 2009;92:1856–9.
- [74] Yang D, Conrad H. Enhanced sintering rate of zirconia (3Y-TZP) by application of a small AC electric field. *Scr Mater* 2010;63:328–31.
- [75] Raj R, Cologna M, Francis JSC. Influence of externally imposed and internally generated electrical fields on grain growth, diffusional creep,

- sintering and related phenomena in ceramics. *J Am Ceram Soc* 2011;94:1941–65.
- [76] Yang D, Raj R, Conrad H. Enhanced Sintering Rate of Zirconia (3Y-TZP) Through the Effect of a Weak dc Electric Field on Grain Growth. *J Am Ceram Soc* 2010;93:2935–7.
- [77] Cologna M, Prette ALG, Raj R. Flash-sintering of cubic yttria-stabilized zirconia at 750°C for possible use in SOFC manufacturing. *J Am Ceram Soc* 2011;94:316–9.
- [78] Hao X, Liu Y, Wang Z, Qiao J, Sun K. A novel sintering method to obtain fully dense gadolinia doped ceria by applying a direct current. *J Power Sources* 2012;210:86–91.
- [79] Muccillo R, Muccillo ENS, Kleitz M. Densification and enhancement of the grain boundary conductivity of gadolinium-doped barium cerate by ultra fast flash grain welding. *J Eur Ceram Soc* 2012;32:2311–6.
- [80] Francis JSC, Raj R. Influence of the field and the current limit on flash sintering at isothermal furnace temperatures. *J Am Ceram Soc* 2013;96:2754–8.
- [81] Axel J, Downs M. Mechanism of flash-sintering. University of Trento, 2013.
- [82] Abdelkader M, Daher, Abdelkareem R, El-Kashif E. Preparation of zirconium metal by the electrochemical reduction of zirconium oxide. *Metall Mater Trans B* 2007;38:35–44.
- [83] Janek J, Korte C. Electrochemical blackening of yttria-stabilized zirconia – morphological instability of the moving reaction front. *Solid State Ionics* 1999;116:181–95.
- [84] Naik KS, Sglavo VM, Raj R. Field assisted sintering of ceramic constituted by alumina and yttria stabilized zirconia. *J Eur Ceram Soc* 2014;35.
- [85] Vakiv M, Shpotyuk O, Mrooz O, Hadzaman I. Controlled thermistor effect in the system $\text{Cu}_x\text{Ni}_{1-x-y}\text{Co}_2\text{yMn}_{2-y}\text{O}_4$. *J Eur Ceram Soc* 2001;21:1783–5.
- [86] Rousset a., Tenailleau C, Dufour P, Bordeneuve H, Pasquet I, Guillemet-Fritsch S, et al. Electrical properties of $\text{Mn}_{3-x}\text{Co}_x\text{O}_4$ ($0 \leq x \leq 3$) ceramics : An interesting system for negative temperature coefficient thermistors. *Int J Appl Ceram Technol* 2013;10:175–85.

- [87] Klym HI, Hadzaman I V, Shpotyuk OI. Nanostructured thick films based on spinel ceramics for multifunctional. *Nanomater Appl Prop* 2011;1:158–64.
- [88] Morozov I V., Lyubushkin R a., Fedorova a. a., Petrov MN, Burdeinaya TN, Trets'yakov VF. Physicochemical properties of manganese-containing oxides with a spinel structure prepared with the use of ammonium nitrate and their catalytic activity in carbon monoxide oxidation. *Kinet Catal* 2006;47:35–9.
- [89] Xiao J, Wan L, Wang X, Kuang Q, Dong S, Xiao F, et al. Mesoporous Mn_3O_4 -CoO core-shell spheres wrapped by carbon nanotubes: a high performance catalyst for the oxygen reduction reaction and CO oxidation. *J Mater Chem A* 2014;2:3794.
- [90] Liang Y, Wang H, Zhou J, Li Y, Wang J, Regier T, et al. Covalent hybrid of spinel manganese-cobalt oxide and graphene as advanced oxygen reduction electrocatalysts. *J Am Chem Soc* 2012;134:3517–23.
- [91] Edition I, Pirogova GN, Panich NM, Korosteleva RL. Regularities of formation and catalytic properties of supported cobaltites in the oxidation of CO and hydrocarbons and in the reduction of nitrogen oxides 2000;49:0–3.
- [92] Uusi-Esko K, Rautama E-L, Laitinen M, Sajavaara T, Karppinen M. Control of Oxygen Nonstoichiometry and Magnetic Property of $MnCo_2O_4$ Thin Films Grown by Atomic Layer Deposition. *Chem Mater* 2010;22:6297–300.
- [93] Bazuev GV, Korolyov a. V. Magnetic behavior of $MnCo_2O_{4+\delta}$ spinel obtained by thermal decomposition of binary oxalates. *J Magn Magn Mater* 2008;320:2262–8.
- [94] Joy PA, Date SK. Unusual magnetic hysteresis behavior of oxide spinel $MnCo O$ 2000;210:31–4.
- [95] Sakai N, Yokokawa H, Horita T, Yamaji K. Lanthanum Chromite-Based Interconnects as Key Materials for SOFC Stack Development. *Int J Appl Ceram Technol* 2005;1:23–30.
- [96] Fergus J. Lanthanum chromite-based materials for solid oxide fuel cell interconnects. *Solid State Ionics* 2004;171:1–15.
- [97] Yang Z, Xia G-G, Maupin GD, Stevenson JW. Evaluation of Perovskite Overlay Coatings on Ferritic Stainless Steels for SOFC Interconnect Applications. *J Electrochem Soc* 2006;153:A1852.

- [98] Bi ZH, Zhu JH, Batey JL. CoFe_2O_4 spinel protection coating thermally converted from the electroplated Co–Fe alloy for solid oxide fuel cell interconnect application. *J Power Sources* 2010;195:3605–11.
- [99] Qu W, Jian L, Hill JM, Ivey DG. Electrical and microstructural characterization of spinel phases as potential coatings for SOFC metallic interconnects. *J Power Sources* 2006;153:114–24.
- [100] Bordeneuve H, Rousset A, Tenailleau C, Guillemet-Fritsch S. Cation distribution in manganese cobaltite spinel $\text{Co}_{3-x}\text{Mn}_x\text{O}_4$ ($0 < x < 1$) determined by thermal analysis. *J Therm Anal Calorim* 2010;101:137–42.
- [101] Lange F, Martin M. The Electrical conductivity of CoO: Experimental results and a new conductivity model. *Ber Bunsenges Phys Chemi* 1997;101:176–84.
- [102] Yin Q, Lin YS. Effect of dopant addition on oxygen sorption properties of La-Sr-Co-Fe-O perovskite type oxide. *Adsorption* 2006;12:329–38.
- [103] Conductivity E. Electrical Conductivity and Seebeck Coefficient of Nonstoichiometric 1989;136:2082–8.
- [104] Patcas F, Buciuman FC, Zsako J. Oxygen non-stoichiometry and reducibility of B-site substituted lanthanum manganites. *Thermochim Acta* 2000;360:71–6.
- [105] Sebastian L, Shukla AK, Gopalakrishnan J. metal-substituted derivatives of lanthanum – strontium – gallium – magnesium (LSGM) perovskite oxide ion conductor. *Bull Mater Sci* 2000;23:169–73.
- [106] Lee M, Jun J, Jung J, Kim Y, Lee S. Catalytic Activities of Perovskite-type LaBO_3 (B = Fe , Co , Ni) Oxides for Partial Oxidation of Methane. *Bull Korean Chem Sociey* 2005;26:1591–6.
- [107] Yarbay RZ, Figen HE, Baykara SZ. Effects of Cobalt and Nickel Substitution on Physical Properties of Perovskite Type Oxides Prepared by the Sol – Gel Citrate Method. *Acta Phys Pol A* 2012;121:44–6.
- [108] Silva GRO, Santos JC, Martinelli DMH, Pedrosa AMG, Souza MJB, Melo DMA. Synthesis and Characterization of $\text{LaNi}_x\text{Co}_{1-x}\text{O}_3$ Perovskites via Complex Precursor Methods. *Mater Sci Appl* 2010;01:39–45.

- [109] Sun C, Hui R, Roller J. Cathode materials for solid oxide fuel cells: a review. *J Solid State Electrochem* 2009;14:1125–44.
- [110] Shuk P, Jantz R, Guth U. Advanced oxygen sensor with oxide electrode materials. 2011 Fifth Int. Conf. Sens. Technol., IEEE; 2011, p. 129–33.
- [111] Teraoka Y, Honbe Y, Ishii J, Furukawa H, Moriguchi I. Catalytic effects in oxygen permeation through mixed-conductive LSCF perovskite membranes 2002;153:681–7.
- [112] Habib M a., Ben Mansour R, Nemit-allah M a. Modeling of oxygen permeation through a LSCF ion transport membrane. *Comput Fluids* 2013;76:1–10.
- [113] Tan X, Liu N, Meng B, Sunarso J, Zhang K, Liu S. Oxygen permeation behavior of $\text{La}_{0.6}\text{Sr}_{0.4}\text{Co}_{0.8}\text{Fe}_{0.2}\text{O}_3$ hollow fibre membranes with highly concentrated CO_2 exposure. *J Memb Sci* 2012;389:216–22.
- [114] Jin W, Li S, Huang P, Xu N, Shi J. Preparation of an asymmetric perovskite-type membrane and its oxygen permeability 2001;185:237–43.
- [115] Zeng Y, Lin YS, Swartz SL. Perovskite-type ceramic membrane: synthesis, oxygen permeation and membrane reactor performance for oxidative coupling of methane. *J Memb Sci* 1998;150:87–98.
- [116] Kusaba H, Shibata Y, Sasaki K, Teraoka Y. Surface effect on oxygen permeation through dense membrane of mixed-conductive LSCF perovskite-type oxide. *Solid State Ionics* 2006;177:2249–53.
- [117] Kostogloudis GC, Ftikos C. Properties of A-site deficient $\text{La}_{0.6}\text{Sr}_{0.4}\text{Co}_{0.2}\text{Fe}_{0.8}\text{O}_{3-d}$ -based perovskite oxides. *Solid State Ionics* 1999;126:143–51.
- [118] Cullity BD. *Elements of X-ray Diffraction*. second edi. Addison-Wesley Publishing Company Inc.; 1977.
- [119] Hua B, Kong Y, Lu F, Zhang J, Pu J, Li J. The electrical property of MnCo_2O_4 and its application for SUS 430 metallic interconnect. *Chinese Sci Bull* 2010;55:3831–7.
- [120] Vivet N, Chupin S, Estrade E, Richard a., Bonnamy S, Rochais D, et al. Effect of Ni content in SOFC Ni-YSZ cermets: A three-dimensional study by FIB-SEM tomography. *J Power Sources* 2011;196:9989–97.

- [121] Bauerle JE. Study of solid electrolyte polarization by a complex admittance method. *J Phys Chem Solids* 1969;30:2657–70.
- [122] Ergant ZOB, Rum JAG. Porosity evaluation of flame-sprayed and heat-treated nickel-based coatings using image analysis. *J Image Anal Stereol* 2011;30:53–62.
- [123] Mohiddon a., Yadav KL. Reaction kinetics of PLZT formation and its effect on structural and dielectric properties. *Adv Appl Ceram* 2008;107:354–9.
- [124] Rajeevan NE, Kumar R, Shukla DK, Pradyumnan PP, Arora SK, Shvets IV. Structural, electrical and magnetic properties of Bi-substituted Co_2MnO_4 . *Mater Sci Eng B* 2009;163:48–56.
- [125] Moure C, Fernandez JF, Villegas M, Duran P. Non-Ohmic Behaviour and Switching Phenomena in YMnO_3 -Based Ceramic Materials 1999;19:131–7.
- [126] Zhang J, Cui W, Juda M, McCammon D, Kelley R, Moseley S, et al. Non-Ohmic effects in hopping conduction in doped silicon and germanium between 0.05 and 1 K. *Phys Rev B* 1998;57:4472–81.
- [127] Ganichev S, Ziemann E, Prettl W, Yassievich I, Istratov a., Weber E. Distinction between the Poole-Frenkel and tunneling models of electric-field-stimulated carrier emission from deep levels in semiconductors. *Phys Rev B* 2000;61:10361–5.
- [128] Tribelis GP, Dimakogianni M. Field and temperature dependence of the small polaron hopping electrical conductivity in 1D disordered systems. *J Phys Condens Matter* 2009;21:385406.
- [129] Kusmartseva, Yang M, Oro-Solé J, Bea. M, Fuertes, Atfield JP. Large magnetoresistances and non-Ohmic conductivity in $\text{EuWO}_{1+x}\text{N}_{2-x}$. *Appl Phys Lett* 2009;95:022110.
- [130] Belyaev AE, Semenow YG, Shevchenko NV. Non-ohmic conductivity in semimagnetic semiconductor $\text{p-MnxHg}_{1-x}\text{Te}$. *Am Inst Phys* 1990:164–6.
- [131] Govor L V., Bashmakov I a., Boehme K, Parisi J. Electrical field dependence of hopping conduction in self-organized carbon networks. *J Appl Phys* 2002;91:739.

- [132] Katzenmeyer AM, Léonard F, Talin a A, Wong P-S, Huffaker DL. Poole-Frenkel effect and phonon-assisted tunneling in GaAs nanowires. *Nano Lett* 2010;10:4935–8.
- [133] Bryksin V V, Damker T, Bottger H. Motion of localized carriers in a strong electric field. *J Phys Condens Matter* 1998;10:7907–21.
- [134] Liu H, Zhang L, Guo Y, Cheng C, Yang L, Jiang L, et al. Reduction of graphene oxide to highly conductive graphene by Lawesson's reagent and its electrical applications. *J Mater Chem C* 2013;1:3104.
- [135] Cheah CY, Kaiser AB. Variable-range hopping transport : Crossovers from temperature dependence to electric field dependence in disordered carbon materials 2009;x:1–6.
- [136] Schmidt R, Basu a., Brinkman a. Small polaron hopping in spinel manganates. *Phys Rev B* 2005;72:115101.
- [137] Zafar A, Imran Z, Rafiq MA, Hasan MM. Evidence of Pool-Frankel conduction mechanism in Sr-doped Lanthanum Ferrite $\text{La}_{1-x}\text{Sr}_x\text{FeO}_3$ ($0 \leq x \leq 1$) system. *Electron. Commun. Photonics Conf. (SIEPCPC)*, 2011 Saudi Int., vol. 3, 2011, p. 1–4.
- [138] Wang Z, Yu H, Su H. The transport properties of oxygen vacancy-related polaron-like bound state in HfOx. *Sci Rep* 2013;3:3246.
- [139] Zhang Y, Chang A, Cao J, Wang Q, Kim W, Li Y, et al. Electric-field-directed growth of aligned single-walled carbon nanotubes. *Appl Phys Lett* 2001;79:3155.
- [140] Yamazoe N, Teraoka Y, Seiyama T. TPS and XPS study on thermal behavior of absorbed oxygen in $\text{La}_{1-x}\text{Sr}_x\text{CoO}_3$. *Chem Lett* 1981:1767–70.
- [141] Teraoka Y, Masahiro Y, Yamazoe N, Tetesuro S. Oxygen-sorptive properties and defect structure of perovskite-type oxides. *Chem Lett* 1984:893–6.
- [142] Naik K, Raj R, Sglavo VM. Flash Sintering as a nucleation phenomenon and a model thereof. *J Eur Ceram Soc* 2014.
- [143] Nenashev A V, Jansson F, Baranovskii SD, Osterbacka R, Dvurechenskii A V, Gebhard F. Hopping conduction in strong electric fields: Negative differential conductivity 4 ~ 2008:1–12.

- [144] Santos S., Salazar I. High electric field effect on hopping conduction in molecularly doped polymer systems. *Polymer (Guildf)* 1999;40:4415–8.

Curriculum Vitae

Education:

Doctor of Philosophy (2011-2014)

Materials Science and Engineering

University of Trento, Italy

Title: 'Flash-sintering of MnCo_2O_4 and $(\text{La}, \text{Sr})(\text{Co}, \text{Fe})\text{O}_3$ Ceramics for Potential Application in SOFC'

Masters of Technology (2009)

Solid State Electronic Materials

Indian Institute of Technology Roorkee, India

Masters of Science (2006)

Physics

DDU Gorakhpur University, India

Bachelors of Science (2004)

St. Andrew's College, Gorakhpur, India

Research Experience:

M. Tech. Project (July 2008-December 2008)

Title: Structural and optical studies of BiFeO_3 thin film'

Supervisor: Dr. Davinder Kaur, Assistant Professor,
Department of Physics, IIT Roorkee

M. Tech. Dissertation (July 2008- June 2009)

Title: 'Synthesis and characterization of pulsed laser deposited Nd doped BiFeO_3 thin films'

Supervisor: Dr. Davinder Kaur, Assistant Professor,
Department of Physics, IIT Roorkee

Senior Research Fellow (September 2009- December 2010)

Title: 'Technology Development and Research with Photonic Crystal Fibers and Components for Advanced Photonic Sensor System'

Supervisor: Dr. Partha Roychoudhary, Assistant Professor,
Department of Physics and Meteorology, IIT Kharagpur

Papers in Referred Journals:

- 1) A. Gaur, V.M. Sglavo, 'Flash-sintering of MnCo_2O_4 and its relation to phase stability', J. Eur. Ceramic Society 34 (2014) 2391-2400.
- 2) A. Gaur, V.M. Sglavo, 'Densification of $(\text{La}, \text{Sr})(\text{Co}, \text{Fe})\text{O}_3$ ceramic by flash-sintering at 100°C ', J. Mate. Sci. 2014, DOI: 10.1007/s10853-014-8357-2.
- 3) R.S. Pillai, A. Gaur, S. Dirè, V.M. Sglavo, 'Effect of MgO incorporation on the synthesis temperature and high temperature phase stability of beta tricalciumphosphate', 2014, (manuscript under preparation).
- 4) A. Gaur, V.M. Sglavo, 'Flash-sintering of $(\text{La}, \text{Sr})(\text{Co}, \text{Fe})\text{O}_3$ and Gd doped CeO_2 composites'(manuscript under preparation).
- 5) A. Gaur, P. Singh, N. Choudhary, D. Kumar, M. Shariq, K. Singh, N. Kaur, D. Kaur 'Structural, optical and magnetic properties of Nd-doped BiFeO_3 thin films prepared by pulsed laser deposition', Physica B: Condensed Matter, 406 (2011) 1877- 1882.

Conference and Proceeding:

- 1) A. Gaur, D. Montinaro, V. M. Sglavo, 'Electric field assisted-sintering of LSCF and LSCF/GDC composites', Proceedings of EFC2013 Fifth European Fuel Cell Technology & Applications Conference - Piero Lunghi Conference December 11-13, 2013, Rome, Italy, Pages: 225-226
- 2) J. A. Downs, K. Naik, A. Gaur, V. M. Sglavo, 'Electric field assisted sintering in advanced ceramics', Proceedings of XI Convegno Nazionale AIMAT, Gaeta (LT), 16-19 September 2012, Pages 213-216
- 3) A. Gaur, D. Montinaro, V. M. Sglavo, 'Production of pore-free protective coatings on crofer steel interconnect via the use of an electric field during sintering', 10th European SOFC Forum, 26th-29th June, 2012, B1208 Pages 44-49
- 4) Participated in Conference on Mesogenic and Ferroic Materials (CMFM09) held at Department of Physics, Banaras Hindu University, Varanasi from 9-11th Jan, 2009.

Book Chapters:

“Changing trends in Silicon Nanotechnology” in the book on
"Nantotechnology" Edited by Dr. J. N Govil, Vol.8: Electronics and
Photovoltaics, Pages: 411, 2013

Md. Ahamad Mohiddon, Anshu and M. Ghanashyam Krishna
Studium Press LLC, USA. ISBN: 1-62699-008-5.

Teaching Experience:

Laboratory Assistant:

- BTech. First Year (July 2008-June 2009)
- BTech First Year (Jan 2010- December 2010)
- MSc Physics 2nd Year labs (Jan 2010- December 2010)

Awards/Achievements:

- B.Sc. Gold Medalist 2004 (Shri Sheonidhi Lal Srivastava Memorial Medal).
- National Level Graduate Aptitude Test in Engineering (GATE) 2007
All India Rank: 93, GATE Score: 488, GATE Percentile: 98.24.
- Joint CSIR-UGC test for Junior Research Fellowship and eligibility for
Lectureship (NET) for UGC JRF+ Lectureship.

Acknowledgments

I reach on the culminating point of my thesis, a sense of achievement with satisfaction has transcended in me and it is pleasant and exciting moment of my life when I want to reminisce and acknowledge all those who are associated directly or indirectly with me during this period.

Foremost, I would like to express my sincere gratitude to my tutor Prof. Vincenzo M. Sglavo for his all time enthusiasm and encouraging remark. His pertinent suggestions strengthened my skill in research methodology and also helped me to develop a positive outlook towards problems or issues. His guidance helped me in all the time of research and writing of the thesis.

I am also thankful to faculty members of Materials Science and Engineering Department, University of Trento, Italy for their kind suggestions and help whenever it needed during the research work. I would extend my heartily thanks to Livio Zottele and Alexia Conci for providing all needful help in the lab.

I would like to thank my colleagues and friends from ceramics lab, John, Lam, Francesca, Andrea, and Michele for their co-operation during the work. A special thanks to my friends Zolzaya Dashdorj and Galena Kostoska who helped to live a lively life in Trento away from India.

I am in dearth of words in expressing my warm feelings to 'Mesiano Guys': Kiran Pradnyesh, Pradeep, Rahul, Piyush and Pushker who made me feel like being with family in Trento. Their presence made my life and stay in Trento cheerful and colorful. I must accolade the versatile, convivial and vibrant company of my friends from India, Nami, Bari, Shalinji and Chandaniji. I will always remain grateful to them for the time they have shared with me, to keep joyous environment. In fact, my life is shared with them.

The words are not enough to express all my regards, love and thankfulness to my Mummy (Mrs. Rajni Gaur) and Papa (Mr. Surendra Nath Gaur) for their blessings, love and support at every moment. I would like to abound my feelings for my sisters Priti, Parul and Shikha with a special attention to a new member of the family 'Saanvi', her presence made our lives more

livable and enjoyable. I would like to include my brother-in-law Mr. Siva Kumar Kotla for being with my family as a support.

My acknowledgments would never be complete if I do not include 'sir' (Dr. Ahmed Mohiddon) whose presence, even, means a lot in every part of my carrier and life. His suggestions and constructive criticism strengthened my research skill and helped me to develop a love of knowledge. I deeply appreciate all his prudent support, forbearance and invaluable and timely help.

Last but not least I wish to acknowledge all those whose names have not figured above, but helped me directly or indirectly during the entire period of my work.

God is above all.

ANSHU